An in-depth study of DOPE:DOPC liposomes to maximize targeted drug delivery to cancer-associated cells

by

Tanzeel Ur Rehman

A dissertation submitted to the graduate faculty

in partial fulfillment of the requirements for the degree of

DOCTOR OF PHILOSOPHY

Major: Materials Science and Engineering

Program of Study Committee:
Surya Mallapragada, Co-major Professor
Chris Cornelius, Co-major Professor
Shan Jiang
Rizia Bardhan
Marit Nilsen-Hamilton

The student author, whose presentation of the scholarship herein was approved by the program of study committee, is solely responsible for the content of this dissertation. The Graduate College will ensure this dissertation is globally accessible and will not permit alterations after a degree is conferred.

Iowa State University

Ames, Iowa

2023

DEDICATION

To the man who taught me the value of hard work, dedication, and perseverance - my father. Though he is no longer with me, his unwavering belief in my abilities and unwavering support in my pursuit of education lives on. I dedicate this thesis to his memory and honor, as a testament to the sacrifices he made and the love he instilled in me. This accomplishment is not mine alone, but a shared achievement between us. Thank you for being my guiding light and for always believing in me. This one is for you…!

TABLE OF CONTENTS

Page

ACKNOWLEDGMENTS

I express my deepest gratitude to the individuals who have supported me throughout my academic journey. Firstly, I would like to thank my major professors, Dr. Surya Mallapragara and Dr. Chris Cornelius, for their unwavering support and guidance toward the completion of my Ph.D. I am also grateful to my committee members, Dr. Marit Nilsen-Hamilton, Dr. Shan Jiang, and Dr. Rizia Bardhan, for their invaluable feedback and mentorship throughout my research.

Furthermore, I would like to extend my thanks to Dr. Kaitlin Bratlie, who played an instrumental role in the inception of my research project. I am also thankful to Dr. Sarah Huffman and Chris Myers for their continued support and encouragement in my academic pursuits at Iowa State University.

I would like to acknowledge the contributions of my colleagues Zhuqing Li, Zihao Xu, Susheel Nethi, and Brianna White, as well as the department faculty and staff, Julie, Makayla, and Andrea, for making my time at Iowa State University truly memorable. Finally, I express my heartfelt gratitude to my dear friends Abdullah, Kamran, Mayyda, and others for providing me with an incredible support system, making my journey all the more rewarding, and providing me with a family away from home.

ABSTRACT

Cancer is a global health concern, with chemotherapy being the primary treatment for many cancer types. Despite advances in cancer treatment, chemotherapy remains the most common treatment modality for many cancer types with various side effects, including hair loss, nausea, vomiting, fatigue, and decreased immune function. These side effects can be debilitating and may not effectively eradicate cancer cells, leading to drug resistance. Therefore, the development of new and more effective cancer therapies with fewer side effects is crucial to improve patient outcomes and quality of life. Liposomes are spherical nanoparticles composed of a phospholipid bilayer that can encapsulate both hydrophobic and hydrophilic drugs. They are an attractive delivery system for cancer chemotherapy due to their ability to improve the pharmacokinetics and biodistribution of drugs, reduce toxicity, and enhance therapeutic efficacy by targeted drug delivery of single drugs as well as combinations of drugs, to the tumor site. In this dissertation, the first study examined the effects of liposome size on cellular uptake and toxicity. Four different liposome sizes, ranging from 50 to 400 nm, were loaded with the chemotherapy drug doxorubicin (DOX) and rigorously tested for their cellular uptake and toxicity, in vitro. The results showed that the 100 nm liposomes were most efficiently taken up by the cells, whereas toxicity levels were similar across all four sizes, with no significant difference observed among the half-minimal inhibitory concentration (IC_{50}) values. Based on these findings, the 100 nm liposomes were selected for further studies. The second study focused on modifying the surface of 100 nm DOPE:DOPC liposomes with 17 new arginine-like molecules to enhance their targetability towards myofibroblasts, which are cancer-associated fibroblasts found in the presence of a tumor. Results showed that 15 of the 17 molecules effectively targeted myofibroblasts more compared to fibroblasts, with higher cellular uptake and

lower IC50 values, demonstrating the potential for these modifications to be used for improved drug delivery in cancer therapy. In the third study, we investigated the use of a combination of doxorubicin and ibuprofen-loaded liposomes (IBLL) against macrophages and their phenotypes (M0, M1, and M2). After testing nine different concentrations of IBLL in combination with a constant concentration of doxorubicin-loaded liposomes (DLL), the three highest concentrations of IBLL showed synergistic results against macrophages. While toxicity was increased, the cellular uptake remained similar. However, to effectively target M2-type macrophages which transform into tumor-associated macrophages in the presence of a tumor, more targeting strategies must be included on the surface of the liposomes. The results demonstrated that this combination could significantly increase the efficacy of doxorubicin while reducing its toxic effects on healthy cells, highlighting the potential of combination therapies and drug delivery systems for improving cancer treatment outcomes. In the fourth study, DOPE was modified by attaching a cysteine to it with the aim of using the -SH bond of cysteine to click with any targeting agent using the thiol-ene/yne click chemistry. Folic acid was used as a proof of concept and modified to have a triple bond at the terminal end. The click reaction was executed, and folic acid was successfully attached to the surface of liposomes encapsulated with DOX. These liposomes were then tested against M0, M1, and M2-type macrophages, where it was observed that M2-type macrophages showed a higher cellular uptake due to the folic acid modification. As M2-type macrophages act as tumor-associated macrophages in the vicinity of a tumor, this modification could prove useful in targeting them specifically. Overall, these studies demonstrate the potential of liposomes as a promising targeted drug delivery system for combination cancer treatments. Further optimization and modification of liposome formulations could lead to more effective and targeted therapies with reduced toxicity.

CHAPTER 1. GENERAL INTRODUCTION

Cancer is a significant global health concern that affects millions of people worldwide. In 2023, 1.9 million new cancer cases are expected, with around 600,000 projected cancer deaths in the United States [1]. While the overall number of cancer cases has decreased since 1991, some types, such as prostate, liver, and breast cancer, have been increasing in recent years [2]. According to the World Health Organization, cancer is the second leading cause of death globally. The increasing incidence of cancer and the limitations of current treatments highlight the need to develop new and more effective therapies. Chemotherapy remains one of the most commonly used treatments for certain types of cancer, such as breast and lung cancer, despite its well-known side effects [3,4].

Chemotherapy targets rapidly dividing cells, including cancer cells, and damages their DNA, ultimately leading to their death [5]. However, chemotherapy drugs can also damage healthy cells, leading to a range of side effects. Hair loss, nausea, vomiting, fatigue, and decreased immune function are among the most common side effects associated with chemotherapy [6]. These side effects can significantly impact a patient's quality of life, and they can persist long after the end of treatment. Moreover, chemotherapy can lead to drug resistance, a significant challenge in cancer treatment [7,8]. As cancer cells become resistant to the drugs used to treat them, they continue to grow and divide, making the cancer more difficult to treat. Therefore, there is an urgent need to develop new and more effective cancer therapies to overcome these limitations and provide better outcomes for patients. The development of new therapies, such as targeted therapy, combination therapy, immunotherapy, and nanomedicine, offers the promise of more precise and less toxic cancer treatment.

Chemotherapy, as mentioned earlier, is a common treatment for cancer, but it has limitations due to its adverse effects and drug resistance. In addition to cancer cells, tumors contain a diverse range of cells, including cancer-associated cells that promote tumor growth and metastasis. These cells can include cancer-associated fibroblasts (CAFs) and tumor-associated macrophages (TAMs), which play critical roles in tumor progression and resistance to chemotherapy [9,10]. CAFs are cells that support tumor growth by secreting growth factors, remodeling the extracellular matrix, and promoting angiogenesis [11]. TAMs, on the other hand, are immune cells that infiltrate tumors and can have both pro-tumor and anti-tumor effects depending on their activation state [12]. Cancer-associated cells, including CAFs and TAMs, promote tumor growth and resistance to chemotherapy. Despite their profound impact, these cells have received limited attention in cancer therapy, and few drugs have been developed to target them specifically. Therefore, it is imperative to prioritize research efforts to unravel the complex interplay between cancer-associated cells and tumor microenvironments to identify novel therapeutic targets. Developing targeted therapies that can modulate these cells may offer new hope for patients and improve cancer treatment outcomes.

Liposomes are a type of nanoparticle that have been studied for their potential use in drug delivery. They were first discovered in the 1960s by Alec Bangham, who observed the self-assembly of phospholipids into spherical structures resembling biological membranes [13,14]. They are composed of phospholipids, similar to the lipids found in cell membranes. This composition makes the liposomes biocompatible and non-toxic [15,16]. Additionally, the size of liposomes can be controlled to optimize their performance for specific applications. Liposomes can be modified by attaching different functional groups to their surface, enhancing their stability, increasing their circulation time in the body, and targeting them to specific tissues or cells. Moreover, liposomes

have a hollow, spherical cavity that can easily encapsulate both hydrophobic and hydrophilic drugs, making them a versatile drug delivery system [17,18]. Since then, liposomes have been extensively studied and have shown promise as a delivery vehicle for a wide range of drugs.

One of the earliest Food and Drug Administration (FDA) -approved liposomal drugs was Doxil, a liposomal formulation of the chemotherapy drug doxorubicin, approved in 1995 for treating ovarian and breast cancer [19]. Another example is Ambisome, a liposomal formulation of the antifungal drug amphotericin B, which was approved in 1997 for treating systemic fungal infections [20]. Liposomal formulations of other drugs, such as cytarabine and daunorubicin, have also been approved to treat cancer [21,22].

Recently, liposomes have also been used to develop vaccines, including the COVID-19 vaccine. The Pfizer-BioNTech and Moderna COVID-19 vaccines both use mRNA encapsulated in lipid nanoparticles, which protect the mRNA from degradation and aid in its delivery to cells [23,24]. The use of liposomes in vaccine development is a promising area of research, as they can improve the stability and efficacy of vaccines. In summary, liposomes have a rich history in drug delivery to effectively treat various diseases, including cancer. They have also been included in developing COVID-19 vaccines, highlighting their potential in immunization. Due to the flexibility in size, drug encapsulation, and surface modification, among other advantages, liposomes have emerged as an ideal choice for targeted drug delivery to treat cancers, making them an area of active research in the field of nanomedicine.

The remainder of this chapter provides an in-depth exploration of the crucial role played by cancer-associated cells, including CAFs and TAMs, in tumor growth and resistance to chemotherapy. Subsequently, the history of liposomes is discussed, alongside examples of FDA-approved liposomes, focusing on their potential as an effective delivery system, especially

targeted to CAFs and TAMs for cancer therapy. Chapter two delves into the effect of liposome size on cellular uptake and toxicity. Chapter three explores how modifying the surface of liposomes can enhance their targetability towards myofibroblasts, which are CAFs found in the presence of a tumor. Chapter four investigates the use of a combination of doxorubicin and ibuprofen-loaded liposomes against macrophages and their phenotypes (M0, M1, and M2), while chapter five focuses on the modification of DOPE by attaching a cysteine to it to click with any targeting agent using the thiol-ene/yne click chemistry and how this could prove useful in targeting M2-type macrophages specifically. Ultimately, chapter six provides a comprehensive conclusion, emphasizing the significant potential impact of this work in cancer research and drug delivery systems, particularly in developing new targeted therapies that can modulate cancer-associated cells to improve cancer treatment outcomes.

1.1 Fibroblasts, Macrophages, and Their Phenotypes

Fibroblasts are a type of cell found in connective tissue throughout the body. They are responsible for producing and maintaining the extracellular matrix (ECM), a network of proteins and other molecules that provide structural support for tissues and organs. Fibroblasts secrete collagen, elastin, and other proteins that make up the ECM, as well as enzymes that help to remodel it [25]. In addition to their role in tissue maintenance and repair, fibroblasts also play a key role in wound healing and immune responses. They are involved in the production of growth factors and cytokines that attract and activate immune cells, as well as in the formation of scar tissue.

A study by Desmoulière et al. found that fibroblasts secrete cytokines, such as interleukin-1 (IL-1), during the inflammatory phase of wound healing. These cytokines are essential for attracting immune cells to the wound site and promoting tissue repair [26]. Another study showed that fibroblasts produce growth factors, such as transforming growth factor beta

(TGF-β), during the proliferative phase of wound healing. These growth factors are essential for stimulating the growth and proliferation of new cells in the wound bed [27]. A study by Eming et al. identified several growth factors and cytokines involved in scar formation. They found that fibroblasts produce and secrete transforming growth factor beta 1 (TGF-β1), which promotes collagen synthesis and deposition. The researchers also noted that fibroblasts produce connective tissue growth factor (CTGF), which is involved in various cellular processes, including wound healing and fibrosis. Furthermore, the study demonstrated that fibroblasts secrete interleukin-6 (IL-6), a cytokine that is involved in the immune response and inflammation, and that it plays a role in scar formation [28].

When activated by injury or inflammation, fibroblasts can differentiate into myofibroblasts, which have contractile properties and are involved in tissue contraction and remodeling [29,30]. Myofibroblasts are characterized by the presence of alpha-smooth muscle actin (α-SMA) filaments, which enable them to contract and exert mechanical forces on the ECM [31]. These cells are critical during wound healing, where they promote tissue repair by contracting the wound edges and generating mechanical tension that promotes cell proliferation and migration. Myofibroblasts also secrete extracellular matrix proteins, such as collagen and fibronectin, contributing to scar formation. While myofibroblasts play an essential role in wound healing, excessive or prolonged myofibroblast activation can lead to tissue fibrosis, a pathological condition characterized by excessive deposition of ECM proteins and tissue stiffening.

Myofibroblasts are highly specialized cells crucial in wound healing and tissue repair. They secrete various cytokines, including transforming growth factor beta (TGF-β), a key regulator of ECM synthesis and deposition. According to Hinz et al., myofibroblasts in human

skin wounds express high levels of TGF-β, which stimulate the production and secretion of fibronectin. This ECM protein promotes cell adhesion and migration [32]. Another review by Darby et al. discusses that myofibroblasts also secrete a protein called periostin, which regulates collagen deposition during wound healing [33]. Additionally, myofibroblasts have been shown to play a role in scar formation by producing excessive amounts of collagen, leading to the development of hypertrophic scars [34].

Macrophages are immune cells that play a crucial role in maintaining tissue homeostasis and responding to infections and injuries. They are derived from monocytes, which circulate in the blood and can differentiate into macrophages upon tissue infiltration [35]. Once activated, macrophages can phagocytose and eliminate foreign invaders and dead or damaged cells [36]. Additionally, they secrete various cytokines and growth factors that can stimulate other immune cells, promote tissue repair and regeneration, and modulate the immune response. Macrophages are also involved in regulating inflammation and can switch between different phenotypes depending on the microenvironment they encounter [37,38].

Macrophages are highly heterogeneous cells that can undergo phenotypic changes in response to various stimuli. There are two major macrophage phenotypes, M1 and M2, representing the extremes of a spectrum of activation states [39,40]. M1 macrophages, also known as classically activated macrophages, are involved in pro-inflammatory responses and the killing of pathogens. They secrete cytokines such as tumor necrosis factor-alpha (TNF-α), interleukin-1 beta (IL-1β), interleukin-6 (IL-6), and interleukin-12 (IL-12), which activate immune cells and induce an inflammatory response. M1 macrophages also produce reactive oxygen and nitrogen species (ROS and RNS) to kill pathogens and infected cells.

Studies have found that M1 macrophages produce high levels of TNF-α, which plays a critical role in the immune response to pathogens. Moreover, TNF-α produced by M1 macrophages can activate other immune cells, such as T cells and natural killer cells, to fight off infection [41–43]. Another study found that IL6 produced by M1 macrophages is involved in the pro-inflammatory response to pathogens. The researchers found that IL6 stimulates the production of other pro-inflammatory cytokines and chemokines, which recruit immune cells to the site of infection [44,45].

On the other hand, M2 macrophages, also known as alternatively activated macrophages, are involved in tissue repair and immune regulation. They secrete cytokines such as interleukin-10 (IL-10), transforming growth factor-beta (TGF-β), and interleukin-1 receptor antagonist (IL-1RA), which inhibit pro-inflammatory responses and promote tissue remodeling and repair [46,47]. M2 macrophages are also involved in the clearance of apoptotic cells and debris, and they play a role in wound healing and tissue regeneration.

A study by Kigerl et al. showed that M2 macrophages release anti-inflammatory cytokines, such as IL-10 and TGF-β, which inhibit pro-inflammatory responses and promote tissue remodeling [48]. Another study explored the role of M2 macrophages in liver fibrosis. The researchers found that M2 macrophages secrete factors that inhibit pro-inflammatory responses and promote tissue remodeling, leading to the resolution of liver fibrosis. Specifically, M2 macrophages secrete IL-10, which inhibits the production of pro-inflammatory cytokines, and TGF-β, which promotes the differentiation of fibroblasts into myofibroblasts and the production of extracellular matrix proteins [49].

In the presence of a tumor, the behavior of fibroblasts and macrophages is altered, and they become corrupted into cancer-associated fibroblasts (CAFs) and tumor-associated macrophages (TAMs), respectively. These cells in the tumor microenvironment (TME) often have an abnormal phenotype and produce factors that support tumor growth, invasion, and metastasis. CAFs secrete growth factors and extracellular matrix components, creating a pro-tumorigenic microenvironment [50]. At the same time, TAMs can promote tumor growth by releasing cytokines that inhibit the immune response and promote angiogenesis [51]. Therefore, understanding the behavior and functions of these cells in the TME is essential for developing effective cancer treatments. Targeting CAFs and TAMs in the TME could be a promising strategy to prevent tumor progression and enhance the efficacy of cancer therapies.

1.2 Cancer-Associated Cells

Cancer-associated cells are normal cells in the body that have been transformed by the presence of cancer cells or the TME. These cells can include fibroblasts, immune cells such as macrophages, as well as endothelial cells that make up blood vessels. In response to the presence of a tumor, these cells can undergo changes that promote tumor growth and progression.

Cancer-associated fibroblasts (CAFs) and tumor-associated macrophages (TAMs) are two major types of cancer-associated cells that have been widely studied in cancer research. These cells are known to promote tumor growth and metastasis by secreting growth factors, cytokines, and ECM components that support tumor cell survival and invasion. Below, the specific characteristics and functions of CAFs and TAMs are discussed in more detail.

1.2.1 Cancer-Associated Fibroblasts

Cancer-associated fibroblasts (CAFs) are a type of activated fibroblast that is found within the tumor microenvironment. CAFs can be derived from numerous sources, including resident tissue fibroblasts, bone marrow-derived mesenchymal stem cells and endothelial cells. These cells are characterized by their ability to promote tumor growth and progression, and to modify the surrounding extracellular matrix to enhance tumor invasion and metastasis.

One of the key functions of CAFs is to produce and deposit extracellular matrix components, such as collagen and fibronectin, which can create a stiff and dense matrix that supports tumor growth and progression. CAFs can also secrete a range of growth factors, cytokines, and chemokines that promote tumor cell proliferation, migration, and invasion. For example, CAFs can produce fibroblast growth factor (FGF), which can promote the growth and survival of cancer cells, and transforming growth factor-beta (TGF-β), which can suppress the immune response and promote tumor cell invasion [52,53].

Numerous studies have shown that CAFs promote tumor growth, invasion, and metastasis. CAFs secrete various growth factors, cytokines, and extracellular matrix components, creating a supportive environment for cancer cells. For instance, a study published by Grugan et al. showed that CAFs secrete hepatocyte growth factor (HGF), which promotes tumor cell proliferation, survival, and invasion [54]. Subramaniam et al. demonstrated that CAFs secrete interleukin-6 (IL-6), which activates the STAT3 signaling pathway and promotes tumor cell growth and survival [55]. Additionally, CAFs can remodel the ECM and create a stiffer and more fibrotic environment that facilitates tumor invasion and metastasis. Another study showed that CAFs secrete lysyl oxidase (LOX), an enzyme that cross-links collagen fibers and increases ECM stiffness, thereby promoting tumor cell migration and metastasis [56].

In addition to promoting tumor growth, CAFs can contribute to developing drug resistance in cancer cells [57,58]. CAFs can secrete factors that activate signaling pathways involved in drug resistance, such as the Notch and Wnt pathways. They can also modify the extracellular matrix to create a physical barrier that prevents drugs from reaching the cancer cells. As such, targeting CAFs has emerged as a potential therapeutic strategy for cancer treatment.

1.2.2 Tumor-Associated Macrophages

Tumor-associated macrophages (TAMs) are immune cells that infiltrate the TME and play a significant role in tumor progression and metastasis. TAMs are typically classified into two subtypes: M1 and M2. While both subtypes are present in the TME, M2 TAMs are more commonly associated with tumor progression and metastasis than M1 TAMs.

M2 TAMs have been shown to promote tumor growth and metastasis through various mechanisms. For example, they secrete cytokines such as TGF-β and IL-10 that suppress the immune response and promote tumor cell proliferation, migration, and invasion [59,60]. They also promote angiogenesis, which is the formation of new blood vessels that supply oxygen and nutrients to the tumor, by secreting pro-angiogenic factors such as VEGF [61,62].

Pollard et al. found that TAMs produce VEGF, which promotes angiogenesis and tumor growth. The researchers demonstrated that blocking VEGF production by TAMs reduced tumor growth in mice [63]. Another showed that TAMs produce TGF-β, which has immunosuppressive effects and promotes tumor growth. It was seen that blocking TGF-β production by TAMs inhibited tumor growth and improved the antitumor immune response in mice [64]. Targeting TAMs and their associated cytokines represents a promising strategy for developing novel anti-cancer therapies.

1.3 Liposomes and Their Use in Drug Delivery

Liposomes are spherical structures composed of a phospholipid bilayer that encapsulates an aqueous core. These structures were first discovered in the 1960s, and since then, they have been widely studied as drug delivery systems. One of the most important characteristics of liposomes is their biocompatibility, which is due to the fact that they are composed of phospholipids, the same components that make up cell membranes in the body. This biocompatibility allows liposomes to be used for drug delivery without causing adverse reactions or immune responses in the body.

Moreover, the ability to modify the surface of liposomes is a critical aspect of their versatility in drug delivery. The surface of liposomes can be easily functionalized by attaching various ligands, such as antibodies or peptides, which can target specific cells or tissues [65,66]. Furthermore, different surface coatings can be applied to liposomes to alter their pharmacokinetics and biodistribution. This has led to the development of "stealth" liposomes, which are coated with polyethylene glycol (PEG) to prolong their circulation time and reduce clearance by the immune system [67,68]. Additionally, surface modifications can be used to promote the uptake of liposomes by specific cells or to enhance their stability in harsh environments. Therefore, the ability to modify the surface of liposomes adds to their diversity and makes them a promising tool in drug delivery for a variety of applications.

Liposomes can encapsulate a wide range of drugs, both hydrophilic and hydrophobic, due to the fact that their bilayer structure can contain both polar and non-polar substances [69,70]. This versatility in drug encapsulation has made liposomes an attractive option for drug delivery in various therapeutic areas, including cancer, infectious diseases, and inflammatory disorders.

Several liposomal agents have been approved by the FDA for cancer therapy, including Doxil and DaunoXome, which are used to treat ovarian and breast cancer, respectively[19,71]. Additionally, liposomes have been used as a delivery system for the mRNA vaccines developed by Pfizer and Moderna to combat COVID-19 [72–74].

1.3.1 The Role of Liposomes in Combination Therapies for Cancer

Combination therapy is a treatment approach that involves combining two or more therapies to treat a disease or medical condition. In the context of cancer treatment, combination therapy is often used to increase the effectiveness of the treatment and reduce the risk of drug resistance. By combining different types of therapies, such as chemotherapy, targeted therapy, immunotherapy, and radiation therapy, combination therapy can target cancer cells in multiple ways, potentially leading to better outcomes [75]. Moreover, combination therapy can also reduce the side effects of treatment by using lower doses of each therapy while maintaining or even enhancing their therapeutic effects [76,77]. In recent years, combination therapy has emerged as a promising treatment approach for cancer, and liposomes have gained attention as an effective platform for delivering combination therapies to cancer cells.

A study by Cui et al. used liposomes to co-deliver curcumin and doxorubicin to treat breast cancer [78]. The study found that the combination therapy enhanced cytotoxicity and induced apoptosis, resulting in a higher anti-tumor effect compared to single-drug treatments. Another study by Mylonakis et al. used liposomes to deliver gemcitabine and cisplatin to treat non-small cell lung cancer [79]. The study found that the combination therapy enhanced cellular uptake of the drugs and showed a synergistic effect, resulting in higher cytotoxicity and tumor growth inhibition compared to single-drug treatments.

A study by Li et al. used liposomes to co-deliver two drugs, camptothecin and quercetin, to treat breast cancer [80]. The study found that the combination therapy enhanced anti-tumor efficacy, as the liposomes were able to increase drug accumulation in tumor tissue and reduce drug toxicity in healthy tissues.

In addition to small molecule drugs, liposomes have been used to deliver therapeutic proteins as part of combination therapies. A study by Huang et al. used liposomes to co-deliver TRAIL, a protein that induces apoptosis, and doxorubicin to treat hepatocellular carcinoma [81]. The study found that the combination therapy enhanced apoptosis and showed a synergistic effect, resulting in higher anti-tumor efficacy compared to single-drug treatments.

Overall, these studies demonstrate the potential of liposomes as delivery systems for combination therapies in cancer treatment. By co-delivering two or more drugs, liposomes can enhance drug accumulation in tumor tissue and reduce toxicity in healthy tissues, resulting in higher anti-tumor efficacy. Liposomes can also be used to deliver therapeutic proteins as part of combination therapies, further expanding the range of treatment options for cancer.

With all the advantages and flexibility, liposomes can specifically target cancer-associated fibroblasts and tumor-associated macrophages. As discussed above, CAFs and TAMs are known to play a significant role in the development and progression of tumors and can contribute to resistance to chemotherapy and immunotherapy. Targeting these cells using liposomes offers a promising approach to cancer treatment, as liposomes can be engineered to carry drugs specifically to these cells. For example, liposomes can be modified to target proteins expressed on the surface of CAFs or TAMs or to release drugs. This targeted approach can potentially increase cancer treatment's efficacy while minimizing side effects.

1.4 References

1. Siegel, R. L., Miller, K. D., Wagle, N. S. & Jemal, A. Cancer statistics, 2023. CA. Cancer J. Clin. 73, 17–48 (2023).

2. Eide, M. J. & Weinstock, M. A. Association of UV index, latitude, and melanoma incidence in nonwhite populations—US Surveillance, Epidemiology, and End Results (SEER) Program, 1992 to 2001. Arch. Dermatol. 141, 477–481 (2005).

3. Presley, C. J. et al. Functional trajectories before and after a new cancer diagnosis among community-dwelling older adults. J. Geriatr. Oncol. 10, 60–67 (2019).

4. Howlader, N. et al. The effect of advances in lung-cancer treatment on population mortality. N. Engl. J. Med. 383, 640–649 (2020).

5. A Baudino, T. Targeted cancer therapy: the next generation of cancer treatment. Curr. Drug Discov. Technol. 12, 3–20 (2015).

6. Masood, A. I., Sheikh, R. & Anwer, R. A. BIOBRAN MGN-3: Effect of reducing side effects of chemotherapy in breast cancer patients. Prof. Med. J. 20, 13–16 (2013).

7. Mansoori, B., Mohammadi, A., Davudian, S., Shirjang, S. & Baradaran, B. The different mechanisms of cancer drug resistance: a brief review. Adv. Pharm. Bull. 7, 339 (2017).

8. Luqmani, Y. A. Mechanisms of drug resistance in cancer chemotherapy. Med. Princ. Pract. 14, 35–48 (2005).

9. Liao, D., Luo, Y., Markowitz, D., Xiang, R. & Reisfeld, R. A. Cancer associated fibroblasts promote tumor growth and metastasis by modulating the tumor immune microenvironment in a 4T1 murine breast cancer model. PLoS One 4, e7965 (2009).

10. Zhou, N. et al. Exposure of tumor-associated macrophages to apoptotic MCF-7 cells promotes breast cancer growth and metastasis. Int. J. Mol. Sci. 16, 11966–11982 (2015).

11. Tyan, S.-W. et al. Breast cancer cells induce cancer-associated fibroblasts to secrete hepatocyte growth factor to enhance breast tumorigenesis. PLoS One 6, e15313 (2011).

12. Goswami, K. K. et al. Tumor promoting role of anti-tumor macrophages in tumor microenvironment. Cell. Immunol. 316, 1–10 (2017).

13. Abdul Ghaffar, K., Kumar Giddam, A., Zaman, M., Skwarczynski, M. & Toth, I. Liposomes as nanovaccine delivery systems. Curr. Top. Med. Chem. 14, 1194–1208 (2014).

14. Weissig, V. Liposomes came first: The early history of liposomology. Liposomes Methods Protoc. 1–15 (2017).

15. Dua, J. S., Rana, A. C. & Bhandari, A. K. Liposome: methods of preparation and applications. Int J Pharm Stud Res 3, 14–20 (2012).

16. Dymek, M. & Sikora, E. Liposomes as biocompatible and smart delivery systems–The current state. Adv. Colloid Interface Sci. 102757 (2022).

17. Ge, L., Tan, X., Sheng, R. & Xiao, J. Layer-by-layer self-assembly of giant polyelectrolyte microcapsules templated by microbubbles as potential hydrophilic or hydrophobic drug delivery system. Colloid Interface Sci. Commun. 47, 100603 (2022).

18. Chen, Y. et al. Double mesoporous silica shelled spherical/ellipsoidal nanostructures: synthesis and hydrophilic/hydrophobic anticancer drug delivery. J. Mater. Chem. 21, 5290–5298 (2011).

19. Barenholz, Y. C. Doxil®—the first FDA-approved nano-drug: lessons learned. J. Control. release 160, 117–134 (2012).

20. Boswell, G. W., Buell, D. & Bekersky, I. AmBisome (liposomal amphotericin B): a comparative review. J. Clin. Pharmacol. 38, 583–592 (1998).

21. Salehi, B. et al. Liposomal cytarabine as cancer therapy: from chemistry to medicine. Biomolecules 9, 773 (2019).

22. Fassas, A. & Anagnostopoulos, A. The use of liposomal daunorubicin (DaunoXome) in acute myeloid leukemia. Leuk. Lymphoma 46, 795–802 (2005).

23. Khurana, A. et al. Role of nanotechnology behind the success of mRNA vaccines for COVID-19. Nano Today 38, 101142 (2021).

24. Schoenmaker, L. et al. mRNA-lipid nanoparticle COVID-19 vaccines: Structure and stability. Int. J. Pharm. 601, 120586 (2021).

25. Brett, D. A review of collagen and collagen-based wound dressings. Wounds 20, 347–356 (2008).

26. Desmoulière, A., Chaponnier, C. & Gabbiani, G. Tissue repair, contraction, and the myofibroblast. Wound repair Regen. 13, 7–12 (2005).

27. Shah, M., Foreman, D. M. & Ferguson, M. W. Neutralising antibody to TGF-beta 1, 2 reduces cutaneous scarring in adult rodents. J. Cell Sci. 107, 1137–1157 (1994).

28. Eming, S. A., Krieg, T. & Davidson, J. M. Inflammation in wound repair: molecular and cellular mechanisms. J. Invest. Dermatol. 127, 514–525 (2007).

29. Grinnell, F. Fibroblasts, myofibroblasts, and wound contraction. J. Cell Biol. 124, 401–404 (1994).

30. Baum, J. & Duffy, H. S. Fibroblasts and myofibroblasts: what are we talking about? J. Cardiovasc. Pharmacol. 57, 376 (2011).

31. Rao, B., Malathi, N., Narashiman, S. & Rajan, S. T. Evaluation of myofibroblasts by expression of alpha smooth muscle actin: a marker in fibrosis, dysplasia and carcinoma. J. Clin. diagnostic Res. JCDR 8, ZC14 (2014).

32. Hinz, B. The role of myofibroblasts in wound healing. Curr. Res. Transl. Med. 64, 171–177 (2016).

33. Darby, I. A., Laverdet, B., Bonté, F. & Desmoulière, A. Fibroblasts and myofibroblasts in wound healing. Clin. Cosmet. Investig. Dermatol. 301–311 (2014).

34. Goel, A. & Boland, C. R. Epigenetics of colorectal cancer. Gastroenterology 143, 1442–1460 (2012).

35. Yang, J., Zhang, L., Yu, C., Yang, X.-F. & Wang, H. Monocyte and macrophage differentiation: circulation inflammatory monocyte as biomarker for inflammatory diseases. Biomark. Res. 2, 1–9 (2014).

36. Martin, P. & Leibovich, S. J. Inflammatory cells during wound repair: the good, the bad and the ugly. Trends Cell Biol. 15, 599–607 (2005).

37. Lee, C.-H. & Choi, E. Y. Macrophages and inflammation. J. Rheum. Dis. 25, 11–18 (2018).

38. Hesketh, M., Sahin, K. B., West, Z. E. & Murray, R. Z. Macrophage phenotypes regulate scar formation and chronic wound healing. Int. J. Mol. Sci. 18, 1545 (2017).

39. Jablonski, K. A. et al. Novel markers to delineate murine M1 and M2 macrophages. PLoS One 10, e0145342 (2015).

40. Liu, Y.-C., Zou, X.-B., Chai, Y.-F. & Yao, Y.-M. Macrophage polarization in inflammatory diseases. Int. J. Biol. Sci. 10, 520 (2014).

41. Sheng, J., Zhang, B., Chen, Y. & Yu, F. Capsaicin attenuates liver fibrosis by targeting Notch signaling to inhibit TNF-α secretion from M1 macrophages. Immunopharmacol. Immunotoxicol. 42, 556–563 (2020).

42. Akhtari, M., Zargar, S. J., Vojdanian, M., Jamshidi, A. & Mahmoudi, M. Monocyte-derived and M1 macrophages from ankylosing spondylitis patients released higher TNF-α and expressed more IL1B in response to BzATP than macrophages from healthy subjects. Sci. Rep. 11, 17842 (2021).

43. Eisenman, S. T. et al. Tumor necrosis factor alpha derived from classically activated “M1” macrophages reduces interstitial cell of Cajal numbers. Neurogastroenterol. Motil. 29, e12984 (2017).

44. Yunna, C., Mengru, H., Lei, W. & Weidong, C. Macrophage M1/M2 polarization. Eur. J. Pharmacol. 877, 173090 (2020).

45. Laria, A. et al. The macrophages in rheumatic diseases. J. Inflamm. Res. 1–11 (2016).

46. Yan, W. et al. Tim-3 fosters HCC development by enhancing TGF-β-mediated alternative activation of macrophages. Gut 64, 1593–1604 (2015).

47. Bingisser, R., Speich, R., Zollinger, A., Russi, E. & Frei, K. Interleukin-10 secretion by alveolar macrophages and monocytes in sarcoidosis. Respiration 67, 280–286 (2000).

48. Kigerl, K. A. et al. Identification of two distinct macrophage subsets with divergent effects causing either neurotoxicity or regeneration in the injured mouse spinal cord. J. Neurosci. 29, 13435–13444 (2009).

49. Mantovani, A. et al. The chemokine system in diverse forms of macrophage activation and polarization. Trends Immunol. 25, 677–686 (2004).

50. Erdogan, B. & Webb, D. J. Cancer-associated fibroblasts modulate growth factor signaling and extracellular matrix remodeling to regulate tumor metastasis. Biochem. Soc. Trans. 45, 229–236 (2017).

51. Lamagna, C., Aurrand-Lions, M. & Imhof, B. A. Dual role of macrophages in tumor growth and angiogenesis. J. Leukoc. Biol. 80, 705–713 (2006).

52. Finch, N. C., Geddes, R. F., Syme, H. M. & Elliott, J. Fibroblast growth factor 23 (FGF-23) concentrations in cats with early nonazotemic chronic kidney disease (CKD) and in healthy geriatric cats. J. Vet. Intern. Med. 27, 227–233 (2013).

53. Calon, A., Tauriello, D. V. F. & Batlle, E. TGF-beta in CAF-mediated tumor growth and metastasis. in Seminars in cancer biology 25, 15–22 (Elsevier, 2014).

54. Grugan, K. D. et al. Fibroblast-secreted hepatocyte growth factor plays a functional role in esophageal squamous cell carcinoma invasion. Proc. Natl. Acad. Sci. 107, 11026–11031 (2010).

55. Subramaniam, K. S. et al. Cancer-associated fibroblasts promote endometrial cancer growth via activation of interleukin-6/STAT-3/c-Myc pathway. Am. J. Cancer Res. 6, 200 (2016).

56. Bielack, S. S., Erttmann, R., Winkler, K. & Landbeck, G. Doxorubicin: effect of different schedules on toxicity and anti-tumor efficacy. Eur. J. Cancer Clin. Oncol. 25, 873–882 (1989).

57. Kinugasa, Y., Matsui, T. & Takakura, N. CD44 expressed on cancer-associated fibroblasts is a functional molecule supporting the stemness and drug resistance of malignant cancer cells in the tumor microenvironment. Stem Cells 32, 145–156 (2014).

58. Bu, L., Baba, H., Yasuda, T., Uchihara, T. & Ishimoto, T. Functional diversity of cancer-associated fibroblasts in modulating drug resistance. Cancer Sci. 111, 3468 (2020).

59. Thepmalee, C., Panya, A., Junking, M., Chieochansin, T. & Yenchitsomanus, P. Inhibition of IL-10 and TGF-β receptors on dendritic cells enhances activation of effector T-cells to kill cholangiocarcinoma cells. Hum. Vaccin. Immunother. 14, 1423–1431 (2018).

60. Mirlekar, B. Tumor promoting roles of IL-10, TGF-β, IL-4, and IL-35: Its implications in cancer immunotherapy. SAGE Open Med. 10, 20503121211069012 (2022).

61. Obeid, E., Nanda, R., Fu, Y.-X. & Olopade, O. I. The role of tumor-associated macrophages in breast cancer progression. Int. J. Oncol. 43, 5–12 (2013).

62. Bolat, F. et al. Microvessel density, VEGF expression, and tumor-associated macrophages in breast tumors: correlations with prognostic parameters. Vascular 14, 15 (2006).

63. Pollard, J. W. Tumour-educated macrophages promote tumour progression and metastasis. Nat. Rev. Cancer 4, 71–78 (2004).

64. Yang, J. et al. Tumor-associated macrophages regulate murine breast cancer stem cells through a novel paracrine EGFR/Stat3/Sox-2 signaling pathway. Stem Cells 31, 248–258 (2013).

65. Nobs, L., Buchegger, F., Gurny, R. & Allémann, E. Current methods for attaching targeting ligands to liposomes and nanoparticles. J. Pharm. Sci. 93, 1980–1992 (2004).

66. Jølck, R. I., Feldborg, L. N., Andersen, S., Moghimi, S. M. & Andresen, T. L. Engineering liposomes and nanoparticles for biological targeting. Biofunctionalization Polym. their Appl. 251–280 (2011).

67. Kataria, S., Sandhu, P., Bilandi, A., Akanksha, M. & Kapoor, B. Stealth liposomes: a review. Int. J. Res. ayurveda Pharm. 2, (2011).

68. Immordino, M. L., Dosio, F. & Cattel, L. Stealth liposomes: review of the basic science, rationale, and clinical applications, existing and potential. Int. J. Nanomedicine 1, 297 (2006).

69. Voinea, M. & Simionescu, M. Designing of ‘intelligent’liposomes for efficient delivery of drugs. J. Cell. Mol. Med. 6, 465–474 (2002).

70. Alavi, M., Karimi, N. & Safaei, M. Application of various types of liposomes in drug delivery systems. Adv. Pharm. Bull. 7, 3 (2017).

71. Forssen, E. A. The design and development of DaunoXome® for solid tumor targeting in vivo. Adv. Drug Deliv. Rev. 24, 133–150 (1997).

72. Abed, O. S. A. Gene therapy avenues and COVID-19 vaccines. Genes Immun. 1–5 (2021).

73. Wilson, B. & Geetha, K. M. Lipid nanoparticles in the development of mRNA vaccines for COVID-19. J. Drug Deliv. Sci. Technol. 74, 103553 (2022).

74. McSweeney, M. D., Mohan, M., Commins, S. P. & Lai, S. K. Anaphylaxis to Pfizer/BioNTech mRNA COVID-19 vaccine in a patient with clinically confirmed PEG allergy. Front. Allergy 2, 57 (2021).

75. Esteva, F. J., Hubbard-Lucey, V. M., Tang, J. & Pusztai, L. Immunotherapy and targeted therapy combinations in metastatic breast cancer. Lancet Oncol. 20, e175–e186 (2019).

76. Su, X. et al. Combination therapy of anti-cancer bioactive peptide with Cisplatin decreases chemotherapy dosing and toxicity to improve the quality of life in xenograft nude mice bearing human gastric cancer. Cell Biosci. 4, 1–13 (2014).

77. Rajkumar, S. V. et al. Combination therapy with lenalidomide plus dexamethasone (Rev/Dex) for newly diagnosed myeloma. Blood 106, 4050–4053 (2005).

78. Cui, T., Zhang, S. & Sun, H. Co-delivery of doxorubicin and pH-sensitive curcumin prodrug by transferrin-targeted nanoparticles for breast cancer treatment. Oncol. Rep. 37, 1253–1260 (2017).

79. Mylonakis, N. et al. Phase II study of liposomal cisplatin (LipoplatinTM) plus gemcitabine versus cisplatin plus gemcitabine as first line treatment in inoperable (stage IIIB/IV) non-small cell lung cancer. Lung cancer 68, 240–247 (2010).

80. Lv, L., Shi, Y., Wu, J. & Li, G. Nanosized drug delivery systems for breast cancer stem cell targeting. Int. J. Nanomedicine 16, 1487 (2021).

81. Huang, S. et al. Improved melanoma suppression with target-delivered TRAIL and Paclitaxel by a multifunctional nanocarrier. J. Control. Release 325, 10–24 (2020).

CHAPTER 2. ANALYZING THE BEST SIZE FOR DOPE:DOPC LIPOSOMES TO TARGET FIBROBLASTS AND CANCER-ASSOCIATED FIBROBLASTS

Tanzeel Ur Rehman [1], Madison A. Rubin [2], Kaitlin M. Bratlie [1,2]

1. Department of Materials Science & Engineering, Iowa State University, Ames, Iowa 50011

2. Department of Chemical & Biological Engineering, Iowa State University, Ames, Iowa, 50011

Modified from a manuscript to be submitted to *ACS Omega*

Abstract

Biocompatibility, surface charge, and the ability to easily alter size are some of the advantages of liposomes. Although surface modification can be performed, the size of the liposomes still plays an essential role in targeting any cell and cellular uptake. Moreover, surface modification adds an additional step in the manufacturing process, costing more time and causing a loss of final product yield. Certainly, it is crucial to understand what size of liposomes works best for certain cell types. Therefore, in this study, we fabricated DOPE:DOPC liposomes with four different sizes: 50, 100, 200, and 400 nm. These different liposomes were tested for their cell viability against fibroblasts and cancer-associated fibroblasts (CAFs). Then, these liposomes were loaded with doxorubicin and were examined for their cytotoxicity through half-minimal inhibitory concentration (IC_{50}) against fibroblasts and CAFs. Subsequently, the cell internalization by fibroblasts and cancer-associated fibroblasts was analyzed by encapsulating fluorescin in all four sizes of liposomes. Finally, statistical analyses were performed on the results to determine which size of DOPE:DOPC liposomes is best suited for targeting CAFs in an environment with healthy fibroblasts. This study serves as the basis of many future studies that propose to use surface modifications on liposomes for CAF targeting.

2.1 Introduction

Liposomes, nano-sized vesicles synthesized from phospholipids, have numerous advantages in drug delivery systems. The most common advantages are their hydrophilic and hydrophobic character, biocompatibility, and flexibility in size. The FDA has approved more than 18 liposomal drugs for a variety of therapeutics (Bozzuto and Molinari, 2015; Gregoriadis, 2016; Kim and Jeong, 2021). As is commonly known, the first FDA-approved liposome was Doxil for the treatment of ovarian cancer and AIDS-related Kaposi's sarcoma. Many other drugs have been approved since then, such as Vyxeos in 2017, for the treatment of therapy-related acute myeloid leukemia (Bulbake et al., 2017; Krauss et al., 2019). Since this initial application, liposomes have become the most common and most investigated nanocarriers for drug delivery (Sercombe et al., 2015a; Zylberberg and Matosevic, 2016) owing to decreased toxicity (Allen, 2012; Allen and Martin, 2004; Grant et al., 1994; Wasan et al., 1994) and increased circulation times (Gabizon, 1995; A. Gabizon and Papahadjopoulos, 1988; Alberto Gabizon and Papahadjopoulos, 1988; Sercombe et al., 2015b).

Fibroblasts are the "most common cell type of connective tissues found throughout the body and the principal source of the extensive extracellular matrix (ECM)" (Kendall and Feghali-Bostwick, 2014). Similarly, fibroblasts can differentiate to myofibroblasts as the result of an inflammatory response to injury (Baum and Duffy, 2011; Fang et al., 2018).

Myofibroblasts are the primary producers of ECM required to restore tissue integrity after injury (Hinz, 2016). However, in cancer stroma, the myofibroblasts significantly impact tumor proliferation due to their production of growth factors and ECM remodeling, acting as cancer-associated fibroblasts (Liu et al., 2016; Sahai et al., 2020). Cancer-associated fibroblasts (CAFs) play essential roles in cancer initiation, progression, and proliferation (Lee et al., 2018; Li et al., 2021). Therefore, it is crucial to develop a drug delivery method that has the capability to target

fibroblast phenotype (myofibroblasts) that act as CAFs in a tumor microenvironment and help in tumor progression, metastatis, and drug resistance, especially in an environment, where regular, healthy cells are also present.

Increased therapeutic indices, enhanced antitumor activity, and decreased toxicity have all been shown by the encapsulation of antitumor drugs in liposomal formations compared to traditional drugs(Huang et al., 1992; Papahadjopoulos et al., 1991). Specifically, cardiac health concerns such as anthracycline-induced cardiotoxicity associated with the use of the anti-cancer drug doxorubicin have been shown to decrease when the drug is used in its liposomal form, along with significantly fewer cardiac events (Safra, 2003). Additionally, and maybe most importantly, the liposomal delivery method has shown an increased concentration of drugs in solid tumor tissue when loaded with anti-cancer drugs (Huang et al., 1992).

Liposomes typically range between 50 and 450 nm for medical applications. Although the size of liposomal formulations appears to affect the circulation time, size directly affects the efficiency of the delivery of an anti-cancer agent to a tumor environment (Liu et al., 1992; Nagayasu et al., 1999; Uchiyama et al., 1995). Previous findings suggest that the size of the liposomal drug delivery system can play a key role in the targeting efficiency of liposomes to tumor tissue, decreasing the release of said drugs within the vicinity of healthy tissue while improving anti-cancer abilities (Nagayasu et al., 1999; Oku et al., 1995). This is due to the fact that cell types are able to be targeted by altering the lipid chemistry and other physical characteristics of the liposomes being used for encapsulation (Neuberger et al., 2018; Storm et al., 1995). Therefore, it is crucial to understand what exact size of liposomes is best suited for specific cell types.

Although doxorubicin has been shown to be quite advantageous in liposomal form, optimal liposome preparation to target tumor tissue has not been clearly identified (Mayer et al., 1989). Researchers in the past have used surface modifications to alter the representation of liposomal formulations in the body, allowing for altered effects or target sites. These may include surface ligands, targeting moieties, biopolymers, etc., added to bind to a target type of cell, system, or tissue (de Lima et al., 2021; Khan et al., 2020; Turánek et al., 2019). Although these modifications may increase circulation time, they also come with their own drawbacks (Nag and Awasthi, 2013). For example, methoxy(polyethylene glycol)-grafted liposomes have been shown to exhibit immediate hypersensitivity reactions in a substantial percentage of human subjects (Moein Moghimi et al., 2006). Up to 45% of patients have been shown to experience hypersensitivity reactions via intravenous injection of liposomal drugs, including hemodynamic, respiratory, and cutaneous manifestations (Fülöp et al., 2019; Szebeni et al., 2007). Although the presence of these anti-cancer drugs in liposomal formulations has improved the targeting of the tumor, the off-target effects demonstrate the need for a targeting method that does not include surface modifications (de Oliveira Silva and de Barros, 2015). Moreover, surface modification adds an extra step in the manufacturing process, which can be time-consuming and complex, and may decrease the yield of liposomes. Thus, it is critical to determine how different liposome sizes can be used to target distinct phenotypes of cells and understand how efficient these size modifications are in targeting different phenotypes.

Herein, we examined how altering the size of DOPE:DOPC liposomes affects cell viability, cytotoxicity, and internalization by fibroblasts (NIH/3T3) and its phenotypes (transforming growth factor- β (TGF-β) activated NIH/3T3) (CAFs). Four different sizes of DOPE:DOPC liposomes (50, 100, 200, and 400 nm) were tested for their cell viability against

fibroblasts and CAFs. Subsequently, these different-sized liposomes were loaded with doxorubicin (DOX). The DOX-loaded liposomes were tested for their half-minimal inhibitory concentration (IC50) against fibroblasts and CAFs. Moreover, these liposomes were loaded with fluorescin (FC) to examine the effects on cell internalization each size would have on both fibroblasts and CAFs. Finally, various statistical analyses were performed on the results to analyze which size of liposomes is best used as a CAF-specific drug delivery agent. The results from this study establish a platform from which further studies, including surface-modified liposomes, can benefit and expand upon. For the rest of this article, we will use myofibroblasts to address the (TGF- β activated NIH/3T3 phenotype).

2.2 Methods

2.2.1 Materials

All materials were purchased through Sigma-Aldrich, St. Louis, MO, and were used as received unless otherwise stated. Fresh deionized (DI) water (Milli-Q, Thermo Scientific Nanopure, Waltham, MA) was used throughout this study.

2.2.2 Liposome Synthesis

All liposomes were synthesized using a previously established method (Rehman and Bratlie, 2022). In a 250 mL round-bottom flask, 1,2-dioleoyl-sn-glycero-3-phosphoethanolamine (DOPE, 100 mg/mL, Avanti Polar Lipids, Inc., Alabaster, AL) and 1,2-dioleoyl-sn-glycero-3-phosphocholine (DOPC, 250 mg/mL, Avanti Polar Lipids, Inc.) were dissolved in 12 mL of chloroform and rotary evaporated at 60 ºC for 5 minutes. These lipids were then mixed with 15 mL phosphate-buffered saline (PBS, diluted from 10X solution to 0.1 M, pH 7.4, Fisher Scientific, Pittsburgh, PA). The liposomes were dialyzed against deionized water overnight. The next day the liposomes were freeze-dried using a lyophilizer (Labconco, 4.5 L, Kansas City, MO) for 3 days. One large batch of liposomes was synthesized and used throughout this study.

2.2.3 Size and Zeta Potential Measurements

Dynamic light scattering (DLS) was used to measure the size and zeta potential values of the liposomes. The resulting liposomes from 2.2 were added to DI water to obtain a final concentration of 1 mg/mL. Zetasizer Nano Z (Malvern Instruments LTD., Malvern, UK) was used to obtain the size and zeta potential measurements for the prepared liposomal solutions.

2.2.4 Drug Loading

Doxorubicin (DOX) was used as a model drug. Dried liposomes, 5 mg isolated using methods found in 2.2, were suspended in 1 mL citric acid (150 nM, pH 4) and vortexed until a homogenous mixture was obtained. This solution was extruded 21 times using an Avanti Mini-Extruder. This process of extrusion was repeated four times, each for a new liposome with a different filter size: 0.05, 0.1, 0.2, and 0.4 μm. A heating block at 50 ºC was used during the extrusion with the 0.05 μm filter to induce passage. Once liposomes of each size were extruded, the solution pH was modified using NaOH or HCl until a pH of 7.4 was achieved. The liposomes were incubated at 65 ºC for 10 minutes. Doxorubicin (PBS, 10 mg/mL) was also incubated at 65 ºC for 10 minutes. Next, 100 μL DOX was added to the suspended liposomes and incubated at 65 ºC for 45 minutes. This mixture was centrifuged at 3000 rpm for 5 minutes, and the supernatant was used to calculate the encapsulation efficiency of DOX in the liposomes by measuring the absorbance at 490 nm with a reference at 630 nm using a plate reader (BioTek Synergy HT Multidetection Microplate Reader, BioTek, Winooski, VT). The encapsulation efficiency (EE) was calculated using Equation 1:

$$EE\ (\%) = \frac{C_{total} - C_{sup}}{C_{total}} * 100 \qquad (1)$$

where C_{total} is the concentration of doxorubicin added to the liposomes, and C_{sup} is the concentration of doxorubicin in the supernatant. Next, the loaded liposomes were tested on cells.

2.2.5 Cell Culture

Fibroblasts (NIH/3T3, ATCC, Manassas, VA) were used in this study, and myofibroblasts were performed by using transforming growth factor- β (TGF-β). Fibroblasts were cultured at 37 ºC with 5% CO2 in complete medium (CM), consisting of 10% bovine calf serum (BCS), 1% penicillin, and 1% streptomycin in Dulbecco's modified Eagle's medium (DMEM). Fibroblasts were passaged every three to four days and sub-cultured between 6.7 x 10^3 and 2.7 x 10^4 cells/cm^2. Fibroblasts were activated to myofibroblasts by adding 100 µL of 1 µg/mL TGF-β to a 10 mL stock solution of fibroblast before transferring the cells to the well plates. The final concentration of TGF-β in each well was 10 ng/mL.

2.2.6 Cell Viability

Cells were seeded into a 96 well plate in 100 µL of growth medium at a density of 5.0 x 10^4 cells/cm^2 for 24 h at 37 ºC in an incubator. After 24 h, the medium was replaced by 100 µL liposome solution (250 µg/mL) in fresh medium. These liposomes were not loaded with DOX, as this experiment aimed to measure the cell viability of DOPE: DOPC liposomes. Moreover, a positive control (PC) of cells without liposomes and a negative control (NC) without cells were added to the plate. The plates were incubated at 37 ºC for 48 h, and the cell viability was determined by a methyl thiazol tetrazolium (MTT) assay. The MTT assay was done by carefully removing the CM from each well and replacing it with 100 µL of 0.5 mg/mL MTT solution. The plates were again incubated at 37 ºC for 2 h. Finally, 85 µL of the solution was removed from each well, and 85 µL dimethyl sulfoxide (DMSO) was added to dissolve the insoluble purple formazan crystals. The plate was read at 540 nm with a reference of 690 nm with the plate reader.

2.2.7 Cellular Uptake of Liposomes

Liposomes were loaded with fluorescein to measure the internalization of the liposomes by the cells. Liposomes, 2 mg, were mixed with 1 mL fluorescein (FC, 1 mg/mL in acetone). The liposomes were extruded with four filters using the method described above. These liposomes were dried at 65 ºC for 4 hours and placed in the freezer overnight. The liposomes were then resuspended in 2 mL of PBS and passed through a Sephadex G-50 column (Fisher) to remove the unencapsulated FC.

Fibroblasts were seeded at a density of 5.0×10^4 cells/cm^2 in a black 96-well plate. Cells were either not activated or activated with the addition of 10 ng/mL TGF-β in each well. Cells without liposomes were used as PC, and wells with liposomes but without cells were NC. The plate was incubated for 24 hours at 37 ºC. Subsequently, the media was aspirated, and 200 µL of each of the four sizes of FC-loaded liposomes was added to the plate. These plates were either incubated at 37 ºC for 4 hours to measure the internalization or at 4 ºC for 4 hours for cold binding experiments.

The medium was then aspirated from each of the 96 wells in the plate, and 100 µL of 0.25% trypan blue (Corning, Manassas, VA) was added to each well and incubated for 1 min to quench extracellular fluorescence. After 1 min, the trypan blue was aspirated, and the fluorescence was measured using an excitation wavelength of 485 nm and an emission wavelength of 528 nm using the plate reader.

2.2.8 Half Maximal Inhibitory Concentration (IC_{50})

Fibroblasts were seeded at 5.0×10^4 cells/cm^2 in 96 well plates and were either not activated or activated using 10 ng/mL TGF-β in each well. An NC of only CM was included on the plate. A serial dilution of DOX loaded liposomes was added to the plate. No liposomes were added to the PC. In addition to the DOX loaded liposomes, a serial dilution of 50 µg/mL DOX

was used to calculate the IC50 value of free DOX. This concentration of free DOX (50 μg/mL) corresponds to the amount of DOX loaded in the liposomes. After incubation for 48 hours at 37 ºC, the media was aspirated, and 10 μL of a 5 mg/mL MTT solution and 100 μL CM was added to each well. The plate was incubated at 37 ºC for 2 hours, after which 85 μL MTT solution was replaced by DMSO (Fisher) to dissolve any formazan crystals. The optical density was measured at 540 nm and a reference of 690 nm. Data were normalized to cells cultured without liposomes, and eight replicates were obtained for each experiment. Origin ® software was used to generate a sigmoidal dose-response curve, y, which was used to calculate the IC_{50} values for each liposome, shown in Equation (2):

$$y = A_2 + \frac{A_1 - A_2}{1 + \left(\frac{x}{x_o}\right)^p} \qquad (2)$$

Where A_1 is the upper limit of the dose curve, A_2 is the lower limit, p is the steepness of the curve, and x is the IC_{50}.

2.2.9 Statistical and Data Analyses

All data are reported as mean ± standard deviation (SD). Statistical analysis was performed using JMP statistical software. The statistical significance of the mean comparison was determined by a two-way ANOVA. Pair-wise comparisons were analyzed with Tukey's honest significant difference test. Differences were considered statistically significant for $p < 0.05$.

2.3. Results

2.3.1 Physicochemical Characterization of Liposomes

Liposomes were formulated using a 2:1 DOPE to DOPC ratio using the thin film method and were extruded using 50, 100, 200, and 400 nm filters. The liposomes were characterized by their size and zeta potential. **Figure 2.1(a)** shows the size measurement of the synthesized liposomes, while **Figure 2.1(b)** demonstrates the zeta potential values of the liposomes. Each

size has a significantly different value compared to others, while only the 50 nm liposomes have a significantly lower zeta potential value of -15.2 ± 0.1 mV compared to all other sized liposomes. Liposomes of sizes 100, 200, and 400 nm resulted in the zeta potential values of -18.2 ± 0.7 mV, -20.6 ± 1.1 mV, and -19.8 ± 1.4 mV, respectively.

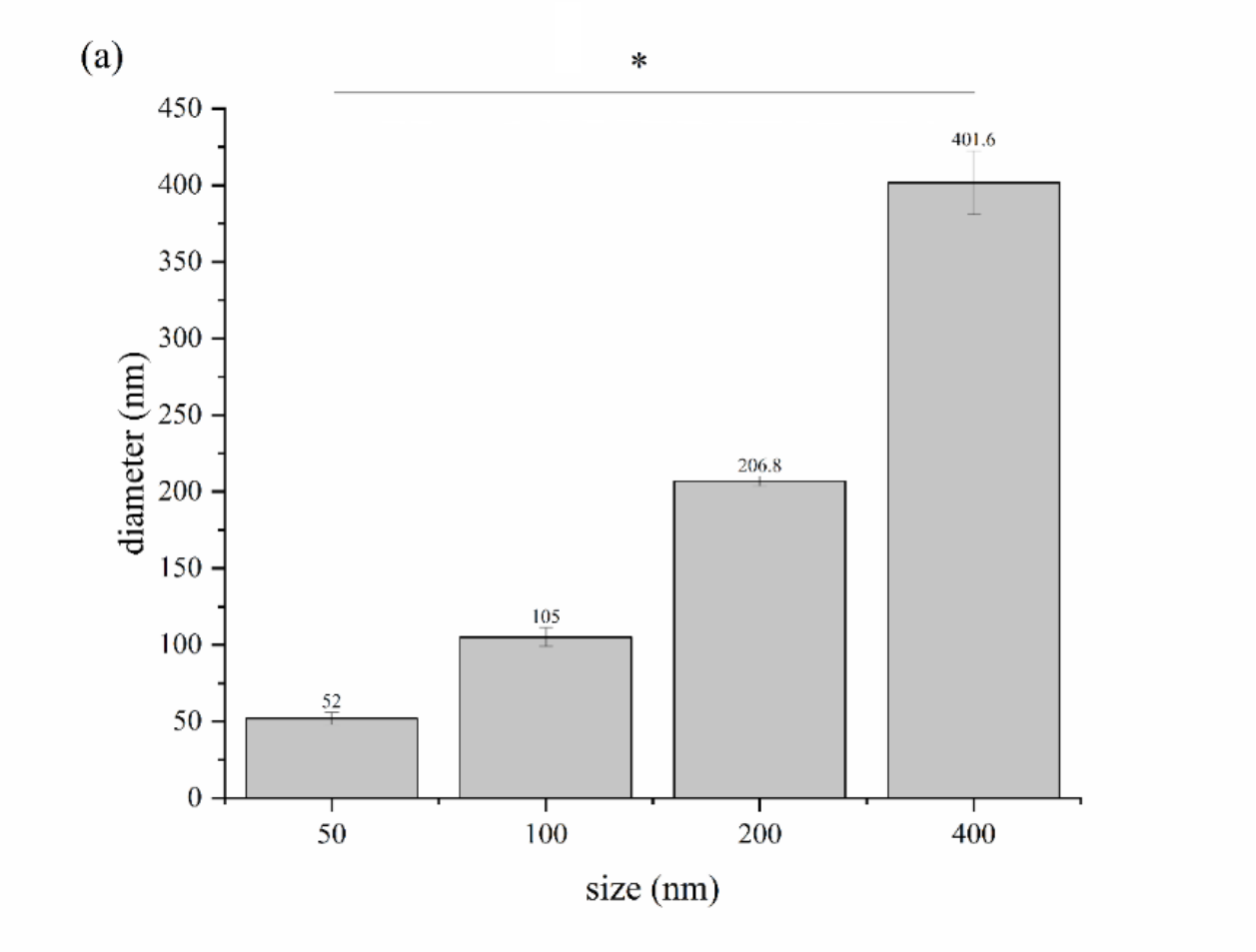

Figure 2.1*: Material characterization of liposomes.* ***(a)*** *DLS and* ***(b)*** *zeta potential measurements of liposomes. Both measurements represent three replicates for each sample. All data are shown by mean ± standard deviation. (*) indicates $p<0.05$ compared with the other sizes.*

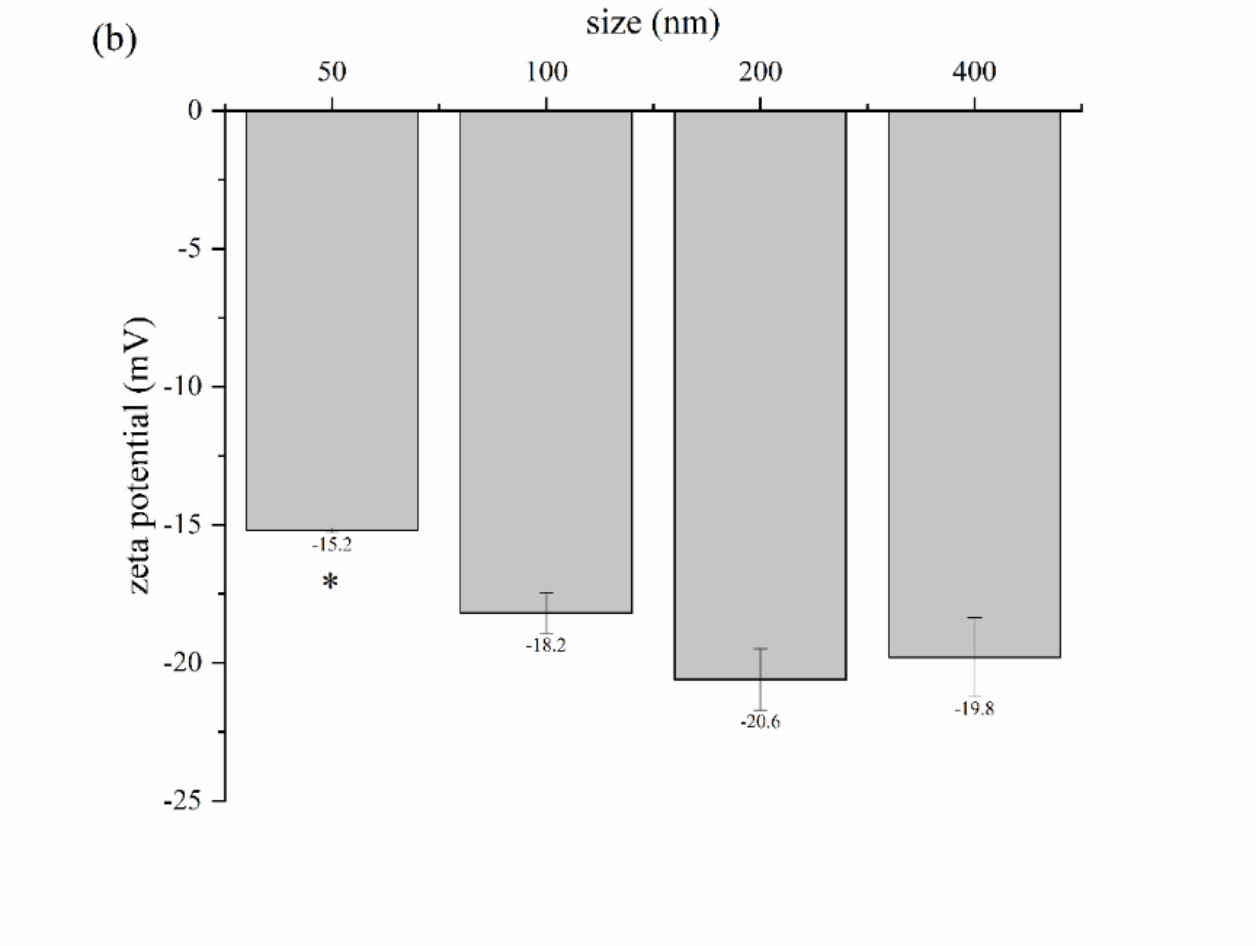

Figure 2.1 continued

2.3.2 Doxorubicin Encapsulation in Different-Sized Liposomes

DOX being an amphipathic drug, can easily be encapsulated in the aqueous cavity of the liposomes using a pH gradient. **Figure 2.2** shows the EE of DOX in the four different sizes of liposomes, which was 94 ± 2%, 93 ± 1%, 96 ± 3%, and 95 ± 2% for sizes 50, 100, 200, and 400 nm, respectively. There were no significant differences for any of the sizes.

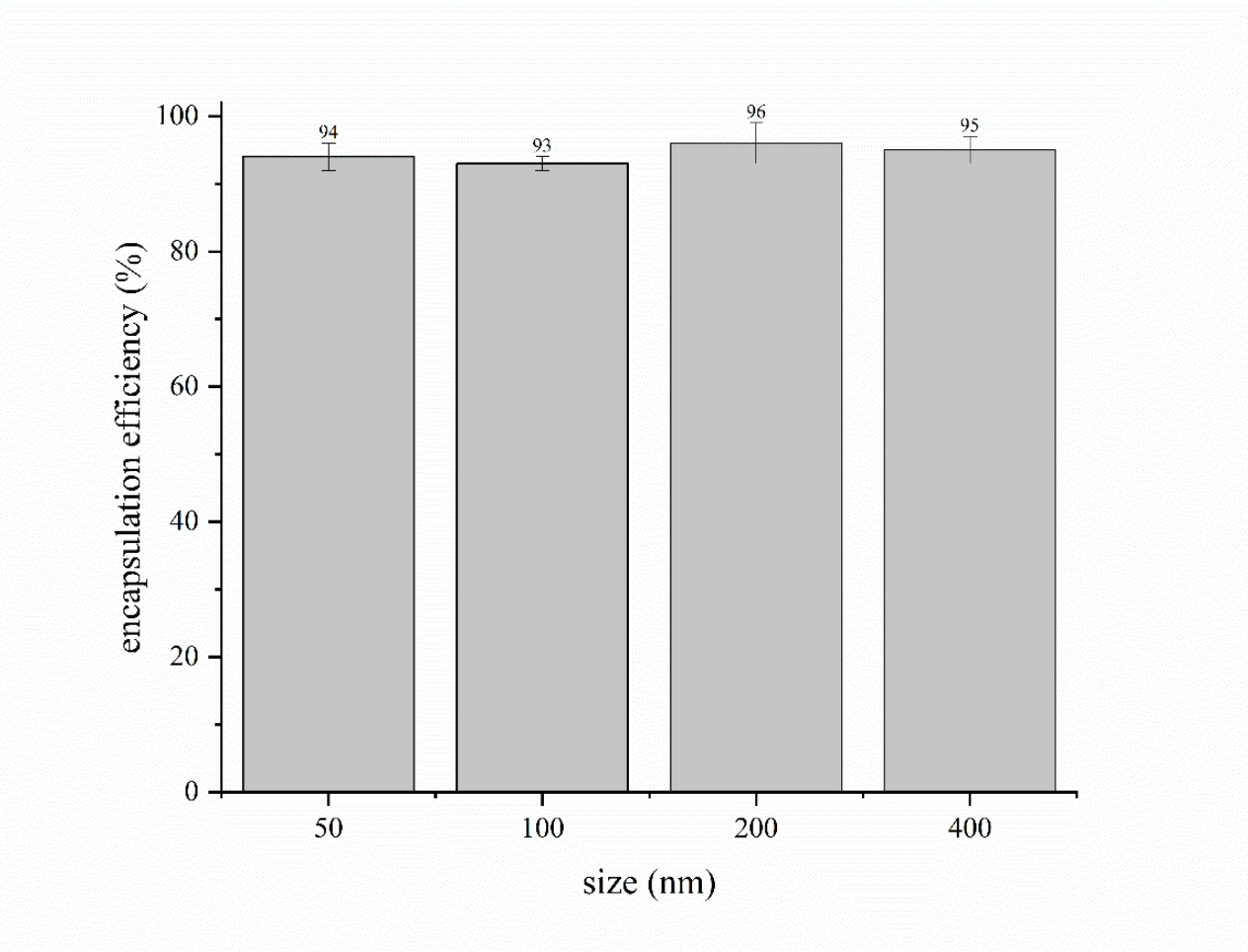

Figure 2.2*: Doxorubicin loading efficiency for each liposome size. Measurements represent three replicates for each sample; all data are shown by mean value ± standard deviation*

2.3.3 Cells are Viable With All Four Sizes of Liposomes

The cell viability of fibroblasts and myofibroblasts in the presence of all four sizes of liposomes were tested. As the purpose of this experiment was to observe whether the DOPE:DOPC liposomes alone are toxic to the cells or not, these liposomes were not loaded with DOX. After the cells were seeded in a 96 well plate for 24 h, 250 µg/mL liposome solution for each size was added to both fibroblasts and myofibroblasts. The cells with liposomes were incubated for another 48 h, after which a viability assay was performed; the plates were then read at 540 nm with a reference of 690 nm using a plate reader. The DOPE:DOPC liposomes resulted

in >94% viability for both fibroblasts and myofibroblasts, and no significant differences were observed, as seen in **Figure 2.3**. For fibroblasts, sizes 50, 100, 200, and 400 nm resulted in cell viability of 95.4 ± 6.7%, 97.4 ± 7%, 97.0 ± 4.7%, and 94.9 ± 5.4%, respectively. Similarly, for myofibroblasts, the cell viability was measured to be 99.2 ± 4%, 95.4 ± 2.5%, 97.5 ± 3.7%, and 98.9 ± 1.8% for sizes 50, 100, 200, and 400 nm, respectively.

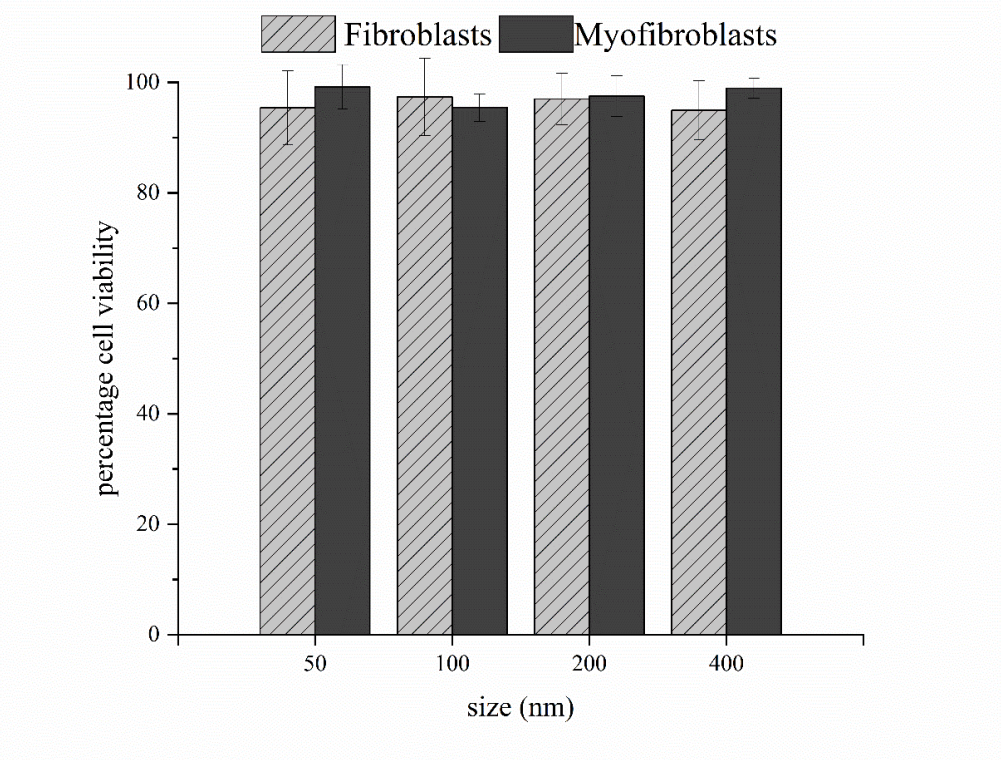

Figure 2.3*: Cell viability of fibroblasts and myofibroblasts incubated with four different sizes of liposomes. Measurements show eight replicates for each sample. All data represent mean value ± standard deviation*

2.3.4 Cellular Uptake of Fluorescent Loaded Luposomes by Fibroblasts and Myofibroblasts

Liposome internalization was measured through the uptake of FC-loaded liposomes by fibroblasts and myofibroblasts. Equal concentrations of all sizes of liposomes (0.25 mg/mL) were added to the cells. As shown in **Figure 2.4(a)**, the uptake of liposomes decreases with size for both myofibroblasts and fibroblasts at 37 ^{o}C. The cold binding, performed at 4 ^{o}C, showed

similar trends in **Figure 2.4(b)**. In general, a similar trend was observed where binding decreased as the size of the liposome increased. Only 200 nm liposomes showed a significantly lower internalization in fibroblasts compared to 50 nm liposomes. No other significant difference was seen.

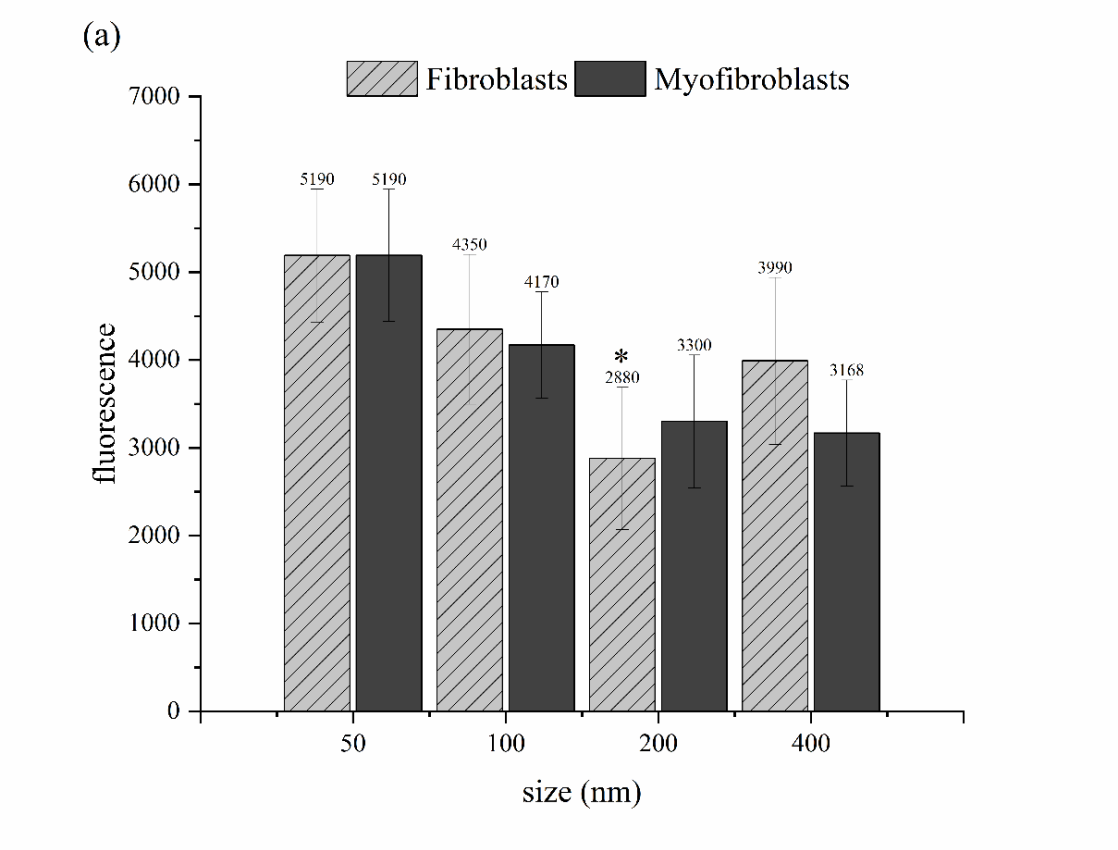

***Figure 2.4**: Fluorescent-loaded liposomes internalized fibroblasts and myofibroblasts at **(a)** 37 °C and **(b)** 4 °C. Data represent the mean value of eight replicates for each sample ± standard deviation. The fluorescence was normalized to the amount of FC added to each well. (*) indicates $p<0.05$ for values compared to 50 nm size.*

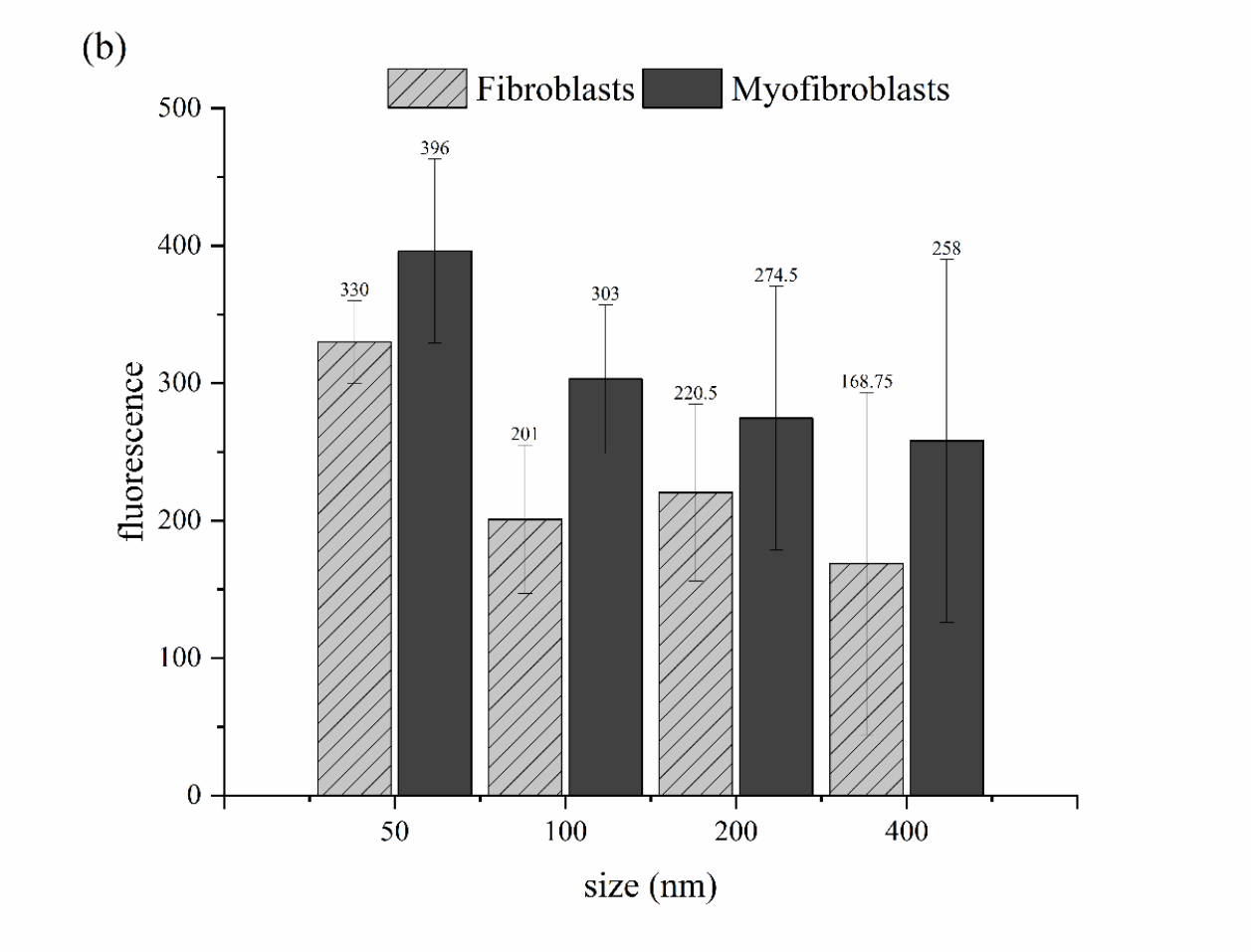

Figure 2.4 continued

For fibroblasts, at 37 ºC, liposomes of sizes 50, 100, 200, and 400 nm showed internalization values of 5190 ± 757, 4350 ± 853, 2880 ± 809, and 3990 ± 950 a.u., respectively. Similarly, for myofibroblasts, the internalization of liposomes of sizes 50, 100, 200, and 400 nm at 37 ºC resulted in the values of 5190 ± 752, 4170 ± 606, 3300 ± 756, and 3168 ± 603 a.u., respectively.

Less internalization of liposomes was observed for the cold binding experiments performed at 4 ºC. For fibroblasts, the liposomes of sizes 50, 100, 200, and 400 nm resulted in internalization values of 330 ± 30, 201 ± 54, 220 ± 65, and 169 ± 120, respectively. For

myofibroblasts, the liposomes of size 50 nm showed the highest internalization value for cold binding at 396 ± 68. For liposomes 100, 200, and 400, the cold binding experiments resulted in internalization values of 303 ± 54, 275 ± 96, and 258 ± 132, respectively.

2.3.5 The Effect of Liposome Size on Half Maximum Inhibitory Concentration (IC_{50})

To define the efficacy of the encapsulated drug, we measured the IC_{50} (half-maximum inhibitory concentration) of the DOX-loaded liposomes in the presence of fibroblasts and myofibroblasts. The IC_{50} value reflects the concentration of the drug at which half of the cells are dead, providing a potency of an antagonist drug. Higher IC50 values indicate lower toxicity. **Figure 2.5** shows the IC_{50} values for liposomes of different sizes incubated with fibroblasts and myofibroblasts.

As liposome size increases, the IC_{50} increases for both cell types (**Figure 2.5**). The exception to this trend was 400 nm liposomes incubated with fibroblasts, which resulted in an IC_{50} value of 1.83 ± 0.3 μM. For sizes 50, 100, and 200 nm, the IC_{50} values for fibroblasts were 1.13 ± 0.15, 1.58 ± 0.24, and 2.76 ± 0.34 μM, respectively. The 'DOX only IC_{50}' refers to the IC_{50} value of free DOX, which was added to the cells without the addition of liposomes and was calculated to be 0.83 ± 0.3 μM. The Dox only IC_{50} value is consistent with the previous literature (Chen et al., 2013; Rehman and Bratlie, 2022; Toffoli et al., 1989; Wang et al., 2017). The IC_{50} values for sizes 50, 100, 200, and 400 nm incubated with myofibroblasts were 2.34 ± 0.39, 3.87 ± 0.22, 4.48 ± 0.4, and 4.96 ± 0.12 μM, respectively. For free DOX, the IC_{50} was calculated to be 0.93 ± 0.57 μM for myofibroblasts, supported by the previously published data (Rehman and Bratlie, 2022). Thus, the least toxic DOX-loaded liposomes for myofibroblasts were 400 nm, and the most toxic was free DOX.

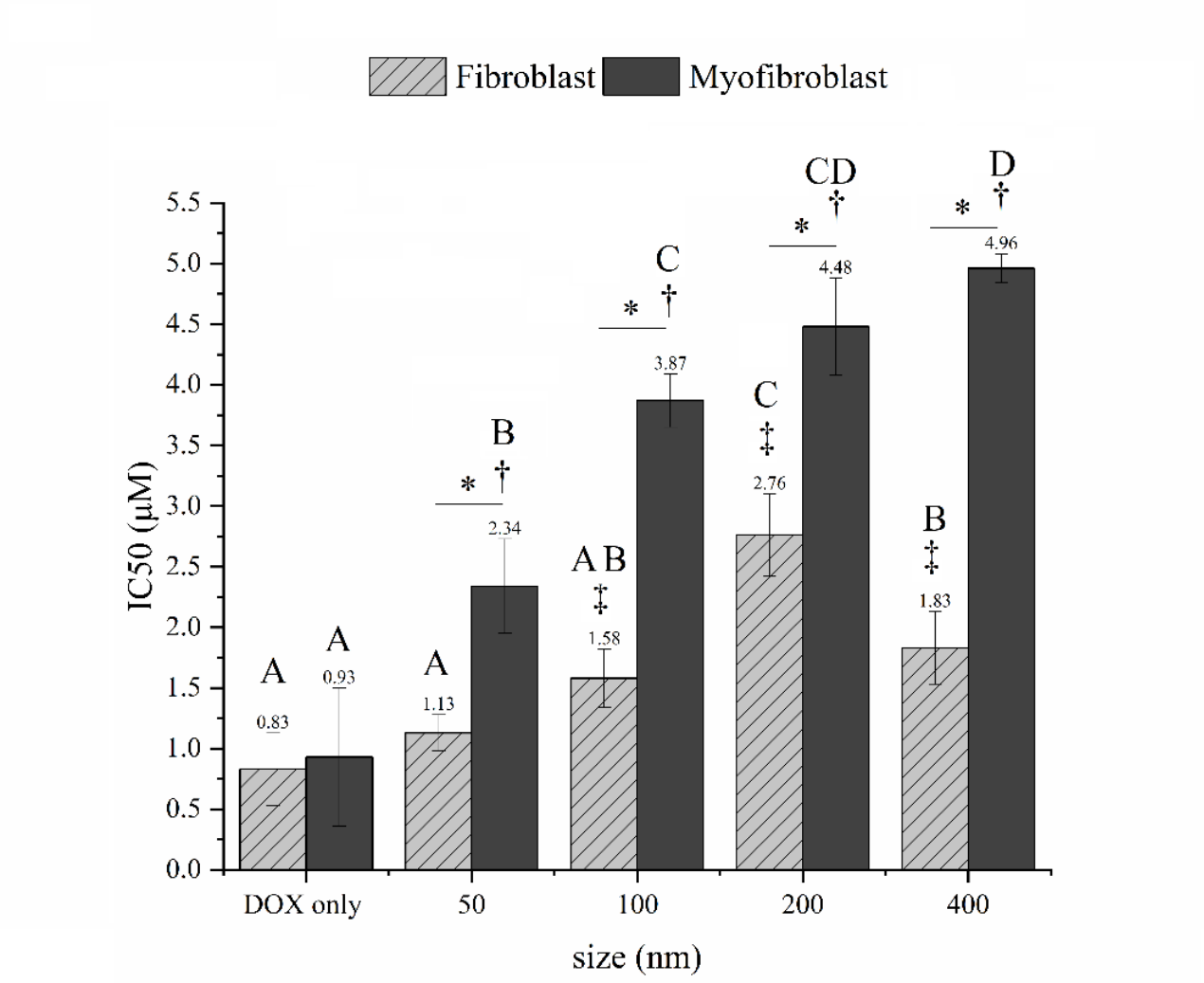

***Figure 2.5**: IC_{50} concentration for fibroblasts and myofibroblasts. Data represent the mean value of eight replicates for each sample ± standard deviation. (*) indicates $p<0.05$ for values of IC_{50} for fibroblasts compared with myofibroblasts of the same size. (‡)indicates $p<0.05$ for IC_{50} values for fibroblasts at different sizes compared with Dox only value. (†) indicates $p<0.05$ for IC_{50} values for myofibroblasts at different sizes compared with Dox only value. Bars with the same letters (A-D) are not statistically different ($p<0.05$) from data points of the same phenotype.*

Furthermore, the letters (A-D) on the bars in **Figure 3.5** represent a significant difference in the IC_{50} values for fibroblasts and myofibroblasts when each size was compared to other sizes within the same phenotype. Bars with the same letter show no significant difference. For fibroblasts, Only 200 nm liposomes showed a significantly higher IC_{50} value for fibroblasts compared to all other sizes. On the other hand, for myofibroblasts, size 50 nm liposomes resulted

in a significantly lower IC_{50} value compared to sizes 100, 200, and 400 nm. In comparison, size 400 nm liposomes showed a significantly higher IC_{50} value compared to size 50 and 100 nm, but not 200 nm.

2.4 Discussion

2.4.1 Surface Charge of Liposomes is Affected by the Liposome Size

Zeta potential can help to predict the fate of liposomes in vivo (Malvern Panalytical, 2019). Specifically, zeta potential can affect the pharmacokinetic behavior of the delivery system (Honary and Zahir, 2013). The attachment of liposomes to cell membranes is altered when physiochemical modification of liposomes takes place and is most affected by changes in the surface charge of the particles (Honary and Zahir, 2013). This has the potential to affect the internalization of the drug in the cells. Nanoparticles with a higher magnitude of surface charge bind more strongly to the cell membrane than those with a surface charge near 0 mV, and these more negative values result in a higher cellular uptake (Honary and Zahir, 2013).

As liposome size increases, the zeta potential becomes more negative. Prior work has suggested that as liposome size increases, cellular uptake increases (Lee et al., 2015; Sakai-Kato et al., 2019). However, there was a negative trend between liposome size and cellular uptake, which was not statistically significant. This negative linear trend is shown for both types of cells incubated at both 37 ^{o}C and 4 ^{o}C (**Figures 2.4 (a) and (b)**). The results, however, are not statistically significant. Nonetheless, it was seen that all sizes of liposomes were able to target and were internalized by both phenotypes of fibroblasts, which was the main goal of the study.

2.4.2 Increasing Liposome Size Decreases Liposome Toxicity

Fibroblasts compose the basic framework for tissues and organs responsible for maintaining the ECM (Dick et al., 2021). Microenvironments marked by the presence of a cancerous tumor can often lead to an undesirable transformation of fibroblasts into

myofibroblasts, known to promote tumor progression and metastasis (Rehman and Bratlie, 2022; Yazdani et al., 2017). Selective targeting of these tumor-promoting cells may be a useful method for treating cancer.

We have seen that toxicity and cellular uptake decrease as liposome size increases. These higher IC_{50} values (**Figure 2.5**) lead to lower efficacy of doxorubicin. Similarly, cellular uptake decreases as liposome size increases, though not statistically significant (**Figures 2.4 (a) and (b)**). This relationship indicates a more efficient method of targeting tumor-supporting cells using smaller liposomes. Utilization of DOX without encapsulation by liposomes leads to the death of both fibroblasts and myofibroblasts, shown by the lack of differentiation between the two in statistical analysis.

In summary, the results from this study provide us with evidence that DOX-loaded DOPE:DOPC liposomes can be used to target both phenotypes of fibroblasts (fibroblasts and myofibroblasts/CAFs). The size of the liposomes can be used to control the toxicity of liposomes. Furthermore, these results provide us with a foundation for future work that smaller liposomes (50 and 100 nm) are better candidates to use surface modifications for targeted drug delivery.

2.5 Conclusions

Herein, we investigated the cell viability, cytotoxicity, and cell internalization of DOPE:DOPC liposomes against fibroblasts and myofibroblasts (acting as CAFs in a tumor microenvironment). Four different sizes of liposomes (50, 100, 200, and 400 nm) were used to examine how the targetability towards different phenotypes changes with size. Both fibroblasts and myofibroblasts were viable when incubated with DOPE:DOPC liposomes before the encapsulation of DOX. Only size 50 nm liposomes showed a significantly lower zeta potential value compared to the other three sizes, which influences cell internalization. It was observed

that lower liposome sizes (50 and 100 nm) are more toxic to both phenotypes and can be further used in future studies. The findings of this study establish a strong foundation to use smaller liposomes for a higher dose of DOX delivery; the surface of these small liposomes can be modified to specifically target CAFs (myofibroblasts) while being more toxic towards CAFs compared to fibroblasts.

2.6 References

1. Allen, T.M., 2012. Liposomal Drug Formulations. Drugs 1998 56:5 56, 747–756.

2. Allen, T.M., Martin, F.J., 2004. Advantages of liposomal delivery systems for anthracyclines. Semin Oncol 31, 5–15.

3. Baum, J., Duffy, H.S., 2011. Fibroblasts and myofibroblasts: what are we talking about? J Cardiovasc Pharmacol 57, 376.

4. Bozzuto, G., Molinari, A., 2015. Liposomes as nanomedical devices. Int J Nanomedicine 10, 975.

5. Bulbake, U., Doppalapudi, S., Kommineni, N., Khan, W., 2017. Liposomal formulations in clinical use: an updated review. Pharmaceutics 9, 12.

6. Chen, X., Ding, G., Gao, Q., Sun, J., Zhang, Q., Du, L., Qiu, Z., Wang, C., Zheng, F., Sun, B., 2013. A human anti-c-Met Fab fragment conjugated with doxorubicin as targeted chemotherapy for hepatocellular carcinoma. PLoS One 8, e63093.

7. de Lima, P.H.C., Butera, A.P., Cabeça, L.F., Ribeiro-Viana, R.M., 2021. Liposome surface modification by phospholipid chemical reactions. Chem Phys Lipids 237, 105084.

8. de Oliveira Silva, J., de Barros, A.L.B., 2015. Toxicological Issues Faced after Liposomes Administration. Peertechz J Clin Pharmacol Clin Pharmacokinet 1 (1): 003 4.

9. Dick, M.K., Miao, J.H., Limaiem, F., 2021. Histology, fibroblast. In: StatPearls [Internet]. StatPearls Publishing.

10. Fang, C.-L., Wang, Y., Tsai, K.H.-Y., Chang, H.-I., 2018. Liposome-encapsulated baicalein suppressed lipogenesis and extracellular matrix formation in Hs68 human dermal fibroblasts. Front Pharmacol 9, 155.

11. Fülöp, T., Kozma, G.T., Vashegyi, I., Mészáros, T., Rosivall, L., Urbanics, R., Storm, G., Metselaar, J.M., Szebeni, J., 2019. Liposome-induced hypersensitivity reactions: Risk reduction by design of safe infusion protocols in pigs. Journal of controlled release 309, 333–338.

12. Gabizon, A.A., 1995. Liposome circulation time and tumor targeting: implications for cancer chemotherapy. Adv Drug Deliv Rev 16, 285–294.

13. Gabizon, Alberto, Papahadjopoulos, D., 1988. Liposome formulations with prolonged circulation time in blood and enhanced uptake by tumors (phospholipid vesicles/drug delivery systems/cancer therapy/glycolipids). Proc. Natl. Acad. Sci. USA 85, 6949–6953.

14. Gabizon, A., Papahadjopoulos, D., 1988. Liposome formulations with prolonged circulation time in blood and enhanced uptake by tumors. Proc Natl Acad Sci U S A 85, 6949.

15. Grant, G.J., Vermeulen, K., Zakowski, M.I., Stenner, M., Turndorf, H., Langerman, L., 1994. Prolonged analgesia and decreased toxicity with liposomal morphine in a mouse model. Anesth Analg 79, 706–709.

16. Gregoriadis, G., 2016. Liposomes in drug delivery: How it all happened.

17. Hinz, B., 2016. The role of myofibroblasts in wound healing. Curr Res Transl Med 64, 171–177.

18. Honary, S., Zahir, F., 2013. Effect of zeta potential on the properties of nano-drug delivery systems-a review (Part 1). Tropical Journal of Pharmaceutical Research 12, 255–264.

19. Huang, S., Lee, K.D., Hong, K., Friend, D.S., Papahadjopoulos, D., 1992. Microscopic localization of sterically stabilized liposomes in colon carcinoma-bearing mice. Cancer Res 52, 5135–5143.

20. Kendall, R.T., Feghali-Bostwick, C.A., 2014. Fibroblasts in fibrosis: novel roles and mediators. Front Pharmacol 5, 123.

21. Khan, A.A., Allemailem, K.S., Almatroodi, S.A., Almatroudi, A., Rahmani, A.H., 2020. Recent strategies towards the surface modification of liposomes: an innovative approach for different clinical applications. 3 Biotech 10, 1–15.

22. Kim, E.-M., Jeong, H.-J., 2021. Liposomes: Biomedical Applications. Chonnam Med J 57, 27.

23. Krauss, A.C., Gao, X., Li, L., Manning, M.L., Patel, P., Fu, W., Janoria, K.G., Gieser, G., Bateman, D.A., Przepiorka, D., 2019. FDA approval summary:(daunorubicin and cytarabine) liposome for injection for the treatment of adults with high-risk acute myeloid leukemia. Clinical Cancer Research 25, 2685–2690.

24. Lee, H.-M., Lee, E., Yeo, S.-Y., Shin, S., Park, H.-K., Nam, D.-H., Kim, S.-H., 2018. Drug repurposing screening identifies bortezomib and panobinostat as drugs targeting cancer associated fibroblasts (CAFs) by synergistic induction of apoptosis. Invest New Drugs 36, 545–560.

25. Lee, J.S., Hwang, S.Y., Lee, E.K., 2015. Imaging-based analysis of liposome internalization to macrophage cells: Effects of liposome size and surface modification with PEG moiety. Colloids Surf B Biointerfaces 136, 786–790.

26. Li, C., Li, Z., Gong, X., Liu, J., Zheng, T., Wang, F., Wu, J., Zhang, B., 2021. Acidic tumor microenvironment-sensitive liposomes enhance colorectal cancer therapy by acting on both tumor cells and cancer-associated fibroblasts. Nanoscale 13, 10509–10525.

27. Liu, D., Mori, A., Huang, L., 1992. Role of liposome size and RES blockade in controlling biodistribution and tumor uptake of GM1-containing liposomes. Biochimica et Biophysica Acta (BBA)-Biomembranes 1104, 95–101.

28. Liu, Liu, Liu, Lin, Yao, H.H., Zhu, Z.Q., Ning, Z.L., Huang, Q., 2016. Stromal myofibroblasts are associated with poor prognosis in solid cancers: a meta-analysis of published studies. PLoS One 11, e0159947.

29. Malvern Panalytical, 2019. Liposomes Characterization Including the Size and Zeta Potential Characterisation of Anionic and Cationic Liposomes Using the Zetasizer Nano.

30. Mayer, L.D., Tai, L.C.L., Ko, D.S.C., Masin, D., Ginsberg, R.S., Cullis, P.R., Bally, M.B., 1989. Influence of vesicle size, lipid composition, and drug-to-lipid ratio on the biological activity of liposomal doxorubicin in mice. Cancer Res 49, 5922–5930.

31. Moein Moghimi, S., Hamad, I., Andresen, T.L., Jørgensen, K., Szebeni, J., Moein Moghimi, S., Hamad, I., Andresen, T.L., Jørgensen, K., Szebeni, J., 2006. Methylation of the phosphate oxygen moiety of phospholipid-methoxy (polyethylene glycol) conjugate prevents PEGylated liposome-mediated complement activation and anaphylatoxin production. The FASEB journal 20, 2591–2593.

32. Nagayasu, A., Uchiyama, K., Kiwada, H., 1999. The size of liposomes: a factor which affects their targeting efficiency to tumors and therapeutic activity of liposomal antitumor drugs. Adv Drug Deliv Rev 40, 75–87.

33. Nag, O.K., Awasthi, V., 2013. Surface engineering of liposomes for stealth behavior. Pharmaceutics 5, 542–569.

34. Neuberger, K., Boddupalli, A., Bratlie, K.M., 2018. Effects of arginine-based surface modifications of liposomes for drug delivery in Caco-2 colon carcinoma cells. Biochem Eng J 139, 8–14.

35. Oku, N., Tokudome, Y., Tsukada, H., Okada, S., 1995. Real-time analysis of liposomal trafficking in tumor-bearing mice by use of positron emission tomography. Biochimica et Biophysica Acta (BBA)-Biomembranes 1238, 86–90.

36. Papahadjopoulos, D., Allen, T.M., Gabizon, A., Mayhew, E., Matthay, K., Huang, S.K., Lee, K.D., Woodle, M.C., Lasic, D.D., Redemann, C., 1991. Sterically stabilized liposomes: improvements in pharmacokinetics and antitumor therapeutic efficacy. Proceedings of the National Academy of Sciences 88, 11460–11464.

37. Rehman, T.U., Bratlie, K.M., 2022. Improving selective targeting to cancer-associated fibroblasts by modifying liposomes with arginine based materials. J Drug Target 30, 94–107.

38. Safra, T., 2003. Cardiac safety of liposomal anthracyclines. Oncologist 8, 17–24.

39. Sahai, E., Astsaturov, I., Cukierman, E., DeNardo, D.G., Egeblad, M., Evans, R.M., Fearon, D., Greten, F.R., Hingorani, S.R., Hunter, T., 2020. A framework for advancing our understanding of cancer-associated fibroblasts. Nat Rev Cancer 1–13.

40. Sakai-Kato, K., Yoshida, K., Izutsu, K., 2019. Effect of surface charge on the size-dependent cellular internalization of liposomes. Chem Phys Lipids 224, 104726.

41. Sercombe, L., Veerati, T., Moheimani, F., Wu, S.Y., Sood, A.K., Hua, S., 2015a. Advances and challenges of liposome assisted drug delivery. Front Pharmacol 6, 286.

42. Sercombe, L., Veerati, T., Moheimani, F., Wu, S.Y., Sood, A.K., Hua, S., 2015b. Advances and challenges of liposome assisted drug delivery. Front Pharmacol 6, 286.

43. Storm, G., Belliot, S.O., Daemen, T., Lasic, D.D., 1995. Surface modification of nanoparticles to oppose uptake by the mononuclear phagocyte system. Adv Drug Deliv Rev 17, 31–48.

44. Szebeni, J., Alving, C.R., Rosivall, L., Bünger, R., Baranyi, L., Bedöcs, P., Tóth, M., Barenholz, Y., 2007. Animal models of complement-mediated hypersensitivity reactions to liposomes and other lipid-based nanoparticles. J Liposome Res 17, 107–117.

45. Toffoli, G., Viel, A., Tumiotto, L., Buttazzi, P., Biscontin, G., Boiocchi, M., 1989. Sensitivity pattern of normal and Ha-ras transformed NIH3T3 fibroblasts to antineoplastic drugs. Tumori Journal 75, 423–428.

46. Turánek, J., Mašek, J., Raška, M., Ledvina, M., Paulovičová, E., Hubatka, F., Kotouček, J., 2019. Modification of liposomal surface by polysaccharides: Preparation, characterization, and application for drug targeting. In: Functional Polysaccharides for Biomedical Applications. Elsevier, pp. 433–467.

47. Uchiyama, K., Nagayasu, A., Yamagiwa, Y., Nishida, T., Harashima, H., Kiwada, H., 1995. Effects of the size and fluidity of liposomes on their accumulation in tumors: A presumption of their interaction with tumors. Int J Pharm 121, 195–203.

48. Wang, Y., Cui, Y., Zhao, Y., He, B., Shi, X., Di, D., Zhang, Q., Wang, S., 2017. Fluorescent carbon dot-gated multifunctional mesoporous silica nanocarriers for redox/enzyme dual-responsive targeted and controlled drug delivery and real-time bioimaging. European Journal of Pharmaceutics and Biopharmaceutics 117, 105–115.

49. Wasan, K.M., Morton, R.E., Rosenblum, M.G., Lopez-Berestein, G., 1994. Decreased Toxicity of Liposomal Amphotericin B Due to Association of Amphotericin B with High-Density Lipoproteins. J Pharm Sci 83, 1006–1010.

50. Yazdani, S., Bansal, R., Prakash, J., 2017. Drug targeting to myofibroblasts: Implications for fibrosis and cancer. Adv Drug Deliv Rev 121, 101–116.

51. Zylberberg, C., Matosevic, S., 2016. Pharmaceutical liposomal drug delivery: a review of new delivery systems and a look at the regulatory landscape. Drug Deliv 23, 3319–3329.

CHAPTER 3. IMPROVING SELECTIVE TARGETING TO CANCER-ASSOCIATED FIBROBLASTS BY MODIFYING LIPOSOMES WITH ARGININE BASED MATERIALS

Tanzeel Ur Rehman [1], Kaitlin M. Bratlie [1,2]

1. Department of Materials Science & Engineering, Iowa State University, Ames, Iowa 50011

2. Department of Chemical & Biological Engineering, Iowa State University, Ames, Iowa, 50011

Modified from a manuscript to be published in the *Journal of Drug Targeting*

Abstract

A library of arginine-like surface modifiers was tested to improve the targetability of DOPE:DOPC liposomes towards myofibroblasts in a tumour microenvironment. Liposomes were characterised using zeta potential and dynamic light scattering. Cell viability remained unchanged for all liposomes. Liposomes were encapsulated using doxorubicin (DOX) with an encapsulation efficiency >94%. The toxicity of DOX-loaded liposomes was calculated via half-maximal inhibitory concentration (IC50) for fibroblasts and myofibroblasts. These liposomes resulted in significantly lower IC_{50} values for myofibroblasts compared to fibroblasts, making them more toxic towards the myofibroblasts. Furthermore, a significant increase in cell internalization was observed for myofibroblasts compared to fibroblasts, using fluorescein-loaded liposomes. Most importantly, a novel regression model was constructed to predict the IC_{50} values for different modifications using their physicochemical properties. Fourteen modifications (A–N) were used to train and validate this model; subsequently, this regression model predicted IC_{50} values for three new modifications (O, P, and Q) for both fibroblasts and myofibroblasts. Predicted and measured IC_{50} values showed no significant difference for

fibroblasts. For myofibroblasts, modification O showed no significant difference. This study demonstrates that the tested surface modifications can improve targeting to myofibroblasts in the presence of fibroblasts and hence are suitable drug delivery vehicles for myofibroblasts in a tumour microenvironment.

3.1 Introduction

Arginine is commonly found in cell-penetrating peptides (CPPs) and can transport small molecules, nucleic acid, proteins, and nanoparticles into cells[82–84]. These CPPs can assist in increased cell internalization of the particles through micropinocytosis and non-endocytic pathways, among other phenomena[85–88]. It has also been demonstrated that peptides that contain L- or D-arginine more efficiently enter a cell compared to the peptides containing ornithine, histidine, or lysine. This implies that only the charge on the peptide is not sufficient to promote cell internalization[89,90]. Furthermore, studies have shown that arginine derivatives, when used in liposomal formation, results in lower cytotoxicity, higher transfection, and higher stability of the particles[91–93]. Although arginine and its derivatives have shown promise as CPPs, a clear set of rules relating materials design to biological function is not yet available.

Doxil ® was the first liposomal formulation that the FDA approved in 1995, which uses doxorubicin (DOX) for chemotherapeutic treatment of various cancers[19,94,95]. The major side effect caused by doxorubicin is cardiomyopathy; however, this can be significantly reduced using liposomal DOX while maintaining drug efficacy[96,97]. Numerous other formulation of liposomes have been approved by the FDA. Furthermore, liposomes can be easily modified using different surface modifiers[98–100]. 1,2-dioleoyl-*sn*-glycero-3-phosphocholine (DOPC) and 1,2-dioleoyl-*sn*-glycero-3-phosphoethanolamine (DOPE) are two FDA approved, commonly used phospholipids for liposomal-based carriers[101,102]. DOPE features a primary amine group present on its hydrophilic head, which allows modification through carbodiimide chemistry.

Recently, we modified DOPE: DOPC liposomes to enhance their selective targeting ability toward macrophage subpopulations and Caco-2 human colorectal adenocarcinoma cells using a library of arginine derivatives[97,102,103]. Macrophages play a vital role in pro-inflammatory and wound healing processes[104–109]. Fibroblasts are also critical in wound healing as they synthesize extracellular matrix (ECM), including collagen. Moreover, fibroblasts support the wound healing process by differentiation a myofibroblast phenotype, which can occur due to transforming growth factor- β, among other inflammatory mediators.

Although myofibroblasts promote wound healing and wound closure, however, in the presence of cancer, myofibroblasts can act as cancer-associated fibroblasts (CAFs) and enhance tumor progression and metastasis[110]. Cancer growth imitates the basic wound healing process, sharing various similarities, for example, recruitment of immune cells and deposition and crosslinking of fibronectin and fibrin[111]. Where a wound is restricted to a specific area and follows the typical wound healing steps, cancer cells manipulate the wound-healing process. They can migrate to, expand, and invade adjacent tissues. Here, CAFs aid the tumor in paving its way to neighboring areas through angiogenesis, secreting various growth factors, cytokines, and ECM development[112].

Various studies have shown that CAFs can develop resistance to chemo- and radiotherapy drugs mediated by CAF-secreted soluble factors, promoting cancer stemness, and modulating metabolism[58]. Sun et al. reported that CAFs produce wingless-type mouse mammary tumor virus integration site family member 16B (WNT16B), which decrease the cytotoxicity of chemotherapy and enhance tumor progression in prostate cancer[113]. Another report demonstrated that WNT16B was regulated by nuclear factor kappa light chain enhancer of activated B cells (NF-κB) by a post-DNA damage mechanism, which may be caused by radiotherapy and tumor

necrosis factor-α (TNF- α). Subsequently, this process triggers the canonical Wnt pathway as a paracrine signal, resulting in drug resistance, consequently preventing apoptosis; thus, increasing proliferation, migration, and invasion of the cancer cells[114]. A study regarding pancreatic cancer by Zhang et al. showed that through an NF-κB-dependent manner, CAFs defended the cancer cells from gemcitabine-induced apoptosis[115]. Furthermore, a more recent study demonstrated that CAFs induce interleukin-8 (IL-8) expression. Increased levels of phosphoinositide 3-kinase (P13K), phosphorylated p65 (p-p65), phosphorylated Iκb (p-Iκb), P-glycoprotein 1 (ABCB1), and phosphorylated AKT (p-AKT) were shown when CAFs were cultured in gastric cancer cells conditioned medium. All of these expressions were present along with NF-κB activation, leading to increased cisplatin resistance in cancer cells[116]. CAFs also secrete IL-17A which increased the chemotherapeutic resistance of colorectal cancer-initiating cells when subjected to chemotherapy[117]. As a significant component of tumor microenvironment, CAFs regularly exchange or share metabolites with neighboring cancer cells. This exchange may trigger a series of signaling pathway resulting in drug resistance. Given the pro-tumorigenic role of CAFs, it is critical to eliminate CAFs from the tumor microenvironment after chemotherapy to prevent cancer recurrence[118–121]. Currently, there is no robust mechanism to specifically target CAFs present in the tumor environment, where there is also a presence of fibroblasts. Therefore, there is an urgent need to synthesize a drug delivery vehicle that can differentiate between CAFs and fibroblasts and actively target CAFs, while being more toxic towards CAFs compared to regular fibroblasts.

In this study, we used 17 different arginine derivatives to modify the surface of the DOPE: DOPC liposomes. Our goal was to study the effects of these surface modifications on liposomal properties, toxicity, and cell internalization. We examined the toxicity and cell

internalization using both fibroblasts (NIH/3T3) and activated myofibroblasts phenotype (TGF-β activated NIH/3T3) [117–119]. The surface charge and size of the modified liposomes were characterized as well. Half maximal inhibitory concentration (IC_{50}) is a measure of the toxicity of a drug; the liposomes were loaded with DOX, and the IC_{50} values of the encapsulated DOX in the modified and unmodified (UM) liposomes were compared to the IC_{50} values of free DOX in fibroblasts and myofibroblasts. Finally, cell internalization of the modified liposomes was compared to the UM liposomes to show that surface modifications using arginine derivatives can increase the drug's targetability and cell internalization to myofibroblasts in contrast to fibroblasts. For the rest of this article, we will use 'fibroblasts' to address the NIH/3T3 cells and myofibroblasts for TGF-β activated NIH/3T3 cells.

3.2 Methods

3.2.1 Materials

All materials were purchased through Sigma-Aldrich, St. Louis, MO, and were used as received unless otherwise stated. Fresh deionized (DI) water (Milli-Q, Thermo Scientific Nanopure, Waltham, MA) was used throughout this study.

3.2.2 Liposome Synthesis

The liposomes were synthesized using the thin-film hydration method (23). Briefly, in a 250 mL round bottom flask, 117.5 µM 1, 2-dioleoyl-sn-glycero-3-phosphoethanolamine (DOPE, Avanti Polar Lipids, Inc., Alabaster, AL) and 58.8 µM 1, 2-dioleoyl-sn-glycero-3-phosphocholine (DOPC, Avanti Polar Lipids, Inc.) were dissolved in 15 mL chloroform. Subsequently, the solution was evaporated at 40 ^{o}C for five minutes using a rotary evaporator. Once the solvent was evaporated, a thin layer of lipids was observed at the bottom of the flask. This film was rehydrated using 15 mL phosphate-buffered saline (PBS, diluted from 10X solution to 0.1 M, pH 7.4, Fisher Scientific, Pittsburgh, PA). The flask was shaken thoroughly

and placed in a sonication bath for 15 minutes to complete the film's hydration. The solution turned milky white as the film hydrated. The solution was then dialyzed against DI water overnight. Afterward, the liposomes were lyophilized and kept at -20 ^{o}C for further use.

3.2.3 Liposome Modification

Seventeen different molecules were used as surface modifiers for the liposomes: (A) 2-amino-3-guanidinopropionic acid, (B) 3-guanidinopropionic acid, (C) nitroarginine, (D) creatine (Fisher Scientific), (E) carnitine, (F) citrulline, (G) 5-hydroxylysine, (H) acetylglutamine, (I) N-carbamyl-α-aminoisobutyric acid, (J) acetylcarnitine, (K) 2,4-diaminobutyric acid, (L) acetylornithine, (M) albizziin, (N) arginine, (O) lysine, (P) ornithine, and (Q) 3-ureidopropionic acid (**Figure 3.1**). Unmodified liposomes (UM) were prepared without any modifications as a positive control. For each modification, 10 mg lyophilized liposomes along with 2 mL of PBS and 2 mg surface modifier were resuspended in PBS at 5 w/v%, followed by the addition of 20 mg N-(3-dimethylaminopropyl)-N'-ethylcarbodiimide hydrochloride (EDC). The mixture was stirred overnight, and the modified liposomes were dialyzed against DI water overnight and lyophilized.

3.2.4 Drug Loading

Doxorubicin (DOX) was encapsulated in the liposomes and used as a model drug for this study. To load the liposomes with DOX, 10 mg of modified or UM liposomes were dissolved in 2 mL citric acid (150 mM, pH 4.0). The solution was extruded 21 times using an Avanti Mini-Extruder with a filter size of 100 µm. Subsequently, the pH of the solution was adjusted to 7.4 using HCl and NaOH. Both the DOX solution (PBS, 10 mg mL-1) and the extruded liposome solution were incubated individually at 65 ^{o}C for 10 minutes to equilibrate the temperature of the solutions. DOX solution (200 µL) was then added to the liposome solution, and it was incubated at 65 ^{o}C for an additional 45 minutes. The DOX-loaded liposomes were then centrifuged at 3000 rpm for five minutes, and the supernatant was carefully removed.

To a 96 well plate, 50 µL supernatant and 50 µL PBS were added to each well. A standard curve was made through serial dilutions of 1 mg mL^{-1} DOX solution. The absorbance of the plate was read using a BioTek Synergy HT Multidetection Microplate Reader (BioTek, Winooski, VT) plate reader at 490 nm with a reference at 630 nm. The loading efficiency of the DOX loaded liposomes was calculated by

$$Encapsulation\ efficiency\ (\%) = \frac{(C_{total} - C_{supernatant})}{C_{total}} X\ 100\% \qquad (1)$$

where C_{total} is the concentration of DOX added to the liposomes and $C_{supernatant}$ is the concentration of DOX in the supernatant.

3.2.5 Zeta Potential and Dynamic Light Scattering

The zeta potential of the modified and UM liposomes was performed to measure the surface charge on the liposomes. To 5 mL H_2O, a 100 µL 1% w/v of liposomes in DI water was added and extruded through 100 nm polycarbonate membranes using an Avanti Mini-Extruder (Avanti Polar Lipids, Inc.). The pH of the DI water was adjusted to 7.4 using HCl or NaOH to minimize the interaction of the ions in water with the liposomes during the test. These liposomal solutions were used to measure the zeta potential and size of the liposomes using a Zetasizer Nano Z (Malvern Instruments Ltd, Malvern, UK). Liposomes with modifications O, P, and Q were analyzed for their zeta potential and size. The data for modifications A-N was taken from our previous study [103].

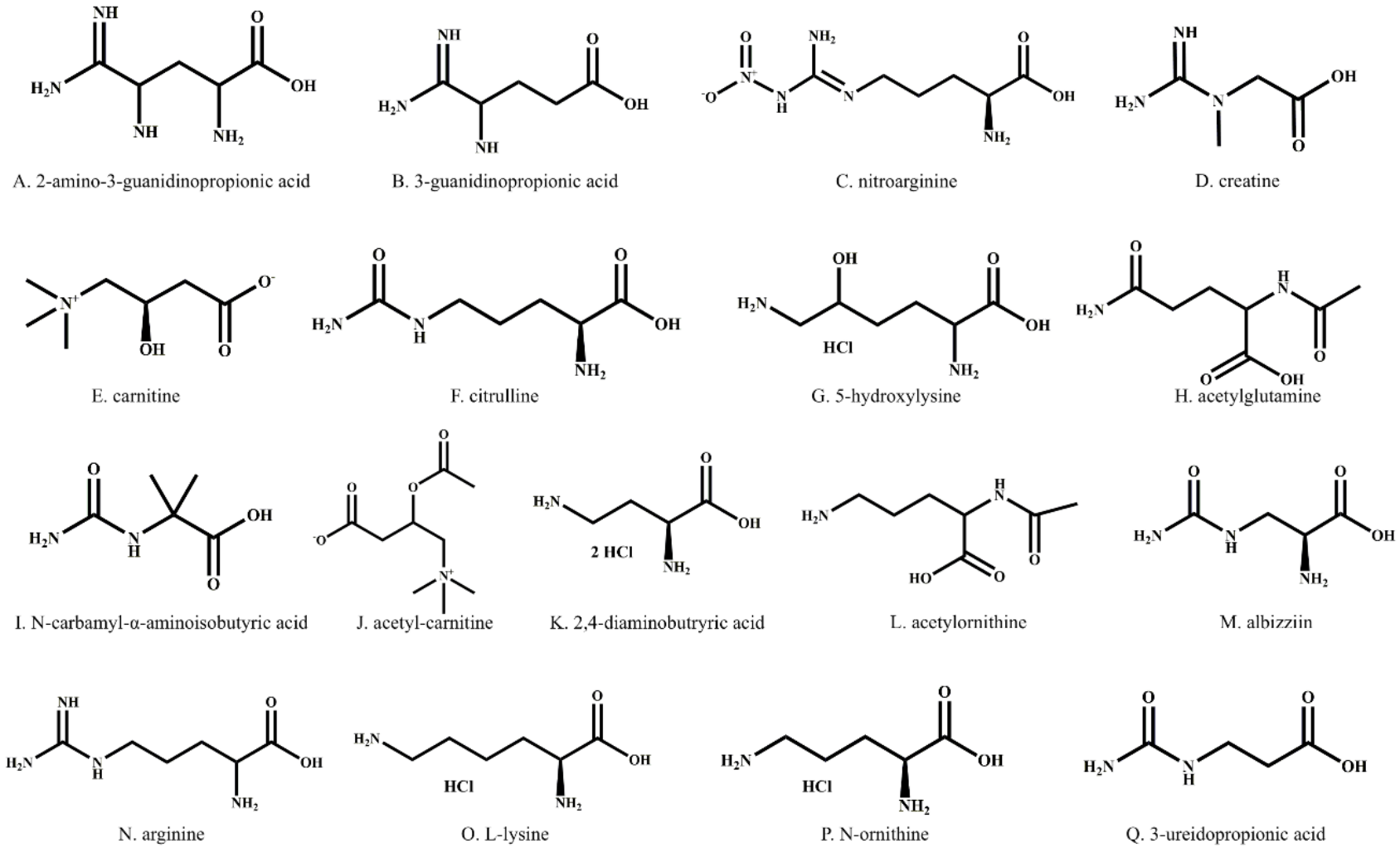

Figure 3.1. Chemical structures of arginine-like molecules used for the modification of liposome surfaces. The different molecules showed here are lettered for easier identification in experiments and discussion throughout the article.

3.2.6 Cell Viability

Fibroblasts (NIH/3T3, ATCC, Manassas, VA) were cultured at 37 ^{o}C with 5% CO_2 with complete medium (CM), consisting of Dulbecco's modified Eagle's medium (DMEM) supplemented with 10% fetal bovine serum (FBS), 1% penicillin, and 1% streptomycin. The cells were passaged every three to four days and sub-cultured between 6.7 x 10^3 and 2.7 x 10^4 cells per cm^2. Differentiation of fibroblasts to myofibroblasts was performed by adding 10 ng mL^{-1} TGF-β to the NIH/3T3 stock solution prior to transferring the cells to the well plates.

3.2.7 Cell Viability

Fibroblasts and myofibroblasts were seeded in a 96-well plate at a density of 5.0 x 10^4 cells cm^{-2} and allowed to grow for 24 h. Subsequently, the media was carefully aspirated, followed by the addition of 100 µL blank liposome solution (500 µg mL^{-1}). The liposomes used to investigate the cell viability were not loaded with DOX, as the purpose was to observe the stand alone cell viability of DOPE:DOPC liposomes. Cells without liposomes served as a positive control (PC), while liposomes in the absence of the cells served as a negative control (NC). All plates were incubated at 37 ^{o}C for 48 h. The cell viability was determined by a methyl thiazol tetrazolium (MTT) assay; CM from each well was carefully replaced with a 100 µL solution of MTT (0.5 mg mL^{-1}), and the plate was incubated at 37 ^{o}C for 2 h. The MTT forms purple insoluble formazan crystals after metabolism in living cells. Subsequently, 85 µL was aspirated from each well, and 100 µL DMSO was added to dissolve the insoluble formazan crystals. The plate was then read at 540 nm and a reference of 690 nm with the plate reader.

3.2.8 Fluoroscent Particles and Cellular Uptake

Cellular uptake of liposomes was measured using fluorescently-loaded liposomes. To encapsulate fluorescein in the liposomes, 10 mg liposomes were mixed with 1 mL fluorescein (FC, 1 mg mL^{-1} in acetone). Subsequently, the liposomes were dried at 55 ^{o}C, and the particles

were resuspended in 1 mL PBS. Afterward, to remove the unencapsulated FC, this liposomal suspension was passed through a Sephadex G-50 column (Fisher Scientific). Fibroblasts and myofibroblasts, at a density of 5.0 x 10^4 cell cm^{-2} in CM, were seeded in a black 96 well plate and incubated for 24 h at 37 ^oC. A negative control without any cells was also present. After the 24 h incubation time, the CM was carefully aspirated and replaced with 200 µL FC loaded liposomes resuspended in CM. The cells were placed at 37 ^oC to measure the internalization of the liposomes, and at 4 ^oC for cold binding experiments.

To observe the internalization of the liposomes, the prepared 96 well plates with fibroblasts and myofibroblasts were incubated at 37 ^oC for 4 h. Subsequently, the media was replaced by 100 µL of 0.25% trypan blue (Corning, Manassas, VA). The addition of trypan blue quenches the extracellular fluorescence. After 1 min, trypan blue solution was replaced with PBS. The level of fluorescence inside the cells, which represents the internalization of liposomes, was then measured at an excitation of 485 nm and emission of 528 nm. The same process was repeated for the cold binding experiments, where the cells were incubated with liposomes at 4 ^oC for 4 h. Eight replicates were obtained for each of the 17 liposomes. Unmodified liposomes were also loaded with FC and tested. The fluorescence was normalized to the amount of FC added to each well.

3.2.9 Half Maximal Inhibitory Concentration (IC_{50})

Fibroblasts and myofibroblasts were seeded at a density of 5.0 x 10^4 cells cm^{-2} onto a 96 well plate for 24 h in CM at 37 ^oC. An NC containing only CM was also included on the plate. A serial dilution of DOX loaded modified or unmodified liposomes was added to the cells. No liposomes were added to the PC. The IC_{50} value of free DOX was also calculated by adding DOX (50 µg mL^{-1}) to the cells and serially diluting the DOX through the plate. The liposomes were incubated with the cells for 48 h at 37 ^oC. Subsequently, an MTT assay was done as

described above. Eight replicates were obtained for each experiment, and the data were normalized to the cells cultured without the liposomes. A sigmoidal dose-response curve was then used to calculate the IC_{50} values for each liposome, shown in Eqn. (2):

$$y = A_2 + \frac{A_1 - A_2}{1 + \left(\frac{x}{x_o}\right)^p} \qquad (2)$$

where A_1 is the upper limit of the dose curve, A_2 is the lower limit, p is the steepness of the curve, and x_o is the IC_{50}.

3.2.10 Statistical and Data Analyses

JMP® statistical software was used to perform various statistical analyses. Data are expressed as the means ± standard deviation (SD). A two-way ANOVA test determined the statistical significance of the mean comparisons. Tukey's honest significant test was performed to analyze pairwise comparisons. The results were considered statistically significant at $P < 0.05$. Three sets of pairwise comparisons were performed on the percentage cell viability, cellular uptake of particles, and IC_{50} values. The first test compared the UM liposomes' values obtained by fibroblasts with the 17 modifications. The second test compared the UM liposomes' values acquired through CAFs with all 17 modifications. The third comparison was performed between fibroblasts and CAFs for each modification to observe which modification results significantly different at which cell type.

Principal component analysis (PCA) was performed to observe the covariance structure. The principal components from PCA are the linear combinations of the original variables, and these are plotted on the axes representing the directions of maximum variance. These plots can be observed to visualize the relationship between through projections of the first principal

component (PC1) and the second principal component (PC2) in a two-dimensional space. Here, we used PCA to demonstrate the relationships between IC_{50} values and different modifiers' physicochemical properties.

Furthermore, a linear regression was performed using the modifiers' physicochemical properties to predict the IC_{50} values for each modified liposome. First, 14 modifiers (A – N) were used to train and validate the regression model, followed by a prediction of the IC_{50} values of the final three modifications (O, P, and Q). This training and validation were performed separately for fibroblasts and myofibroblasts using their respective IC_{50} values. The predicted IC_{50} values were plotted against the true $IC_{50,}$ and a line of best fit was drawn to illustrate the relationship.

3.3 Results

3.3.1 Surface Modifications: physicochemical Characterization of Modified Liposomes

Liposomes were synthesized and their surface was functionalized using 17 different surface modifiers. Modified liposomes were characterized for their size and zeta potential. Differences in the zeta potential values were seen among different modifiers. Zeta potential values for both modified and UM liposomes are presented in **Figure 3.2A**. UM liposomes showed a zeta potential of -16.8 ± 0.8 mV due to the phosphate group in the lipids, and the value aligned with the previously published results [97,103].

For the modified liposomes, the zeta potential ranged from -33.9 to -8.9 mV, which corresponds to the different functional groups of the different modifiers. A connecting letter report was formulated using the student's T-test to observe the significant difference among the 17 modifications. Details for this comparison are provided in **Table S1**. Dynamic light scattering (DLS) was used to measure the size and zeta potential of the liposomes. The UM liposomes resulted in a diameter of 96.3 ± 9.4 nm, whereas the size of modified liposomes ranged from 83.5 to 119.4 nm. All these values fall in the range of the 100 nm extrusion filter, which was

used during liposome extrusion. **Figure 3.2B** shows the sizes of liposomes measured using DLS. Moreover, the polydispersity index (PDI) for these liposomes ranged from 0.096 – 0.167 givecn in **Table S2.**

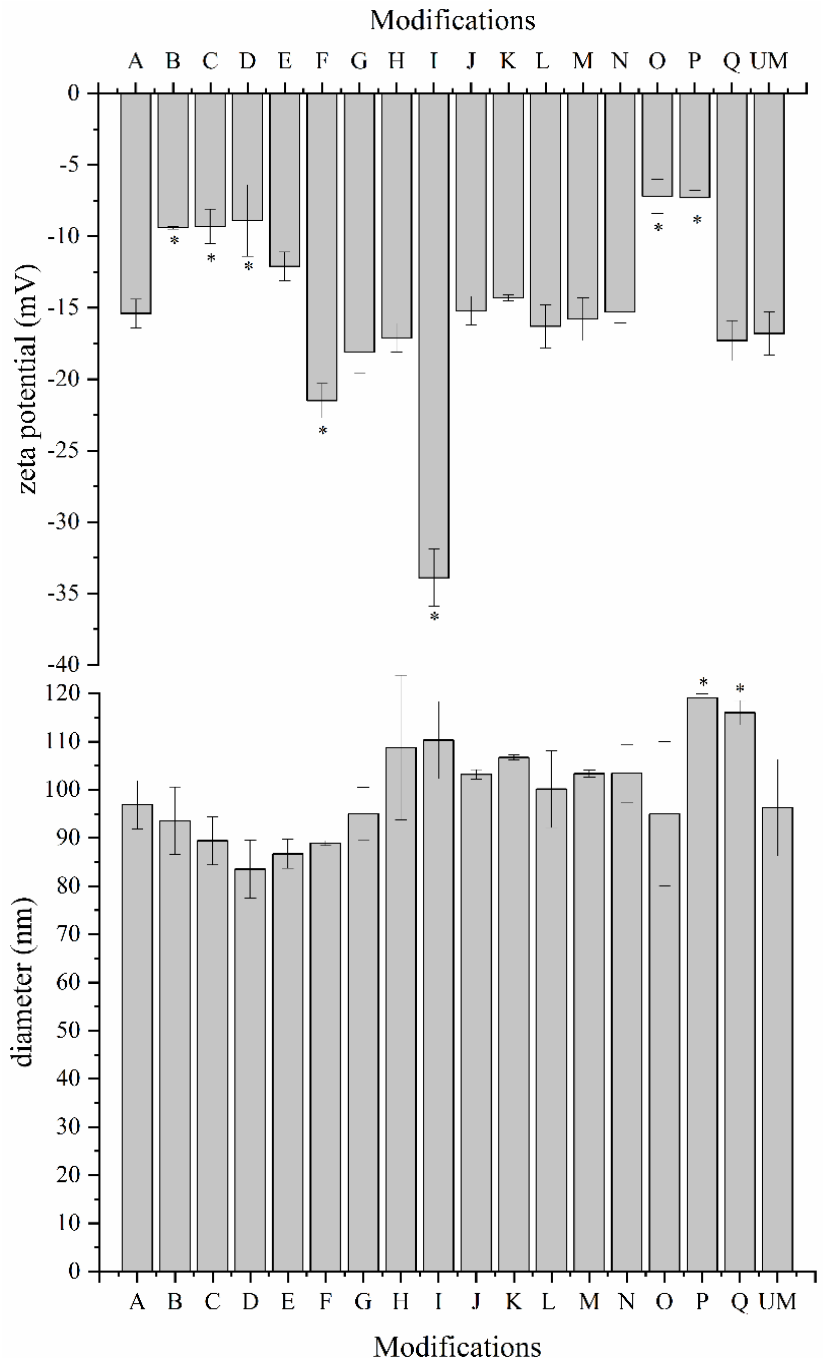

Figure 3.2. Material characterization of modified liposomes. (A) Zeta potential and (B) DLS measurements of the liposomes. *Both measurements represent three replicates for each sample. All data are shown by mean value ± standard deviation. (*) indicates p < 0.05 compared with the unmodified liposomes using pairwise comparison. UM = unmodified liposomes.*

3.3.2 Doxorubicin Encapsulation in Liposomes

Since DOX is an amphipathic drug, it can be encapsulated in the aqueous cavity of the liposome and travel through the pH gradient created by citrate used during drug loading between the inside and the outside of the liposome. This pH gradient method provides optimal encapsulation efficiency (EE). The DOX EE, shown in **Figure 3.3**, indicates that DOX was encapsulated with an efficiency of 94.0% or higher in all of the liposomes. Liposome D showed an EE of 99.60 ± 2% being the highest, while liposome A had an EE of 94 ± 4% being the lowest.

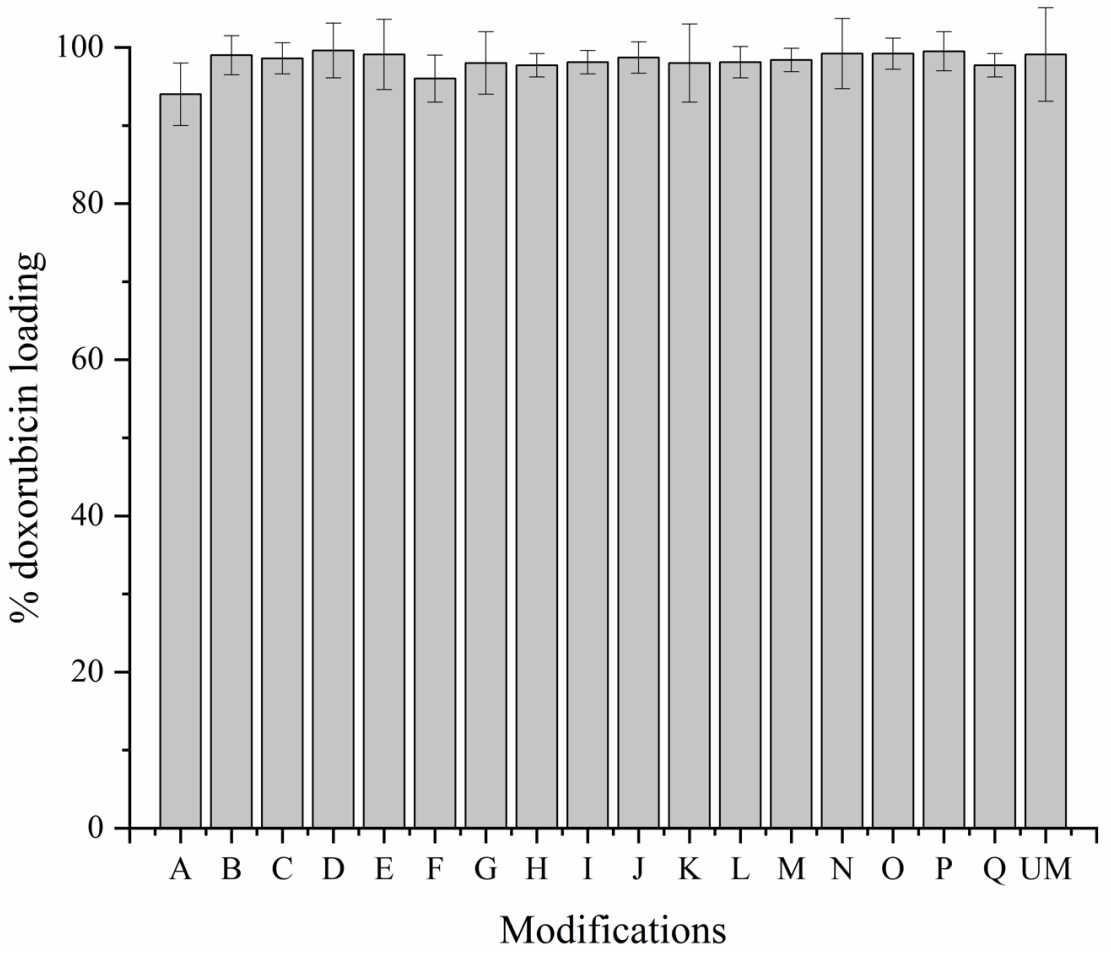

Figure 3.3. Doxoruboicin loading efficiency for modified and unmodified liposomes. *Measurements represent three replicates for each sample; all data are shown by mean value ± standard deviation.*

3.3.3 Cell Viability and Comparison of the Cellular Uptake of Fluorescent Loaded Liposomes Between Fibroblasts and Myofibroblasts

Cell viability of all modified liposomes was tested against fibroblasts and myofibroblasts. These liposomes were not loaded by DOX in order to observe the viability of DOPE:DOPC liposomes alone on the cells. After seeding fibroblasts and myofibroblasts on a 96-well plate for 24 h, a 100 µL liposome solution (500 µg mL^{-1}) was added to the cells, followed by incubation at 37 ºC for 48 h. Subsequently, MTT was performed, and the plates were read at 540 nm and a reference of 690 nm with the plate reader. Both fibroblasts and myofibroblasts showed cell viability greater than 86% and 90%, respectively. The results are shown in **Figure 3.4**.

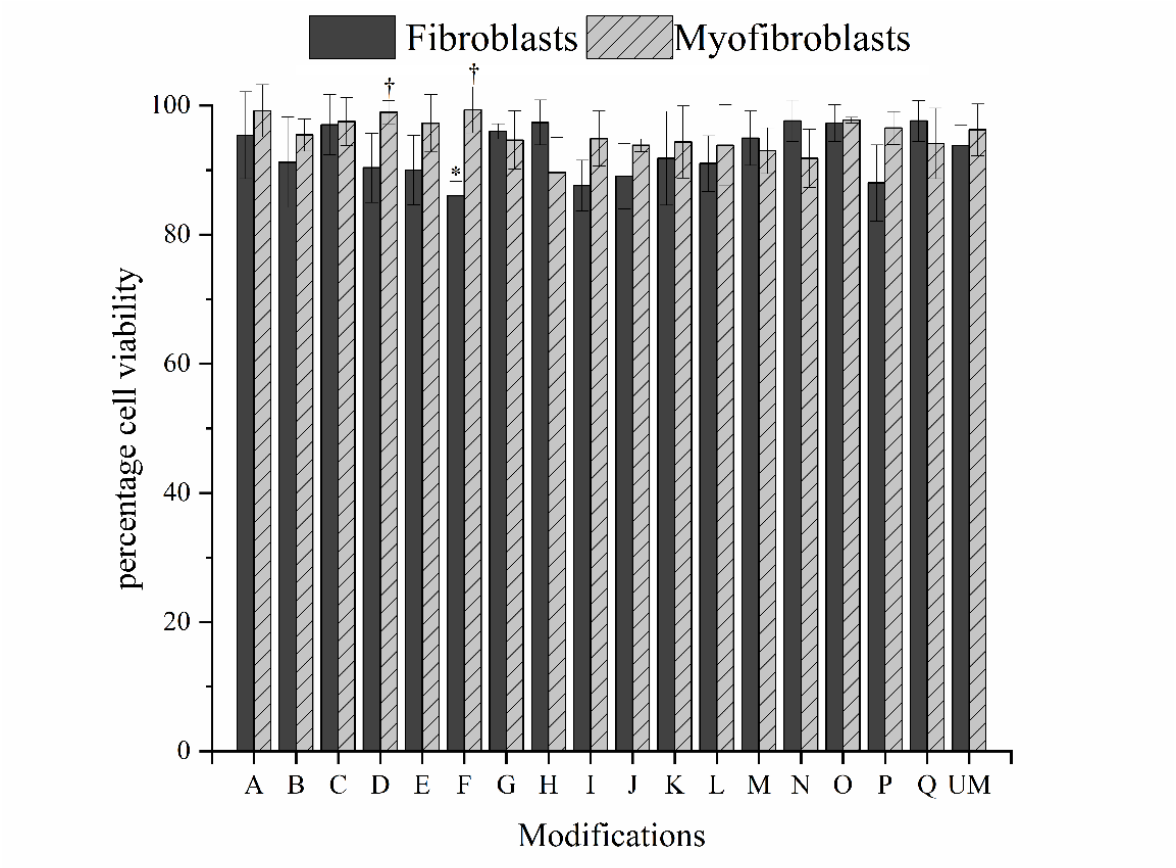

Figure 3.4. Cell viability of fibroblasts and myofibroblasts incubated with modified and unmodified liposomes. *Measurements show eight replicates for each sample. All data represent mean value ± standard deviation. (*) indicates $p < 0.05$ for values compared to their respective UM liposome values using pairwise comparison, while (†) indicates $p < 0.05$ for myofibroblast compared to fibroblast for the same modification. UM = unmodified liposomes.*

The cellular uptake of the liposomes was measured by incubating FC-loaded liposomes, both modified and UM, with the fibroblasts and myofibroblasts for 4 h. An equal amount of all 17 modified FC-loaded liposomes and UM liposomes (0.1 mg mL^{-1}) was added to the cells. Liposomes external to the cells were quenched using trypan blue. **Figure 3.5** visualizes the internalization of FC-loaded liposomes in fibroblasts at (A) 37 ^{o}C and (B) 4 ^{o}, while (C) and (D) show internalization of FC-loaded liposomes in myofibroblasts at 37 ^{o}C and 4 ^{o}C, respectively. Moreover, (E) and (F) display the intensity of fluorescence coming from the liposomes internalized by the fibroblasts. The cold binding experiments were carried out at 4 ^{o}C, where all energy-dependent cell internalization pathways are blocked. Thus, a weak level of fluorescence is seen, demonstrating little particle internalization or adsorption on the cell surface. Conversely, a significant increase in the intensity of fluorescence can be seen at 37 ^{o}C, indicating that the fibroblasts internalize a significant number of liposomes.

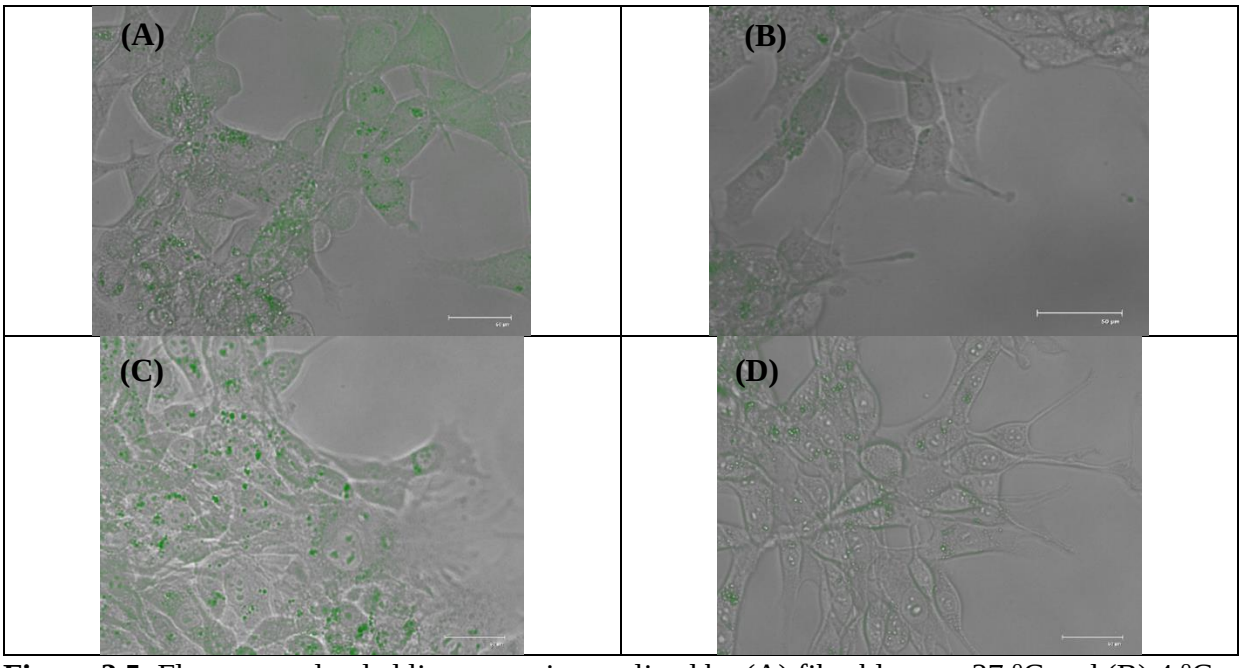

Figure 3.5. Fluorescent loaded liposomes internalized by (A) fibroblasts at 37 ^{o}C and (B) 4 ^{o}C, and (C) myofibroblasts at 37 ^{o}C and (D) 4 ^{o}C. Fluorescence level of FC loaded particles incubated with fibroblasts and myofibroblasts at (E) 37 ^{o}C and (F) 4 ^{o}C. Data represent the mean value of eight replicates for each sample ± standard deviation using pairwise comparison. The fluorescence was normalized to the amount of FC added to each well. (*) indicates $p < 0.05$ for

values compared to their respective UM liposome values using pairwise comparison. (†) indicates $p < 0.05$ for myofibroblast compared to fibroblast for the same modification. UM = unmodified liposomes.

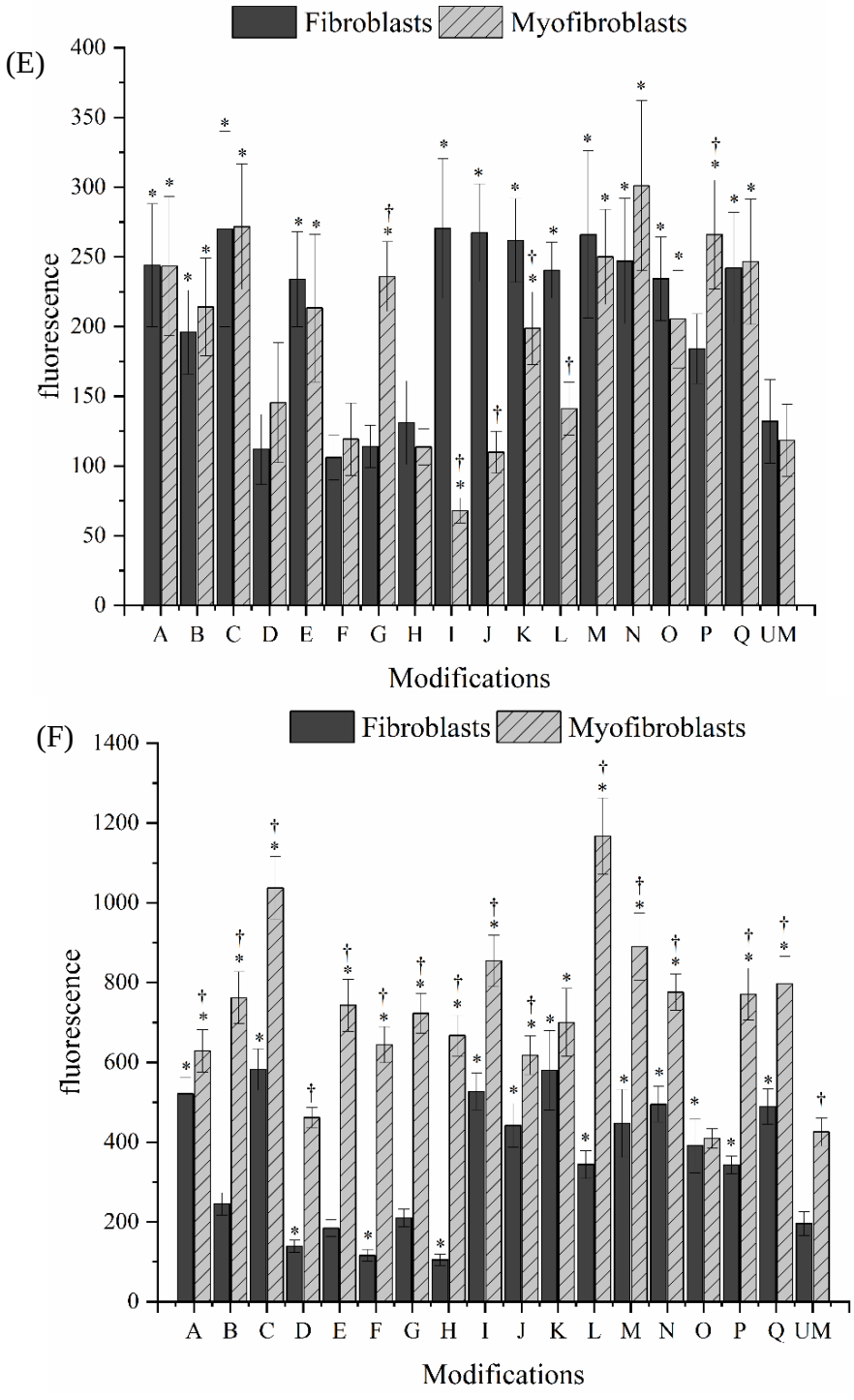

Figure 3.5 continued

At low temperatures, such as 4 ^{o}C, the energy dependent endocytic pathways are inhibited and the surface modification does not play an active role in cell internalization. At 4 ^{o}C, the fluorescence values for fibroblasts, modifications D, F, G, and H were similar to those of the UM liposomes, and there is no statistically significant difference between these liposomes. All other modifications had statistically significantly higher fluorescence values. When the same particles were tested on myofibroblasts, modifications D, F, H, J, and L showed no statistically significant difference compared to UM liposomes. Modification I demonstrated a significantly lower value than UM liposomes. All other modifications resulted in statistically significant higher values compared to the UM liposomes. When the cellular uptake of each modified liposome between each cell type was compared, modifications G and P showed a statistically significantly higher intensity of fluorescence for myofibroblasts than fibroblasts. On the other hand, modifications I, J, K, and L displayed statistically significantly lower fluorescence intensities for myofibroblasts than fibroblasts. No statistically significant difference was found in all other modifications' fluorescence intensities between fibroblasts and myofibroblasts.

In contrast to cellular uptake at 4 ^{o}C, endocytosis is energy dependent. Therefore, at 37 ^{o}C, the surface modifications play a significant role in cellular uptake as they may bind to surface receptors involved in endocytosis. For fibroblasts, similar results were seen at 37 ^{o}C, where modifications D, F, and H had lower fluorescence values compared to UM liposomes, and modifications E and G were not significantly different. All other modifications had a statistically significant higher amount of fluorescence. Unlike fibroblasts, myofibroblasts showed higher cellular uptake for all modifications compared to the UM liposomes. The fluorescence intensity for modification D was higher than that of the UM liposomes, however, it was not statistically significant. All other modifications demonstrated a statistically significant increase in the cellular

uptake for myofibroblasts. When the fluorescence intensities were compared between fibroblasts and CAFs for each modification, cellular uptake for CAFs was statistically significantly higher for all modifications except modifications K and O. Details of comparison and connecting letter reports are provided in **Tables S3, S4, S5, and S6**.

3.3.4 The Liposome Modifications were Cytocomaptible with Fibroblasts And Myofibroblasts

Unmodified DOPE: DOPC liposomes are commonly used in the clinic. Epaxal® is the first DOPE: DOPC based liposome that was approved by the FDA in 1994. It was the first adjuvant virosomal vaccine for the hepatitis A virus and was developed by Crucell Berna Biotech, Switzerland [122]. Therefore, these liposomes were not anticipated to significantly alter the cell viability. However, the modified liposomes used needed to be analyzed for cytocompatibility. Cell viability assay was used to determine the cytotoxicity of the modified liposomes. The viability of the cells (both fibroblasts and myofibroblasts) exposed to the modified or UM liposomes was normalized to the cells without the addition of liposomes. All modified liposomes showed a cell viability of 86% or higher (**Figure 3.4**).

3.3.5 Measuring the Toxicity of Doxorubicin Encapsulated Liposomes via IC_{50}

IC_{50} is the half-maximal inhibitory concentration, which is used to define the efficacy of drugs. It indicates what concentration of the drug is required to inhibit a biological process by half, thus providing a potency of an antagonist drug. MTT assay was used to determine the IC_{50} values for fibroblasts and myofibroblasts. Both fibroblasts and myofibroblasts were incubated with DOX loaded modified liposomes for 48 h, and their IC_{50} values were calculated. The experiments were repeated for all modified liposomes, UM liposomes, and free DOX and the results are listed in Table 3.1.

For fibroblasts, the surface modifiers altered the IC_{50} values of the liposomes compared to UM liposomes (**Figure 3.6**). UM liposomes showed an IC_{50} value of 0.39 ± 0.04 µM, whereas the free DOX gave an IC_{50} value of 0.83 ± 0.1 µM. This value of IC_{50} for free DOX is consistent with earlier findings [123–125]. The IC_{50} has an inverse relationship with the toxicity, meaning, the lower IC_{50} value, the higher the toxicity of that particle. Most of the modified liposomes (A – E and G – O) had IC_{50} values lower than the UM liposomes (0.39 ± 0.04 µM). Liposome F showed the lowest toxicity with an IC_{50} value of 1.28 ± 0.05 µM. Liposomes M, N, O, P, and Q showed weak toxicities with IC_{50} values of 0.76 ± 0.2 µM, 1.04 ± 0.2 µM, 1.13 ± 0.3 µM, 1.18 ± 0.2 µM, and 0.96 ± 0.3 µM, respectively. Liposome I showed the highest toxicity with an IC_{50} value of 0.19 ± 0.04 µM, followed by liposomes A and H, both with IC_{50} values 0.22 ± 0.04 µM.

Interesting results were seen when the same modified liposomes were used to calculate the IC_{50} for myofibroblasts. All modifications, except I and UM liposomes, showed a smaller IC_{50} value for myofibroblasts compared to fibroblasts. Modifications A-G and L-Q showed a statistically significant decrease in the IC_{50} for myofibroblasts, some of which were nearly less than half of the IC_{50} values for fibroblasts. Modification E demonstrated the lowest IC_{50} value of 0.1 ± 0.02 µM, while modification M remained at the top with an IC_{50} value of 0.45 ± 0.02 µM. UM liposomes resulted in an IC50 value of 0.40 ± 0.03 µM, which is very close to that of the fibroblasts. The value of IC50 for free DOX was 0.31 ± 0.02 µM for myofibroblasts.

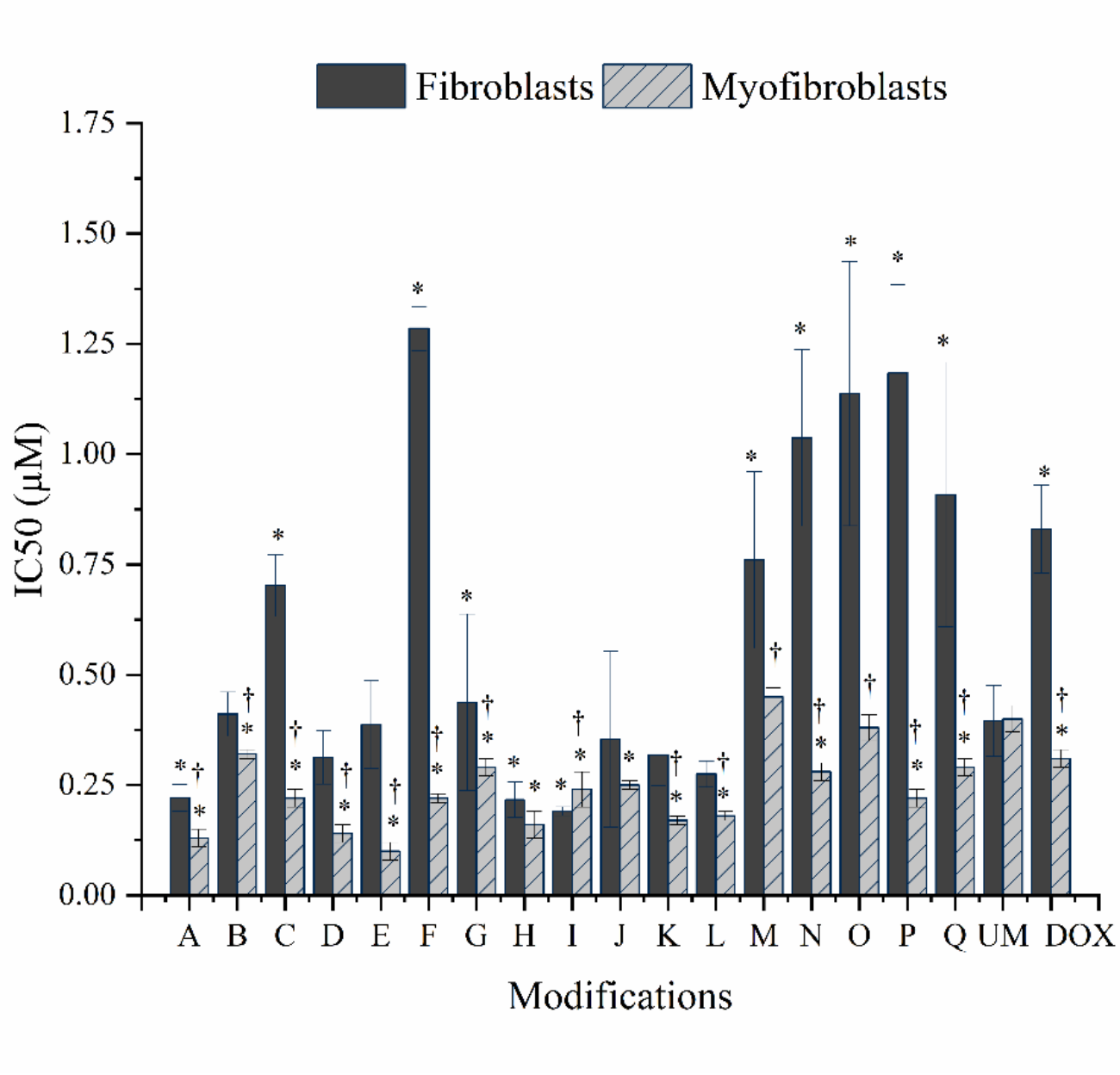

Figure 3.6. IC_{50} concentration for fibroblasts and myofibroblasts. *Data represent the mean value of eight replicates for each sample ± standard deviation. Statistical analysis through two-way ANOVA and Tukey's HSD post-hoc test. (*) indicates $p < 0.05$ for values compared to their respective UM liposome values using pairwise comparison, while (†) indicates $p < 0.05$ for myofibroblast compared with fibroblast for the same modification. UM = unmodified liposomes, DOX = doxorubicin.*

Table 3.1. IC_{50} values for 17 modified liposomes (A-Q), unmodified liposomes (UM), and free doxorubicin (DOX) against fibroblasts and myofibroblasts. (*) indicates $p < 0.05$ for values compared to their respective UM liposome values using pairwise comparison, while (†) indicates $p < 0.05$ for myofibroblast compared to fibroblast for the same modification

	Liposome modification	IC_{50} value against fibroblasts (μM)	IC_{50} value against myofibroblasts (μM)
1	A	0.22 ± 0.03 *	0.13 ± 0.02 *,†
2	B	0.41 ± 0.05	0.32 ± 0.01 *,†
3	C	0.70 ± 0.07 *	0.22 ± 0.02 *,†
4	D	0.31 ± 0.06	0.14 ± 0.02 *,†
5	E	0.39 ± 0.06	0.10 ± 0.02 *,†
6	F	1.28 ± 0.05 *	0.22 ± 0.01 *,†
7	G	0.44 ± 0.2 *	0.29 ± 0.02 *,†
8	H	0.22 ± 0.04 *	0.16 ± 0.03 *
9	I	0.19 ± 0.01 *	0.24 ± 0.04 *,†
10	J	0.35 ± 0.2	0.25 ± 0.01 *
11	K	0.32 ± 0.07	0.17 ± 0.01 *,†
12	L	0.28 ± 0.03	0.18 ± 0.01 *,†
13	M	0.76 ± 0.2 *	0.45 ± 0.02 †
14	N	1.04 ± 0.2 *	0.28 ± 0.02 *,†
15	O	1.13 ± 0.3 *	0.38 ± 0.03 †
16	P	1.18 ± 0.2 *	0.22 ± 0.02 *,†
17	Q	0.90 ± 0.3 *	0.29 ± 0.02 *,†
18	UM	0.39 ± 0.04	0.4 ± 0.03
19	DOX	0.83 ± 0.1 *	0.31 ± 0.02 *,†

The significantly lower IC_{50} values for the liposomes, especially liposomes C, F, M, N, and O, where the difference in IC_{50} values is more than 2-fold, suggest that these modifications could improve targeted delivery to myofibroblasts (or CAFs) in the presence of fibroblasts. Details of comparison and connecting letter reports are provided in **Tables S7 and S8.**

3.3.6 Correlations between IC50 Values and Physicochemical Properties of the Surface Modifiers

The relationship between the IC_{50} values of the modified DOX loaded liposomes and multiple properties of each was investigated through informatics analysis, as shown in **Figure 3.7**. In PCA, the data set was converted through orthogonal transformations to the principal components. We looked at both the angle between the points and the origin and the distance between the points to develop a Euclidian geometric map. This was used to discover the relationship between the IC_{50} values and the physicochemical properties of the modifiers. These data have been plotted as PC1 and PC2, which comprise 47.6% of the total data. PC1 corresponded to 29.6%, while PC2 corresponded to 18% of data. The score plot in **Figure 3.7A** illustrates wide-spread data, indicating that the modified liposomes resulted in a variety of IC_{50} values. The physicochemical properties of the modifiers included polar surface area, surface tension, the enthalpy of vaporization, the number of freely rotating bonds, lipophobicity parameters, and the number of hydrogen bond donors and acceptors. These properties were obtained through a database.[126] Measured zeta potential values were also included as a parameter.

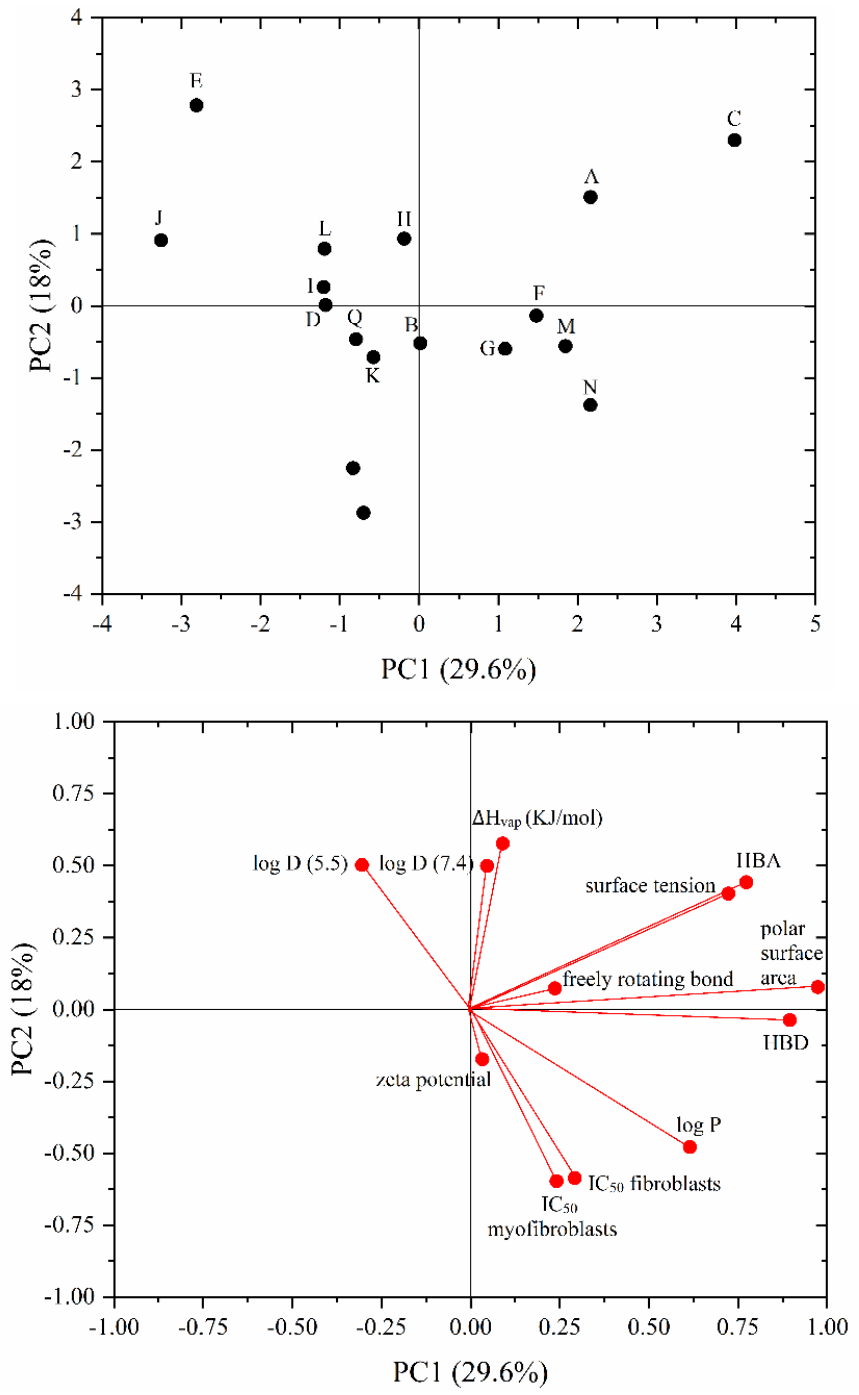

Figure 3.7. Score and loading plots of physicochemical materials properties and their influence on IC_{50} values of doxorubicin loaded modified liposomes. PC1 corresponds to 29.6% data variance and PC2 explains 18% data variance, which total up to 47.6% of the original data information. (A) Score plots of the modified liposomes, and (B) loading plots of the physicochemical properties of the modifiers in PC space. HBA = hydrogen bond acceptors and HBD = hydrogen bond donors.

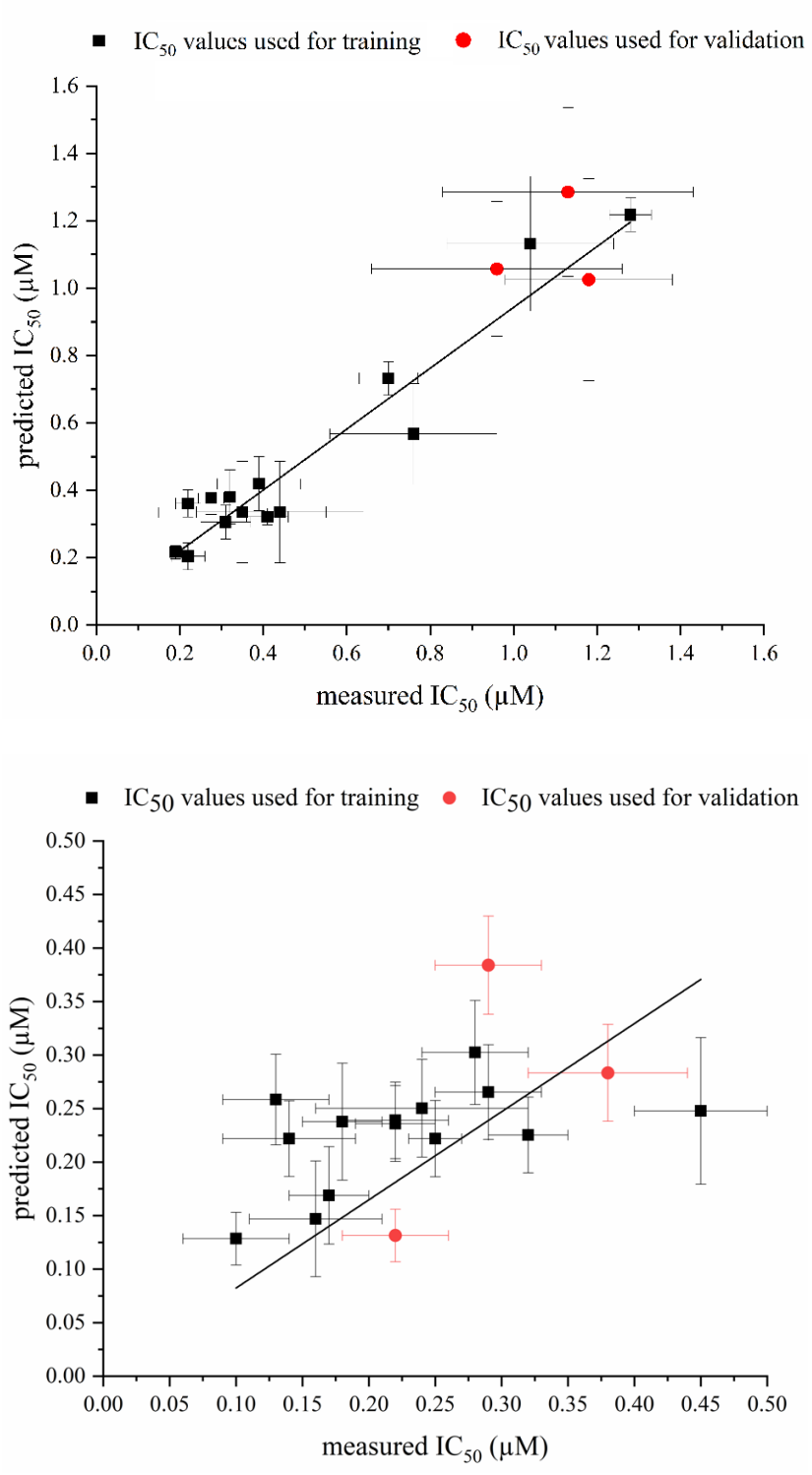

Figure 3.8. Plot of predicted IC_{50} values vs. true IC_{50} values for (A) fibroblasts and (B) myofibroblasts. *A line of best shows a linear relationship between the two set of values. All data represent mean values ± standard deviation.*

Figure 3.7B depicts the loading plot, which shows how strongly or weakly these physicochemical properties influence the IC_{50} values of the modifiers for each cell type. The IC_{50} value for fibroblasts is closely aligned with log P, while a weak relationship can be seen between the IC_{50} for fibroblasts, zeta potential, and hydrogen bond donors. For myofibroblasts, the IC_{50} values are more closely related to zeta potential and show a weak relationship with log P and hydrogen bond donors.

Figure 3.8A and 3.**8B** show the plots for measured IC_{50} vs. predicted IC_{50} values for fibroblasts and myofibroblasts, respectively. Two regression models were created using JMP; the abovementioned physicochemical properties were used as the variables, and the IC_{50} values were predicted for each cell type. All values for the modifiers A through N were used to train and validate each regression model. Subsequently, the models were used to predict the IC_{50} values of the liposomes that were modified using three new modifications: O, P, and Q, for fibroblasts and myofibroblasts. Using this regression model, the predicted IC_{50} values for modifications O, P, and Q for fibroblasts were 1.28 ± 0.3 μM, 1.03 ± 0.2 μM, and 1.06 ± 0.3 μM, respectively (**Figure 3.8A)**. When experimentally measured, the IC_{50} values for the same modifications for fibroblasts were 1.13 ± 0.3 μM, 1.18 ± 0.2 μM, and 0.96 ± 0.3 μM, respectively. There was no significant difference found between the predicted and measured IC_{50} values.

For myofibroblasts, the predicted IC_{50} values for modification O, P, and Q were 0.28 ± 0.05 μM, 0.13 ± 0.02 μM, and 0.38 ± 0.05 μM, respectively. The experimentally measured IC_{50} values were 0.38 ± 0.06 μM, 0.22 ± 0.04 μM, 0.29 ± 0.04 μM, respectively (**Figure 3.8B**). Among these three modifications, modification O did not have a statistically significant difference between the predicted and measured IC_{50} values.

3.4 Discussion

3.4.1 Liposome Properties Are Influenced by Surface Modification

Liposomes have been extensively investigated for their role as delivery agents of drugs, proteins, and DNA [127–131]. Since arginine is considered an essential amino acid, is biocompatible, and plays a significant role in fibroblast proliferation and wound healing, we are using it to improve the targeting of liposomes as a drug delivery agent by modifying the surface of the liposome with arginine-like molecules [132]. The surface charge of the liposomes has a significant effect on encapsulation and targeting capability [133,134]. The 17 arginine-like modifications (**Figure 3.1**) altered the charge on the surface the liposomes. All modified and UM liposomes in this study resulted in a negatively charged liposomal surface, which is more efficient in delivery when compared to liposomes with a neutral surface charge [135]. The phosphate group in the lipid can cause the negative charge on the UM liposome, which agrees with previous studies [136,137]. The negative charge on the modified liposomal surfaces resulted from different functional groups present on the modifiers, hence the variation in the values for zeta potential.

The surface charge of the liposomal surface, which can be altered, can affect cell internalization of the particles [138]. Negatively charged liposomes can become opsonized, making it more favorable for them to enter cell membrane via absorptive endocytosis, which increases the cell internalization efficiency [139]. Positively charged liposomes, on the other hand, can have a toxic effect on the cells due to the presence of stearylamine, which make liposomes with a negative surface charge, for instance those studied here, a more attractive carrier for delivering drugs [140–142]. Furthermore, a more negative zeta potential value results in higher toxicity. A relationship between zeta potential and the IC_{50} values can be seen in our results. For the liposomes having zeta potential values of -15.0 mV or lower, the IC_{50} value for fibroblast is

below 0.5 µM, except for liposomes F, M, and Q. Liposome I further demonstrates the relationship between zeta potential and toxicity, as it has the most negative zeta potential value (-33.9 mV) while having the highest toxicity, with an IC_{50} value of 0.19 ± 0.04 µM.

This relationship between zeta potential and toxicity can be further supported by the results of IC_{50} for myofibroblasts. A significant decrease was observed in IC_{50} values for the modification with a lower zeta potential value. For all the liposomes having a significantly lower zeta potential value, the IC_{50} value was significantly lower compared to the UM liposomes. For liposome I, with the lowest zeta potential value of -33.9 mV, the IC_{50} value was 0.24 ±0.04 µM.

In addition to surface charge, the size of the liposome also affects internalization and drug loading. Several reports have demonstrated that a smaller particle size (~ < 200 nm) can result in a higher accumulation at the drug site through the enhanced permeable and retention (EPR) effect [143–145]. Furthermore, size plays a vital role in altering pharmacokinetics as it influences tissue distribution and clearance. Consequently, to eliminate variables in results and assist the EPR effect, the size of the liposomes was kept uniform. A 100 nm polycarbonate filter was used to extrude all the modified and UM liposomes. No significant difference was observed among the size of the liposomes, which resulted in a uniform diameter and encapsulation volume for DOX. The uniform size of the liposomes leads to similar drug EE among the liposomes, as expected. Collectively, our findings suggest that these arginine derivative modifications on the liposomes have no significant influence on the size and drug loading ability.

3.4.2 Effect of Liposome Modificxations of Toxicity and Cell Internalization

Fibroblasts are typically spindle-shaped cells found in different interstitial spaces of organs and are capable of producing extracellular matrix (ECM) [146]. These fibroblasts transition to myofibroblasts and assist in the production of collagen and the ECM. However, a tumorous environment can take advantage of the myofibroblasts instigating numerous pro-tumorigenic

signals together with the alteration of normal tissue architecture [147]. These myofibroblasts can further make the situation worse by promoting tumor growth and proliferation, accelerating metastasis, inducing angiogenesis, promoting inflammation and immune destruction, regulating tumor metabolism, and inducing chemoresistance [148]. This produces an ideal void to be filled by the extensive growth of cancer cells.

Furthermore, drugs need to cross the cell membrane to perform their function. Similarly, chemotherapeutic agents must also penetrate through the cell membrane to work. Studies have shown that myofibroblasts can promote chemoresistance via biophysical drug scavenging and physical barrier methods. A study showed that fibroblast drug scavenging aggregated intertumoral gemcitabine, which caused the active gemcitabine to be entrapped within the myofibroblasts, making it unavailable to the pancreatic cancer cells [149]. Myofibroblasts can also act as a physical barrier to chemotherapeutic drugs. Myofibroblasts can develop characteristics such as a disorganized and hypovascular stroma and decreased cellular transporters, which are considered as physical barriers to effective drug delivery [150–152]. In a study by Rice et al., it was demonstrated that myofibroblasts caused chemoresistance to paclitaxel through matrix stiffness, implying that rigidity of the environment plays an important aspect of chemoresistance [153]. Therefore, precisely targeting myofibroblasts in a tumor environment and the presence of other cells is an efficient method for drug delivery to tumors. Actively targeting myofibroblasts using DOX loaded liposomes is an effective method of improving passive targeting, which is usually the case with Doxil®. The active targeting of myofibroblasts also lays the foundation to increase intracellular uptake for future *in vivo* studies using these liposomes.

DOX, a common chemotherapeutic drug, is extensively used for treatment of cancer. DOX inhibits the production of topoisomerase II through DNA intercalation [154,155]. This stops the proliferation of cancerous cells and eventually kills the tumor. Even though DOX limits tumor growth, a huge side effect of its usage is that it can cause cardiac toxicity. Thus, modifying the drug carrier to increase its selective targetability is one way of restricting the off-target effects of DOX. In doing so, one might be able to change the biodistribution of DOX, reducing amounts of DOX in healthy tissue.

To measure the degree of toxicity of DOX encapsulated in liposomes, IC_{50} values of each modified liposome were calculated along with UM liposomes for both fibroblasts and myofibroblasts. It was seen that the toxicity of DOX increased when encapsulated in liposomes, as lower IC_{50} values of the liposomes were calculated compared to free DOX. For fibroblasts, free DOX showed an IC_{50} value of 0.83 ± 0.3 µM, which lies in the range of values previously reported [123–125]. Liposomes F, M, N, O, and Q resulted in IC_{50} values higher than free DOX, while all other liposomes demonstrated an IC50 value less than free DOX. The IC_{50} value for UM liposomes was calculated to be 0.39 ± 0.1 µM, whereas liposomes A, D, E, H, I, J, K, and L resulted in toxicity values less than UM liposomes.

When the same modified DOX loaded liposomes were tested on myofibroblasts to measure toxicity, it was seen that all liposomes had lower IC_{50} values than fibroblasts, except liposome I and UM liposomes. Furthermore, all IC_{50} values had a statistically significant difference when compared to the IC_{50} values of fibroblasts, except liposomes H and J. It was interesting to see that for UM liposomes, the IC_{50} values for both fibroblast and myofibroblast were 0.39 ± 0.04 µM and 0.40 ± 0.03 µM, respectively. This result strongly implies that without modification, myofibroblasts and fibroblasts are equally susceptible to DOX loaded liposomes;

however, once modified, the liposomes can be significantly more toxic to myofibroblasts. Therefore, these experiments support our hypothesis that these surface modifications of liposomes can enhance the selective targeting to myofibroblasts in the tumor environment.

Ma et al. used modifications A through M to examined the effect of these modifications on naïve, M1, and M2 macrophages [103]. Neuberger et al. used the same modifications and observed how Caco-2 colon carcinoma cells respond to these modified liposomes [97]. The objective of both of these studies was to increase the toxicity and targetability of DOX to a particular cell type. Similarly, the aim of this study was to analyze the effect of the same modifications on fibroblasts and myofibroblasts and determine if these modifications could increase selective targeting towards myofibroblasts. As expected, the modifications significantly increased the toxicity of the DOX loaded liposomes towards myofibroblasts compared to fibroblasts. According to Neuberger et al., modifications A, C, F, K, L, M, and N showed significantly lower IC_{50} values (all ~0.5 µM or less) compared to free DOX. Similarly, in our experiments, modifications F, M, and N showed a significantly higher IC_{50} value for fibroblasts; however, the IC_{50} values for myofibroblasts decrease by more than two fold. Additionally, Liposomes C, O, P, and Q show a significantly large difference in the IC_{50} values for fibroblasts and myofibroblasts, the latter being much lower. These results strongly suggest that the liposomes modified with the aforementioned modifications are an excellent drug delivery vehicle to target myofibroblasts in a tumor environment.

Like other nanoparticles, the cellular uptake of liposomes occurs through endocytosis, which can be influenced by size, shape, and surface chemistry [156]. As demonstrated by DLS, the size and the shape of liposomes were not affected by the modifications; however, the surface chemistry is different for each modification. Various physicochemical properties of each

modifier were taken into account and correlated with the FC-loaded liposome internalization results. These physicochemical properties included: polar surface area; the number of freely rotating bonds; surface tension; the enthalpy of vaporization; lipophobicity parameters; and the number of hydrogen bond donors and acceptors. Among other properties, lipophobicity is an important factor affecting the internalization, followed by surface tension and polar surface area [103].

Lipophilicity, known as log D here, represents the affinity of a drug for a lipid environment. It can be measured by the distribution of a drug between the organic and the aqueous phases, usually by octanol-water distribution coefficient at various pHs (log D). Usually, nanoparticles utilize hydrophobic interaction to accumulate in the hydrophobic regions of the lipid bilayer when crossing the layer. Therefore, it is beneficial for the nanoparticles to have moderate lipophilicity in order to have better cell internalization [157]. The log D at pH 5.5 for the modifications ranged from -5.41 (being extreme) to -2.62 (being moderate). 37 ^{o}C is an optimum temperature for the cells to proliferate and stay healthy. At this temperature, all of their cell internalization pathways are active, including endocytosis. At 37 ^{o}C, a relatively low internalization was seen in modifications D, F, G, H, and O for both fibroblasts and myofibroblasts. For these modifications, the log D values were < -4.0. At pH 7.4, the log D values ranged from -5.68 – 3.34, where modification H was -5.68. All other modifications had a significant amount of internalization in the cells, and their log D values ranged from –4.56 to -3.55. Modifications A and I, the modifications with the lowest IC_{50} values for fibroblasts, showed higher cellular uptake, whereas modifications A and E (lowest IC_{50} values for myofibroblasts) demonstrated a significant increase in cell internalization compared to UM liposomes. The log D value for modification I at pH 5.5 is -2.82, which is the second highest

compared to other modifications' log D values. It was interesting to see that modification A had a log D value of -4.56, yet it showed promise in lowering the IC_{50} value for both fibroblasts and myofibroblasts. Modification E showed the lowest IC_{50} value for myofibroblasts and has a log D value of -3.61. This log D value lies toward the higher end of the spectrum of the log D values. These results are consistent with previous findings as they demonstrate that higher lipophilicity (log D value) of liposomes can result in higher cell internalization.

Other physicochemical properties, such as surface tension and polar surface area, also affect cell internalization. Studies have demonstrated that hydrophobic liposomes are more susceptible to endocytosis compared to their hydrophilic counterparts [111,135,157]. A modest but direct correlation between surface tension and polar surface area of the modifications was seen with cellular uptake. Most modifications with higher surface tension and polar surface area resulted in a higher fluorescence value, representing a higher uptake. Furthermore, most of these modifications have a lower IC_{50} value than free DOX for fibroblasts and significantly for myofibroblasts, indicating an improvement in selective cytotoxicity.

It was interesting to note that the six modifications, representing six lowest IC_{50} values for fibroblasts (A, D, H, I, K, and L), four modification (A, I, K, and L) demonstrated a significant increase in cell internalization at 37 ^{o}C when compared to UM liposomes. Similarly, for myofibroblasts, all modifications, except D and O, showed a significant increase in cell internalization at 37 ^{o}C compared to UM liposomes. For all these modifications, the IC_{50} values for myofibroblasts were significantly lower compared to UM liposomes (except modification M). These results demonstrate that there is a relationship between toxicity and internalization. More importantly, when the cell internalization for myofibroblasts was compared to fibroblasts, it was clearly seen that all modifications, except K and O, show a significant increase in

internalization for myofibroblasts. This implies that we can actively target myofibroblasts (or CAFs) in a tumor microenvironment using these modified liposomes, as they are significantly more toxic towards myofibroblasts and show greater internalization compared to fibroblasts.

PCA was performed to examine correlations between all the above mentioned physicochemical properties of the modifications, the toxicity (IC_{50}), and the cellular uptake of the liposomes. This multidimensional dataset was reduced to a two-dimensional plot (**Figure 3.7**) to facilitate the analysis of latent relationships. These specific physicochemical properties were chosen based on the previous reports, which describe the attributes of drug molecules, such as Lipinski's rule of five: polar surface area, enthalpy, lipophilicity, charge, and flexibility [97,158,159]. The relationship of the IC_{50} of the liposomes on fibroblasts with each physicochemical property is different compared to the relationship between myofibroblasts and their properties. The IC_{50} for fibroblasts is more strongly related to log P, while it shows a weak relationship to zeta potential and hydrogen bond donors, while the IC_{50} for myofibroblasts is more strongly related to zeta potential and demonstrates a weak relationship with log P and hydrogen bond donors, as seen in **Figure 3.7B**. This suggests that targeting different cell phenotypes through surface modifications can be achieved.

Most importantly, a regression model was designed that uses all the aforementioned physicochemical properties and predicts the IC_{50} values for other arginine-like molecules. The regression model was trained and validated using 14 modifications (A-N). Subsequently, the model was used to predict IC_{50} values for fibroblasts and myofibroblasts for modifications O, P, and Q. The predicted and measured IC_{50} values for fibroblasts showed no significant difference for all three modifications (O, P, and Q). For myofibroblasts, modification O did not show a significant difference between the predicted and measured IC_{50} values. This model has the

potential to predict the IC_{50} values of other similar molecules using their physicochemical properties for IC_{50} values of modified DOPE/DOPC liposomes on fibroblasts and myofibroblasts.

To our knowledge, no study has been performed that utilizes these physicochemical properties and extrapolate them to predict IC_{50} values for fibroblasts or myofibroblasts. This novel method to predict IC_{50} can be applied to a library of arginine-like molecules. Measuring IC_{50} values experimentally is time consuming and can result in use of large number of resources. This regression model can be used to determine which modifiers result in a more desirable IC_{50} value; once shortlisted, those specific molecules can then be tested experimentally. Thus, using this model can be time and cost effective.

Combining all this information, one may elucidate design principles in drug delivery explicitly targeted to the myofibroblasts within a tumor microenvironment. Future work includes investigation of a more extensive library to determine if the relationships between different physicochemical properties, IC_{50} values, and cell internalization hold for fibroblasts, myofibroblasts, and other cell types. Furthermore, which pathways are responsible for an improved toxicity and which are responsible for improved internalization for fibroblasts and myofibroblasts need to be examined and compared. Additionally, a different and new set of molecules can be used as surface modifiers for the validation of the IC_{50} prediction model.

3.5 Conclusions

In this study, DOPE: DOPC liposomes were modified using 17 different arginine-like surface modifiers to enhance the liposomes' targetability to myofibroblasts (CAFs) in a tumor microenvironment. These modifications did not affect the size and drug loading efficiency of the liposomes. Significant differences were seen when the zeta potential was calculated, which influences the cell internalization. Surface modifications and fibroblast phenotype did affect the

cellular uptake of the liposomes. Moreover, different trends between internalization of liposomal FC and IC_{50} values were observed; a more positive correlation was seen between internalization and IC_{50} values for myofibroblasts. For myofibroblasts, 15 out of 17 modifications showed significantly lower IC_{50} values compared to fibroblasts with a significant increase in cell internalization, improving targeted delivery to myofibroblasts in a tumor microenvironment. Furthermore, the IC_{50} prediction model was used to obtain a reasonable estimate for the IC_{50} values for unknown modifiers using their physicochemical properties. This work attests to the significance of investigating the interactions of modified and unmodified liposomes with fibroblasts and myofibroblasts. The finding of this study advocate that liposomes modified with arginine derivations are promising and efficient nanoparticle drug delivery vehicles for myofibroblasts in a tumor microenvironment.

3.6 References

1. Zahid, M. & Robbins, P. D. Cell-type specific penetrating peptides: therapeutic promises and challenges. Molecules 20, 13055–13070 (2015).

2. Deb, P. K., Al-Attraqchi, O., Chandrasekaran, B., Paradkar, A. & Tekade, R. K. Protein/peptide drug delivery systems: practical considerations in pharmaceutical product development. in Basic Fundamentals of Drug Delivery 651–684 (Elsevier, 2019).

3. Patel, S. G. et al. Cell-penetrating peptide sequence and modification dependent uptake and subcellular distribution of green florescent protein in different cell lines. Sci. Rep. 9, 1–9 (2019).

4. Hirose, H. et al. Transient focal membrane deformation induced by arginine-rich peptides leads to their direct penetration into cells. Mol. Ther. 20, 984–993 (2012).

5. Tanaka, G. et al. CXCR4 stimulates macropinocytosis: implications for cellular uptake of arginine-rich cell-penetrating peptides and HIV. Chem. Biol. 19, 1437–1446 (2012).

6. Futaki, S., Hirose, H. & Nakase, I. Arginine-rich peptides: methods of translocation through biological membranes. Curr. Pharm. Des. 19, 2863–2868 (2013).

7. Futaki, S., Nakase, I., Tadokoro, A., Takeuchi, T. & Jones, A. T. Arginine-rich peptides and their internalization mechanisms. Biochem. Soc. Trans. 35, 784–787 (2007).

8. Wender, P. A. et al. The design, synthesis, and evaluation of molecules that enable or enhance cellular uptake: peptoid molecular transporters. Proc. Natl. Acad. Sci. 97, 13003–13008 (2000).

9. Mitchell, D. J., Steinman, L., Kim, D. T., Fathman, C. G. & Rothbard, J. B. Polyarginine enters cells more efficiently than other polycationic homopolymers. J. Pept. Res. 56, 318–325 (2000).

10. Kim, H.-K., Davaa, E., Myung, C.-S. & Park, J.-S. Enhanced siRNA delivery using cationic liposomes with new polyarginine-conjugated PEG-lipid. Int. J. Pharm. 392, 141–147 (2010).

11. Chen, Y., Bathula, S. R., Yang, Q. & Huang, L. Targeted nanoparticles deliver siRNA to melanoma. J. Invest. Dermatol. 130, 2790–2798 (2010).

12. Li, L. et al. Gene transfer efficacies of serum-resistant amino acids-based cationic lipids: Dependence on headgroup, lipoplex stability and cellular uptake. Int. J. Pharm. 408, 183–190 (2011).

13. Barenholz, Y. Doxil-the first FDA-approved nano-drug: from an idea to a product. Handb. Harnessing Biomater. Nanomed 335–398 (2012).

14. 95. Zhong, H., Chan, G., Hu, Y., Hu, H. & Ouyang, D. A comprehensive map of FDA-approved pharmaceutical products. Pharmaceutics 10, 263 (2018).

15. Safra, T. Cardiac safety of liposomal anthracyclines. Oncologist 8, 17–24 (2003).

16. Neuberger, K., Boddupalli, A. & Bratlie, K. M. Effects of arginine-based surface modifications of liposomes for drug delivery in Caco-2 colon carcinoma cells. Biochem. Eng. J. 139, 8–14 (2018).

17. Storm, G., Belliot, S. O., Daemen, T. & Lasic, D. D. Surface modification of nanoparticles to oppose uptake by the mononuclear phagocyte system. Adv. Drug Deliv. Rev. 17, 31–48 (1995).

18. Lestini, B. J. et al. Surface modification of liposomes for selective cell targeting in cardiovascular drug delivery. J. Control. Release 78, 235–247 (2002).

19. Nguyen, T. X., Huang, L., Gauthier, M., Yang, G. & Wang, Q. Recent advances in liposome surface modification for oral drug delivery. Nanomedicine 11, 1169–1185 (2016).

20. Chang, H.-I. & Yeh, M.-K. Clinical development of liposome-based drugs: formulation, characterization, and therapeutic efficacy. Int. J. Nanomedicine 7, 49 (2012).

21. Bygd, H. C., Ma, L. & Bratlie, K. M. Physicochemical properties of liposomal modifiers that shift macrophage phenotype. Mater. Sci. Eng. C 79, 237–244 (2017).

22. Ma, L., Bygd, H. C. & Bratlie, K. M. Improving selective targeting to macrophage subpopulations through modifying liposomes with arginine based materials. Integr. Biol. 9, 58–67 (2017).

23. Bygd, H. C., Forsmark, K. D. & Bratlie, K. M. Altering in vivo macrophage responses with modified polymer properties. Biomaterials 56, 187–197 (2015).

24. Akilbekova, D., Philiph, R., Graham, A. & Bratlie, K. M. Macrophage reprogramming: influence of latex beads with various functional groups on macrophage phenotype and phagocytic uptake in vitro. J. Biomed. Mater. Res. Part A 103, 262–268 (2015).

25. Wang, D. & Bratlie, K. M. Influence of polymer chemistry on cytokine secretion from polarized macrophages. ACS Biomater. Sci. Eng. 1, 166–174 (2015).

26. Nagata, S. & Tanaka, M. Programmed cell death and the immune system. Nat. Rev. Immunol. 17, 333–340 (2017).

27. Martinez, F. O. & Gordon, S. The M1 and M2 paradigm of macrophage activation: time for reassessment. F1000Prime Rep. 6, (2014).

28. Murray, P. J. et al. Macrophage activation and polarization: nomenclature and experimental guidelines. Immunity 41, 14–20 (2014).

29. Lee, H.-M. et al. Drug repurposing screening identifies bortezomib and panobinostat as drugs targeting cancer associated fibroblasts (CAFs) by synergistic induction of apoptosis. Invest. New Drugs 36, 545–560 (2018).

30. Liu, T., Zhou, L., Li, D., Andl, T. & Zhang, Y. Cancer-associated fibroblasts build and secure the tumor microenvironment. Front. cell Dev. Biol. 7, 60 (2019).

31. Botti, G. et al. Microenvironment and tumor progression of melanoma: new therapeutic prospectives. J. Immunotoxicol. 10, 235–252 (2013).

32. Sun, Y. et al. Treatment-induced damage to the tumor microenvironment promotes prostate cancer therapy resistance through WNT16B. Nat. Med. 18, 1359–1368 (2012).

33. Sun, Y. et al. SFRP2 augments WNT16B signaling to promote therapeutic resistance in the damaged tumor microenvironment. Oncogene 35, 4321–4334 (2016).

34. Zhang, D. et al. Tumor–stroma IL1β-IRAK4 feedforward circuitry drives tumor fibrosis, Chemoresistance, and poor prognosis in pancreatic cancer. Cancer Res. 78, 1700–1712 (2018).

35. Zhai, J. et al. Cancer-associated fibroblasts-derived IL-8 mediates resistance to cisplatin in human gastric cancer. Cancer Lett. 454, 37–43 (2019).

36. Lotti, F. et al. Chemotherapy activates cancer-associated fibroblasts to maintain colorectal cancer-initiating cells by IL-17A. J. Exp. Med. 210, 2851–2872 (2013).

37. Orimo, A. et al. Stromal fibroblasts present in invasive human breast carcinomas promote tumor growth and angiogenesis through elevated SDF-1/CXCL12 secretion. Cell 121, 335–348 (2005).

38. O'Connell, J. T. et al. VEGF-A and Tenascin-C produced by S100A4+ stromal cells are important for metastatic colonization. Proc. Natl. Acad. Sci. 108, 16002–16007 (2011).

39. Bergers, G. et al. Matrix metalloproteinase-9 triggers the angiogenic switch during carcinogenesis. Nat. Cell Biol. 2, 737–744 (2000).

40. Muñoz-Galván, S., Gutierrez, G., Perez, M. & Carnero, A. MAP17 (PDZKIP1) expression determines sensitivity to the proteasomal inhibitor Bortezomib by preventing Cytoprotective autophagy and NFκB activation in breast Cancer. Mol. Cancer Ther. 14, 1454–1465 (2015).

41. Moser, C., Müller, M., Kaeser, M. D., Weydemann, U. & Amacker, M. Influenza virosomes as vaccine adjuvant and carrier system. Expert Rev. Vaccines 12, 779–791 (2013).

42. Toffoli, G. et al. Sensitivity pattern of normal and Ha-ras transformed NIH3T3 fibroblasts to antineoplastic drugs. Tumori J. 75, 423–428 (1989).

43. Chen, X. et al. A human anti-c-Met Fab fragment conjugated with doxorubicin as targeted chemotherapy for hepatocellular carcinoma. PLoS One 8, e63093 (2013).

44. Wang, Y. et al. Fluorescent carbon dot-gated multifunctional mesoporous silica nanocarriers for redox/enzyme dual-responsive targeted and controlled drug delivery and real-time bioimaging. Eur. J. Pharm. Biopharm. 117, 105–115 (2017).

45. The Free Chemical Database, Royal Society of Chemistry. Available at: www.chemspider.com.

46. Yagi, N. et al. A surface-modified functional liposome capable of binding to cell membranes. Chem. Commun. 1687–1688 (1999).

47. Connor, J. & Huang, L. pH-sensitive immunoliposomes as an efficient and target-specific carrier for antitumor drugs. Cancer Res. 46, 3431–3435 (1986).

48. Ropert, C., Malvy, C. & Couvreur, P. Inhibition of the Friend retrovirus by antisense oligonucleotides encapsulated in liposomes: mechanism of action. Pharm. Res. 10, 1427–1433 (1993).

49. Holmberg, E. G., Reuer, Q. R., Geisert, E. E. & Owens, J. L. Delivery of plasmid DNA to glial cells using pH-sensitive immunoliposomes. Biochem. Biophys. Res. Commun. 201, 888–893 (1994).

50. Templeton, N. S. et al. Improved DNA: liposome complexes for increased systemic delivery and gene expression. Nat. Biotechnol. 15, 647–652 (1997).

51. Kocic, H. et al. Proliferative, anti-apoptotic and immune-enhancing effects of L-arginine in culture of skin fibroblasts. J. Biol. Regul. Homeost. Agents 31, 667–672 (2017).

52. Mirahmadi, N., Babaei, M. H., Vali, A. M. & Dadashzadeh, S. Effect of liposome size on peritoneal retention and organ distribution after intraperitoneal injection in mice. Int. J. Pharm. 383, 7–13 (2010).

53. Şalva, E., Turan, S. Ö., Eren, F. & Akbuğa, J. The enhancement of gene silencing efficiency with chitosan-coated liposome formulations of siRNAs targeting HIF-1α and VEGF. Int. J. Pharm. 478, 147–154 (2015).

54. Ahsan, F., Rivas, I. P., Khan, M. A. & Suárez, A. I. T. Targeting to macrophages: role of physicochemical properties of particulate carriers—liposomes and microspheres—on the phagocytosis by macrophages. J. Control. release 79, 29–40 (2002).

55. Campos-Martorell, M. et al. Charge effect of a liposomal delivery system encapsulating simvastatin to treat experimental ischemic stroke in rats. Int. J. Nanomedicine 11, 3035 (2016).

56. Krasnici, S. et al. Effect of the surface charge of liposomes on their uptake by angiogenic tumor vessels. Int. J. cancer 105, 561–567 (2003).

57. Patil, S., Sandberg, A., Heckert, E., Self, W. & Seal, S. Protein adsorption and cellular uptake of cerium oxide nanoparticles as a function of zeta potential. Biomaterials 28, 4600–4607 (2007).

58. Epstein-Barash, H. et al. Physicochemical parameters affecting liposomal bisphosphonates bioactivity for restenosis therapy: internalization, cell inhibition, activation of cytokines and complement, and mechanism of cell death. J. Control. Release 146, 182–195 (2010).

59. Nishiya, T., Lam, R. T. T., Eng, F., Zerey, M. & Lau, S. Mechanistic study on toxicity of positively charged liposomes containing stearylamine to blood. Artif. Cells, Blood Substitutes, Biotechnol. 23, 505–512 (1995).

60. Smistad, G., Jacobsen, J. & Sande, S. A. Multivariate toxicity screening of liposomal formulations on a human buccal cell line. Int. J. Pharm. 330, 14–22 (2007).

61. Kelly, C., Jefferies, C. & Cryan, S.-A. Targeted liposomal drug delivery to monocytes and macrophages. J. Drug Deliv. 2011, (2011).

62. Maruyama, K. Intracellular targeting delivery of liposomal drugs to solid tumors based on EPR effects. Adv. Drug Deliv. Rev. 63, 161–169 (2011).

63. Rehman, T. U. et al. Development of acoustically active nanocones using the host–guest interaction as a new histotripsy agent. ACS omega 4, 4176–4184 (2019).

64. Mikada, M. et al. Evaluation of the enhanced permeability and retention effect in the early stages of lymph node metastasis. Cancer Sci. 108, 846–852 (2017).

65. Firestein, G. S., Budd, R. C., Gabriel, S. E., McInnes, I. B. & O'Dell, J. R. Kelley and Firestein's textbook of rheumatology e-book. (Elsevier Health Sciences, 2016).

66. Alkasalias, T., Moyano-Galceran, L., Arsenian-Henriksson, M. & Lehti, K. Fibroblasts in the tumor microenvironment: shield or spear? Int. J. Mol. Sci. 19, 1532 (2018).

67. Sun, Q. et al. The impact of cancer-associated fibroblasts on major hallmarks of pancreatic cancer. Theranostics 8, 5072 (2018).

68. Hessmann, E. et al. Fibroblast drug scavenging increases intratumoural gemcitabine accumulation in murine pancreas cancer. Gut 67, 497–507 (2018).

69. Provenzano, P. P. et al. Enzymatic targeting of the stroma ablates physical barriers to treatment of pancreatic ductal adenocarcinoma. Cancer Cell 21, 418–429 (2012).

70. Pries, A. R., Höpfner, M., Le Noble, F., Dewhirst, M. W. & Secomb, T. W. The shunt problem: control of functional shunting in normal and tumour vasculature. Nat. Rev. Cancer 10, 587–593 (2010).

71. Hesler, R. A. et al. TGF-β-induced stromal CYR61 promotes resistance to gemcitabine in pancreatic ductal adenocarcinoma through downregulation of the nucleoside transporters hENT1 and hCNT3. Carcinogenesis 37, 1041–1051 (2016).

72. Rice, A. J. et al. Matrix stiffness induces epithelial–mesenchymal transition and promotes chemoresistance in pancreatic cancer cells. Oncogenesis 6, e352–e352 (2017).

73. Abraham, S. A. et al. The liposomal formulation of doxorubicin. in Methods in enzymology 391, 71–97 (Elsevier, 2005).

74. Health, D. of. Contraindications and special considerations (Chapter 6). Immun. against Infect. Dis. Green B. (2006).

75. Salatin, S. & Yari Khosroushahi, A. Overviews on the cellular uptake mechanism of polysaccharide colloidal nanoparticles. J. Cell. Mol. Med. 21, 1668–1686 (2017).

76. Zhang, R., Qin, X., Kong, F., Chen, P. & Pan, G. Improving cellular uptake of therapeutic entities through interaction with components of cell membrane. Drug Deliv. 26, 328–342 (2019).

Appendix Improving selective targeting to cancer-associated fibroblasts by modifying liposomes with arginine based materials

Table S1. Connecting letters report for zeta potential for modified liposomes

Material							
O	A						
P	A						
D	A						
C	A						
B	A						
E		B					
K		B	C				
J			C	D			
N			C	D			
A			C	D			
M			C	D	E		
L			C	D	E		
UM			C	D	E		
H				D	E		
Q				D	E		
G					E		
F						F	
I							G

Levels not connected by the same letter are significantly different ($p<0.05$)

Table S2. Connecting letters report for diameter for modified liposomes

Material				
P	A			
Q	A			
I	A			
H	A			
K	A			
N	A	B		
M	A	B		
J	A	B		
L	A	B	C	
A	A	B	C	
UM	A	B	C	D
O		B	C	D
G		B	C	D
B		B	C	D
C			C	D
F				D
E				D
D				D

Levels not connected by the same letter are significantly different ($p<0.05$)

Table S3. Connecting letters report for internalization at 4 ºC in fibroblasts

Material						
I	A					
C	A					
J	A					
M	A					
K	A					
N	A					
A	A					
Q	A					
L	A	B				
O		B				
E			C			
B			C			
P				D		
UM				D		
H				D		
G					E	
D					E	
F					E	

Levels not connected by the same letter are significantly different ($p<0.05$)

Table S4. Connecting letters report for internalization at 4 ºC in myofibroblasts

Material					
N	A				
C	A				
P	A				
M	A				
Q	A				
A	A				
G	A				
B	A				
E	A	B			
O		B			
K			C		
D			C	D	
F				D	
L				D	
UM				D	
H				D	
J				D	
I					E

Levels not connected by the same letter are significantly different ($p<0.05$)

Table S5. Connecting letters report for internalization at 37 ^{o}C in fibroblasts

Material					
I	A				
C	A				
J	A				
M	A				
K	A				
N	A				
A	A				
Q	A				
L	A	B			
O		B			
E			C		
B			C		
P				D	
UM				D	
H				D	
G					E
D					E
F					E

Levels not connected by the same letter are significantly different ($p<0.05$)

Table S6. Connecting letters report for internalization at 37 ºC in myofibroblasts

Material							
L	A						
C	A	B					
M		B	C				
I			C	D			
Q				D			
P				D			
N				D			
B				D			
E				D			
G				D			
K				D	E		
H					E		
F					E		
A					E	F	
J						F	
D							G
UM							G
O							G

Levels not connected by the same letter are significantly different ($p<0.05$)

Table S7. Connecting letters report for IC_{50} of free doxorubicin (DOX) and DOX loaded liposomes for fibroblasts

Material					
F	A				
P	A	B			
O	A	B			
N	A	B			
Q	A	B			
DOX		B	C		
M			C		
C			C		
G				D	
B				D	
UM				D	
E				D	
J				D	
K				D	
D				D	
L				D	
A				D	E
H				D	E
I					E

Levels not connected by the same letter are significantly different ($p<0.05$)

Table S8. Connecting letters report for IC_{50} of free doxorubicin (DOX) and DOX loaded liposomes for myofibroblasts

Material						
M	A					
UM	A	B				
O		B				
B			C			
DOX			C			
G			C			
Q			C			
N			C			
J			C	D		
I			C	D		
C				D		
F				D		
P				D		
L					E	
K					E	F
H						F
D						F
A						F
E						F

Levels not connected by the same letter are significantly different ($p<0.05$)

CHAPTER 4. EVALUATING THE SYNERGY EFFECT OF VARIOUS IBUPROFEN-LOADED LIPOSOME CONCENTRATIONS IN COMBINATION WITH DOXORUBICIN-LOADED LIPOSOMES AGAINST MACROPHAGES AND THEIR PHENOTYPES

Tanzeel Ur Rehman [1,3], Susheel K. Nethi [2,3], Chris J. Cornelius [1,2], Surya K. Mallapragada [1,2,3]

1. Department of Materials Science & Engineering, Iowa State University, Ames, Iowa 50011

2. Department of Chemical & Biological Engineering, Iowa State University, Ames, Iowa, 50011

3. Nanovaccine Institute, Iowa State University, Ames, IA, 50011, USA

Modified from a manuscript to be submitted to the *International Journal of Pharmaceutics*

Abstract

This study aimed to investigate the synergistic effect of combination therapies of doxorubicin (DOX) and ibuprofen loaded in liposomes on macrophages and tumor-associated macrophage (TAMs) phenotypes to reduce the dosage of DOX needed for improved therapeutic efficacy. Both drugs were encapsulated in the liposomes separately and were characterized by their size and zeta potential. RAW 264.7 (MØ) macrophages were transformed to M1 and M2 phenotypes using lipopolysaccharide (LPS) and interleukin 4 (IL4). Both DOX-loaded liposomes (DLL) and ibuprofen-loaded liposomes (IBLL) were tested for their toxicity and efficacy on all three types of cells. Finally, 9 different concentrations of IBLL (5-750 µg/mL) were tested in combination with a constant concentration of DLL (25 µg/mL) to investigate the synergistic effects of DLL and IBLL. Out of the 9 combinations of IBLL and DLL concentrations, 550, 650, and 750 µg/mL IBLL in combination with 25 µg/mL DLL showed synergistic results with a

combination index value of < 1 for all three cell types. A combination of 450 µg/mL IBLL and 25 µg/mL DLL also showed synergistic effects for MØ. The findings suggest that the use of a combination of DOX and IBLL could be a potential strategy for cancer treatment.

4.1 Introduction

Cancer is a complex and devastating disease that affects millions of people worldwide. According to the American Cancer Society, there are almost 1.9 million new cases estimated in 2023 in the US alone, with 0.6 million cancer deaths [1]. Although chemotherapy is one of the most common treatments for cancer, it has several limitations, including toxicity, drug resistance, and low efficacy [160,161]. To overcome these limitations, researchers are constantly seeking new strategies to improve the efficacy and reduce the toxicity of chemotherapy drugs. One such breakthrough was made in 1995 when the Food and Drug Administration (FDA) approved the first liposomal Doxorubicin (DOX) injection, Doxil ® [162,163].

Doxorubicin is a widely used chemotherapy drug that has shown efficacy in the treatment of various types of cancer, including breast cancer, ovarian cancer, and leukemia [162]. However, DOX has several side effects, which limits its use in high doses [56,164,165]. A recent study by Brown et al. explained how DOX and chemotherapy could result in inflammation of the gut, liver, and central nervous system (CNS) [166]. Moreover, previous studies have indicated that DOX may induce inflammation by disrupting the regular cytokine regulation in both human and rodent models. Additionally, it has been observed to cause monocytic migration to regions of inflammation within the body and the (CNS) [167,168]. Therefore, there is a need to find new strategies to enhance the efficacy and reduce the toxicity of DOX, especially chemotherapy-induced inflammation.

In comparison with DOX, ibuprofen is a nonsteroidal anti-inflammatory drug (NSAID) that is commonly used to treat pain and inflammation. Ibuprofen has the ability to inhibit cyclooxygenase enzymes (COX-1 and COX-2) and has been the subject of research for several decades, revealing other potential therapeutic benefits [169]. Recent studies have shown that ibuprofen has anti-cancer properties and can enhance the efficacy of chemotherapy drugs. A study by Akrami et al. demonstrated that ibuprofen has an anti-proliferative effect on cancer stem cells derived from AGS and MKN-45 cells [170]. In another study, it was shown that ibuprofen was able to decrease the transcript levels of CD44 and OCT3/4, indicating the capability of ibuprofen to reduce the stemness of AGS cells, making it a promising candidate for an antitumor drug [171]. Furthermore, there have been reports that ibuprofen can reduce chemotherapy-induced inflammation and help inhibit cell migration [172,173]. Nonetheless, the potential of ibuprofen to reduce inflammation associated with cancer and serve as an anti-cancer drug is a recent development that necessitates further exploration.

Encapsulation of drugs inside liposomes is a well-established strategy to improve the efficacy and reduce the toxicity of chemotherapy drugs and small molecules. Liposomes are spherical vesicles composed of a phospholipid bilayer that can encapsulate both hydrophilic and hydrophobic drugs [174]. Liposomes can improve the bioavailability of drugs, increase their circulation time, and target them to specific cells and tissues [175]. To mitigate the side effects of DOX, various strategies have been employed, such as encapsulating DOX in the liposomal aqueous cavity [176]. Numerous studies have shown the potential of DOX and ibuprofen inside a liposomal cavity [177–182]. While this approach has shown promise in reducing the toxicity and side effects of DOX, it is important to note that the adverse effects of chemotherapy extend beyond inflammation, and other factors such as drug resistance and treatment-related cardiotoxicity

remain major obstacles to successful cancer treatment [183,184]. In addition, it is becoming increasingly clear that a combination therapy approach may be more effective in treating cancer compared to a single-drug strategy [185]. The use of ibuprofen as an adjuvant therapy to DOX in a liposomal formulation is an area of active research that holds promise for improving treatment outcomes and reducing toxicity [186,187]. Therefore, we hypothesize that the efficacy and safety would be enhanced by combining DOX and ibuprofen in a liposomal formulation, which could have significant implications for cancer treatment. We hypothesize that DOX-loaded liposomes (DLL) and ibuprofen-loaded liposomes (IBLL) can effectively target various cancer types. DLL can target tumor reduction and mitigation by inhibiting topoisomerase II, while IBLL can target cancer-related inflammation.

We chose to work with RAW 264.7 macrophages (MØ), a tumor-derived murine macrophage cell line, to investigate the effects of DLL and IBLL on macrophages and their phenotypes (M1 and M2 type). Depending on the stimuli present in their microenvironment, macrophages can polarize towards different phenotypes, including the classically activated M1 phenotype and the alternatively activated M2 phenotype [188,189]. M1 macrophages are pro-inflammatory immune cells and are responsible for promoting inflammation, phagocytosis of pathogens, and antigen presentation to initiate adaptive immunity[190]. On the other hand, the M2 macrophages are involved in tissue remodeling, wound healing, and immunoregulation [191]. However, in a tumor microenvironment, the M2 macrophages play a critical role in promoting tumor growth and progression by suppressing the immune response, promoting angiogenesis, and remodeling the extracellular matrix; they are often referred to as tumor-associated macrophages (TAMs) [192], [193].

While the primary function of M2 macrophages is to reduce inflammation and promote tissue healing by producing anti-inflammatory cytokines, their polarization towards TAMs in the presence of a tumor connects inflammation with cancer and stimulates the proliferation, invasion, and metastasis of tumor cells [194,195]. Moreover, TAMs encourage tumor angiogenesis and suppress the antitumor immune response mediated by T cells, ultimately promoting tumor progression [196,197]. TAMs have been shown to promote chemotherapy resistance and enhance tumor growth and metastasis through various mechanisms, such as secretion of growth factors and cytokines, extracellular matrix remodeling, and inhibition of immune responses [198,199]. Therefore, we examined the synergistic effects of DLL and IBLL on MØ, M1, and M2-type macrophages to determine their potential as immunotherapeutic agents. The goal of this study was to investigate whether the combination of DOX and ibuprofen-loaded liposomes (DLL and IBLL) could synergistically increase cell death in macrophages and their phenotypes. The aim was to potentially reduce the dosage of DOX needed and improve therapeutic efficacy. This combination therapy could be further developed as a targeted therapy agent in future studies.

This study investigated the synergistic relationship between DOX and ibuprofen combination therapies delivered in liposomal formulations. 1,2-Dioleoyl-sn-glycero-3-PE (DOPE) and 1,2-Dioleoyl-sn-glycero-3-PC (DOPC), two FDA-approved liposomal-based carriers were chosen for liposomal synthesis, as they have shown promise in the previous studies [101,102,200]. We encapsulated DOX and ibuprofen inside separate liposomes to avoid any potential interactions between the two drugs. Then, we tested the internalization and toxicity of these liposomes on MØ, M1, and M2 macrophages through flow cytometry and half-minimal inhibitory concentration (IC_{50}), respectively. Subsequently, one concentration of DLL and nine distinct concentrations of IBLL were chosen based on the toxicity and IC_{50} results. A synergy

study was conducted to investigate which concentrations of IBLL work in synergy with a fixed concentration of DLL. Promising results were seen as three different concentrations of IBLL demonstrated synergy with the fixed concentration of DLL. The results of this study have significant implications for the development of new and effective strategies to enhance the efficacy and reduce the toxicity of chemotherapy drugs. The potential of combining ibuprofen with doxorubicin liposomes to target cancer-related inflammation and reduce the stemness of cancer cells could open up new avenues for targeted cancer therapies. By understanding the mechanism of action of this combination therapy, we can develop more effective and less toxic approaches to cancer treatment, which could significantly improve the quality of life for cancer patients. For the rest of this article, we will refer to the naïve RAW 264.7 macrophages as MØ, LPS-transformed M1 macrophages as M(LPS), and IL4-transformed M2 macrophages as M(IL4).

4.2 Materials and Methods

4.2.1 Materials

1,2-Dioleoyl-sn-glycero-3-PE (DOPE) and 1,2-Dioleoyl-sn-glycero-3-PC (DOPC) were purchased from Cayman chemicals (Ann Arbor, MI). Doxorubicin (DOX) was purchased from LC Laboratories (Woburn, MA) and (S)-(+)-2-(4-Isobutylphenyl)propionic acid (Ibuprofen) was purchased from TCI America (Portland, OR). Interleukin 4 (IL4) was purchased from Biotechne (Minneapolis, MN) and Lipopolysaccharides (LPS) were purchased from eBiosciences, ThermoFisher Scientific (Waltham, MA). (3-(4,5-Dimethylthiazol-2-yl)-2,5-Diphenyltetrazolium bromide) (MTT), citric acid anhydrous, sodium hydroxide, hydrochloric acid, chloroform, and phosphate buffer saline (PBS) were purchased from Fisher Scientific (Hampton, NH). Dimethyl sulfoxide (DMSO) was purchased from VWR Scientific (Radnor, PA). Fresh deionized (DI) water (Milli-Q, Thermo Scientific Nanopure, Waltham, MA) was used throughout this study.

4.2.2 Methods

4.2.2.1 Synthesis of Doxorubicin-Loaded Liposomes (DLL)

Liposomes were synthesized using a previously reported thin film hydration method [200]. Briefly, 120 µM 1,2-Dioleoyl-sn-glycero-3-PE (DOPE) was dissolved in 15 mL chloroform in a round bottom flask (RBF). Subsequently, 60 µM 1,2-Dioleoyl-sn-glycero-3-PC (DOPC) was added to the same RBF. The organic solvent was evaporated using a rotary evaporator at 40^{o}C for 5 min. A thin layer of lipids was seen at the bottom of the RBF after the solvent was evaporated. This lipid layer was then rehydrated using DI water. The RBF with DI water was placed in a sonication bath for 15 min to rehydrate the lipid film fully. A milky white solution was formed. Finally, the liposomes were lyophilized and kept at -20 ^{o}C for further use.

Doxorubicin (DOX) was encapsulated in these liposomes and used as a model drug for this study. First, a 10 mg/mL DOX solution (in DI water) was prepared to load DOX into these liposomes. Then, 5 mg lyophilized liposomes were dissolved in 1 mL 150 mM citric acid (pH 4.0) and extruded 21 times through a 100 nm polycarbonate filter membrane using an Avanti Mini-Extruder (Avanti Polar Lipids, Inc., Alabaster, AL). Next, the pH of the liposome solution was adjusted to 7.4 using HCl and NaOH. The 10 mg/mL DOX solution and the liposome solution (pH 7.4) were kept at 65 ^{o}C for 10 min to equilibrate the temperature of the solutions. Subsequently, 100 µL DOX solution was added to the liposome solution and kept at 65 ^{o}C for an additional 45 min. Finally, the DOX-loaded liposomes (DLL) solution was centrifuged at 3000 rpm for 10 min; the supernatant (a) was removed carefully and tested for DOX loading efficiency while the liposomes were kept at -20 ^{o}C for cell culture use.

4.2.2.2 Synthesis of Ibuprofen-Loaded Liposomes (IBLL)

Ibuprofen-loaded liposomes (IBLL) were synthesized similarly as described above, with a few changes. 120 µM DOPE and 60 µM DOPC were dissolved in 15 mL chloroform in an RBF. 200 µM ibuprofen (41.2 mg dissolved in 5 mL chloroform) was dissolved in the same RBF, as mentioned in a previous study [181]. The organic solvent was evaporated at 40 ^{o}C for 5 min using a rotary evaporator. Similarly, a thin lipid film was seen at the bottom of the RBF, which was rehydrated using DI water. After sonication for 15 min, the liposome solution was centrifuged at 3000 rpm for 10 min, and the supernatant (b) was collected for drug loading studies.

The liposome solution was placed in a dialysis tube (3,500 mwco) and dialyzed overnight against DI water to remove the excess ibuprofen. Next, the liposome solution was extruded using a 100 nm polycarbonate filter membrane. Finally, the liposome solution was lyophilized, and the liposomes were kept at -20 ^{o}C for use in cell culture.

4.2.2.3 Drug Loading Efficiency

To measure the DOX loading efficiency in the liposomes, a standard calibration curve was made through serial dilution of 1 mg/mL DOX solution in a 96-well plate. To the same well plate, 100 µL supernatant (a) was added. The experiments were conducted in triplicate, and the plate was read using a SpectraMax M3 (Molecular Devices, San Jose, CA) plate reader at 470 nm with a reference at 630 nm. The DOX encapsulation efficiency (EE) was calculated using the following equation:

$$Encapsulation\ efficiency\ (\%) = \frac{(C_{start} - C_{supernatant})}{C_{start}} X\ 100\% \qquad (1)$$

where C_{start} is the concentration of DOX solution added to the liposomes and $C_{supernatant}$ is the concentration of the DOX in the supernatant (a). Similarly, the drug loading efficiency was also calculated for IBLL.

Ibuprofen loading efficiency in the liposomes was calculated in a similar way. A standard calibration curve was made using serial dilutions of 50 mg/mL ibuprofen solution in DI water in a 96-well plate. Next, 100 µL supernatant (b) was added in triplicate to the same plate. The plate was then read using the SpectraMax M3 plate reader at an absorbance and emission wavelength of 262 and 292 nm, respectively. The ibuprofen EE was calculated by

$$Encapsulation\ efficiency\ (\%) = \frac{(C_{start} - C_{supernatant})}{C_{start}} X\ 100\% \qquad (2)$$

where C_{start} is the concentration of Ibuprofen solution added to the RBF and $C_{supernatant}$ is the concentration of the ibuprofen in the supernatant (b).

4.2.2.4 Dynamic Light Scattering (size) and Zeta Potential of DLL and IBLL

To measure the size and zeta potential of unloaded liposomes, DLL, and IBLL, a 100 µL 1% w/v solution of each liposome solution was added to three test tubes containing 5 mL DI water. The solution was extruded through a 100 nm polycarbonate membrane filter using the Avanti Mini-Extruder. Next, the pH of these liposomal solutions was adjusted to 7.4 using HCl and NaOH; this was done to ensure that there was no interaction of the ions in the water with the liposomes during the experiment runs. These freshly extruded liposomes were tested for their size and zeta potential measurements using a Zetasizer Nano Z (Malvern Instruments Ltd, Malvern, UK).

4.2.2.5 Cell Lines and Culture

Macrophages (RAW 264.7, ATCC, Manassas, VA) were cultured at 37 ^{o}C with 5% CO_2 using complete medium. The complete medium consisted of Dulbecco's modified Eagle's medium (DMEM) supplemented with 10% fetal bovine serum (FBS), 1% penicillin, and 1% streptomycin. The cells were passaged every three to four days using a cell scraper and subcultured between ~ 6.4 x 10^3 and 2.7 x 10^4 cells per cm^2. The differentiation from naïve macrophages (MØ) to classically activated or pro-inflammatory macrophages (M1) was performed using 5 µg/mL LPS and herein referred to as M(LPS). The differentiation to alternatively activated or anti-inflammatory (proangiogenic) (M2) phenotype was carried out using 25 ng/mL IL-4, herein referred to as M(IL4).

4.2.2.6 Flow Cytometry

PE-labeled anti-NOS2 (iNOS) and FITC-labeled CD206 are known markers for M(LPS) and M(IL4), respectively. The abovementioned antibodies were used as markers to evaluate the polarization state of cultured macrophages. RAW264.7 (MØ, M(LPS), or M(IL4)) cells were passaged and grown in T75 flasks for 72 h. Subsequently, the cells were digested and rinsed with PBS. The cells were then incubated with iNOS antibody (eBioscience, USA) diluted with PBS at a ratio of 1:50 and FITC-conjugated anti-mouse CD206 antibody (eBioscience, USA) diluted with PBS at a ratio of 1:400 at 4 °C for 30 minutes in the dark. RAW264.7 cells seeded on culture plates were used as a negative control. After being rinsed thrice with PBS, the labeled cells were analyzed using a flow cytometer (Beckman, USA).

4.2.2.7 Cell Viability Assay

Cell viability of unloaded liposomes was measured to confirm that the liposomes are not toxic to the cells. For this reason, MØ, M(LPS), and M(IL4) were seeded at a density of 5 x 10^4 cells/cm^2 in a 96-well plate (Corning, Somerville, MA) and were allowed to grow for 24 h.

Subsequently, the media was carefully aspirated, and 100 µL of unloaded liposomes (250 µg/mL) diluted with the complete medium was added to the cells. A positive control of cells without liposomes and a negative control of liposomes in the absence of cells were also present. The experiment was performed in triplicate. The plate was incubated at 37 ^{o}C for 48 h. The cell viability was then determined using a methyl thiazol tetrazolium (MTT) assay. The complete medium from each well was carefully replaced with a 100 µL solution of MTT (0.5 mg/mL), and the plate was incubated for an additional 2 h at 37 ^{o}C. The MTT forms insoluble purple formazan crystals after metabolism in living cells that could be used for cell viability determination. Subsequently, 85 µL media was carefully removed from each well, and the same amount of DMSO was added to each well to dissolve the purple formazan crystals. The plate was then read at 570 nm with a reference of 630 nm with a plate reader.

4.2.2.8 Half Maximal Inhibitory Concentration (IC_{50})

Naïve macrophages (MØ), M(LPS), and M(IL4) were seeded onto a 96-well plate at a density of 5 x 10^4 cells/cm^2 in complete medium for 24 h at 37 ^{o}C. Cells without liposomes served as positive controls, and liposomes in the absence of cells served as negative control. A serial dilution of DLL and IBLL, starting at 250 µg/mL and 1 mg/mL, respectively, were added to the cells. Free DOX solution (50 µg/mL) and free ibuprofen solution (1 mg/mL) with serial dilutions were also added to calculate their half-minimal inhibitory concentration (IC_{50}) values. The plates with liposomes, free DOX, and free ibuprofen with cells were then incubated for 48 h at 37 ^{o}C.

Next, an MTT assay was performed as described above. Four replicates were obtained for each experiment; the data were normalized to the positive controls. Subsequently, a sigmoidal dose-response curve was used to calculate the IC_{50} values for DLL, IBLL, free DOX, and free ibuprofen, shown in equation (3):

$$y = A_2 + \frac{A_1 - A_2}{1 + \left(\frac{x}{x_o}\right)^p} \qquad (3)$$

where A_1 is the upper limit of the dose curve, A_2 is the lower limit, p is the steepness of the curve, and x_o is the IC_{50}. The IC_{50} values were calculated using Origin(Pro) version 2019 (OriginLab Corporation, Northampton, MA).

4.2.2.9 Synergy Studies

Since the study aimed to identify the synergistic concentrations of IBLL with DLL, based on the IC_{50} values, a fixed concentration of 25 µg/mL concentration of DLL was chosen. A range of values for IBLL was determined based on the IC_{20}, IC_{50}, and IC_{80} values. Nine different concentrations of IBLL were selected: (i) 5 µg/mL, (ii) 50 µg/mL, (iii) 150 µg/mL, (iv) 250 µg/mL, (v) 350 µg/mL, (vi) 450 µg/mL, (vii) 550 µg/mL, (viii) 650 µg/mL, and (ix) 750 µg/mL. As described above, cell viability studies were conducted for given concentrations of IBLL, as well as a constant concentration of 25 µg/mL DLL. Furthermore, combinations of 9 different IBLL concentrations with a fixed DLL concentration of 25 µg/mL were also evaluated for their respective cell viability values. Quadruplicates of each concentration and combinations were carried out. Compusyn® was used to calculate the synergy studies of DLL and IBLL.

The selected concentrations of IBLL (5 – 750 µg/mL) and DLL (25 µg/mL) were tested for their cell viability values separately and also in combination. The combination index (CI) graph is a tool used to assess the degree of synergy or antagonism between two or more drugs or treatments. The cell viability values were inserted in Compusyn software. The x-axis of the

graph is labeled as “Fa”, which stands for fraction affected and represents the percentage of cells affected by the treatment or drug combination. The y-axis of the graph represents the CI value, which is calculated using the formula:

$$CI = \frac{(D)_1}{(D_x)_1} + \frac{(D)_2}{(D_x)_2} \qquad (4)$$

where $(D_x)_1$ and $(D_x)_2$ are the concentrations of drug 1 and drug 2 alone that achieve the same level of effect (Fa) as the combination of the two drugs at a certain concentration $(D)_1$ and $(D)_2$. A CI value of less than 1 indicates synergy, a CI value of 1 indicates additivity and a CI value greater than 1 indicates antagonism. The graph allows for a visual assessment of the degree and direction of interaction between the treatments at different levels of effect.

For DLL, IC_{20}, IC_{50}, and IC_{80} values were added to Compusyn® as’ treatment 1’ in the software. For IBLL, the cell viability values against the above-stated 9 concentrations were added as ‘treatment 2’ in the software. Finally, a combination of IC_{50} value of DLL and 9 different concentrations of IBLL was added, and the test was run. The combination index plot was used to determine the synergistic concentrations; the combinations resulting in a value below 1 were considered synergistic, while the combinations resulting in a value above 1 were considered antagonistic.

4.2.2.10 Statistical Analyses

All experiments were performed in quadruplicate, and data are expressed as mean ± standard deviation (SD). Tukey’s honest significant test was performed to analyze pairwise comparisons. The results were considered statistically significant at $p<.05$. The pairwise comparison was performed for the IC_{50} values of DLL, IBLL, free DOX, and free ibuprofen against MØ, M(LPS), and M(IL4). Moreover, the pairwise comparison was carried out for the cell viability of 9 different concentrations of IBLL alone and in combination with DLL.

4.3 Results

4.3.1 Liposome Characterization

1,2-Dioleoyl-sn-glycero-3-PE (DOPE) and 1,2-Dioleoyl-sn-glycero-3-PC (DOPC) liposomes were synthesized using the thin film hydration method. Doxorubicin (DOX) is an amphipathic chemotherapeutic drug and can be easily encapsulated in the aqueous cavity of liposomes. Therefore, DOX was used as a model drug and loaded inside the liposomes through the pH gradient created by citrate inside and outside the liposomes. This pH gradient loading method is a well-established DOX loading method [201,202]. Through this method, DOX was encapsulated in the liposomes at an encapsulation efficiency of 97.6 ± 3%.

In contrast, ibuprofen, a nonsteroidal anti-inflammatory drug (NSAID), is highly insoluble in water. Hence, encapsulating ibuprofen inside liposomes is an effective way to deliver this drug. The ibuprofen was dissolved in an organic solvent along with the lipids and was rehydrated after complete evaporation of the organic solvent. The liposomes were then dialyzed and filtered through a 100 nm polycarbonate filter membrane. The amount of ibuprofen not loaded in the liposomes was determined using a plate reader, and the resulting liposomes had an encapsulation efficiency of 80.7 ± 4%.

The size and zeta potential of liposomes are crucial factors that influence their cellular uptake. We measured the size and zeta potential of DLL, IBLL, and blank liposomes using a Zetasizer Nano Z. The DLL showed a size of 110 ± 5 nm, while the IBLL and blank liposomes showed sizes of 102 ± 7 nm and 105 ± 4 nm, respectively. There was no significant difference in the size of the liposomes. Similarly, the zeta potential values for DLL, IBLL, and blank liposomes were -17.5 ± 1.5, -19.1 ± 1.9, and -18.2 ± 0.9 mV, respectively, with no significant differences among the liposomes. *Table 4.1* summarizes the drug loading encapsulation efficiency, size, and zeta potential values of the liposomes.

Table 4.1: Characterization of doxorubicin-loaded liposomes, ibuprofen-loaded liposomes, and blank liposomes.

	Size (nm)	Zeta potential (mV)	Encapsulation efficiency (%)
DLL	110 ± 5	-17.5 ± 1.5	97.6 ± 3
IBLL	102 ± 7	-19.1 ± 1.9	80.7 ± 4
Blank liposomes	105 ± 4	-18.2 ± 0.9	- -

.3.2 Lipopolysaccharide (LPS) and Interleukin 4 (IL4) Induce the Polarization of Naïve Macrophages to M(1) and M(2) Phenotype

Macrophages are versatile immune cells that can polarize into two distinct subtypes, M1 and M2, depending on the microenvironmental cues they receive. The classical activation of macrophages, M1 polarization, is induced by microbial products such as lipopolysaccharide (LPS) and pro-inflammatory cytokines such as interferon-gamma (IFN-γ) [203,204]. M1 macrophages are characterized by high expression of pro-inflammatory cytokines, reactive oxygen, and nitrogen species and exhibit strong microbicidal and tumoricidal activity. On the other hand, M2 polarization, also known as alternative activation, is induced by anti-inflammatory cytokines such as interleukin-4 (IL-4) and IL-13, and is characterized by high expression of scavenger receptors, anti-inflammatory cytokines, and tissue remodeling factors. M2 macrophages are involved in tissue repair and remodeling and play a critical role in maintaining tissue homeostasis [203,205]. Although the M2 macrophages used in this study are regular M2 phenotypes, they have the potential to transform into tumor-associated macrophages (TAMs) in a tumor microenvironment, where they promote tumor growth and progression by stimulating angiogenesis, suppressing antitumor immunity, and remodeling the extracellular matrix [194,206].

Here, we differentiated macrophages into M(LPS) and M(IL4) subtypes by treating them with LPS and IL-4, respectively. To confirm the polarization state of macrophages, we used specific antibodies against iNOS and CD206, known markers for M(LPS) and M(IL4), respectively. The cells were stained with PE-labeled anti-Nos2 and FITC-labeled CD206, and tested through flow cytometry to evaluate if the cells were converted to M(LPS) and M(IL4) cells. The results showed that the addition of LPS or IL-4 to M(Ø) polarized the cells into M(LPS) or M(IL4) subtypes, respectively, as confirmed by **Figure 4.1**, which shows the fold of changes in the expression of specific markers. **Figure 4.1(a)** displays that M(LPS) results in 5.92 ± 0.2 folds of changes compared to M(Ø), while **Figure 4.1(b)** demonstrates that M(IL4) shows 6.32 ± 0.3 fold of changes compared to M(Ø). Both of these values are significantly higher compared to both MØ and M(LPS)/M(IL4).

4.3.3 3 Cytotoxicity comparison of Doxorubicin-loaded Liposomes (DLL) and Ibuprofen-loaded Liposomes (IBLL) against free Doxorubicin and free Ibuprofen

Macrophages (RAW 264.7) and their phenotypes were used throughout this study. All cytotoxicity experiments were performed on naïve macrophages (M(Ø)), classically activated macrophages, M(LPS), and alternatively activated (proangiogenic) macrophages, M(IL4). First, the cell viability of blank liposomes was tested on all three phenotypes to make sure that the liposomes, on their own, do not cause any cytotoxic effects, assuring that all the cytotoxic results for the later experiments are the result of the encapsulated drug inside the liposomes. The blank liposomes resulted in cell viability of 91 ± 3, 93 ± 5, and 93 ± 4% for M(Ø), M(LPS), and M(IL4), respectively. No significant difference was seen among these values.

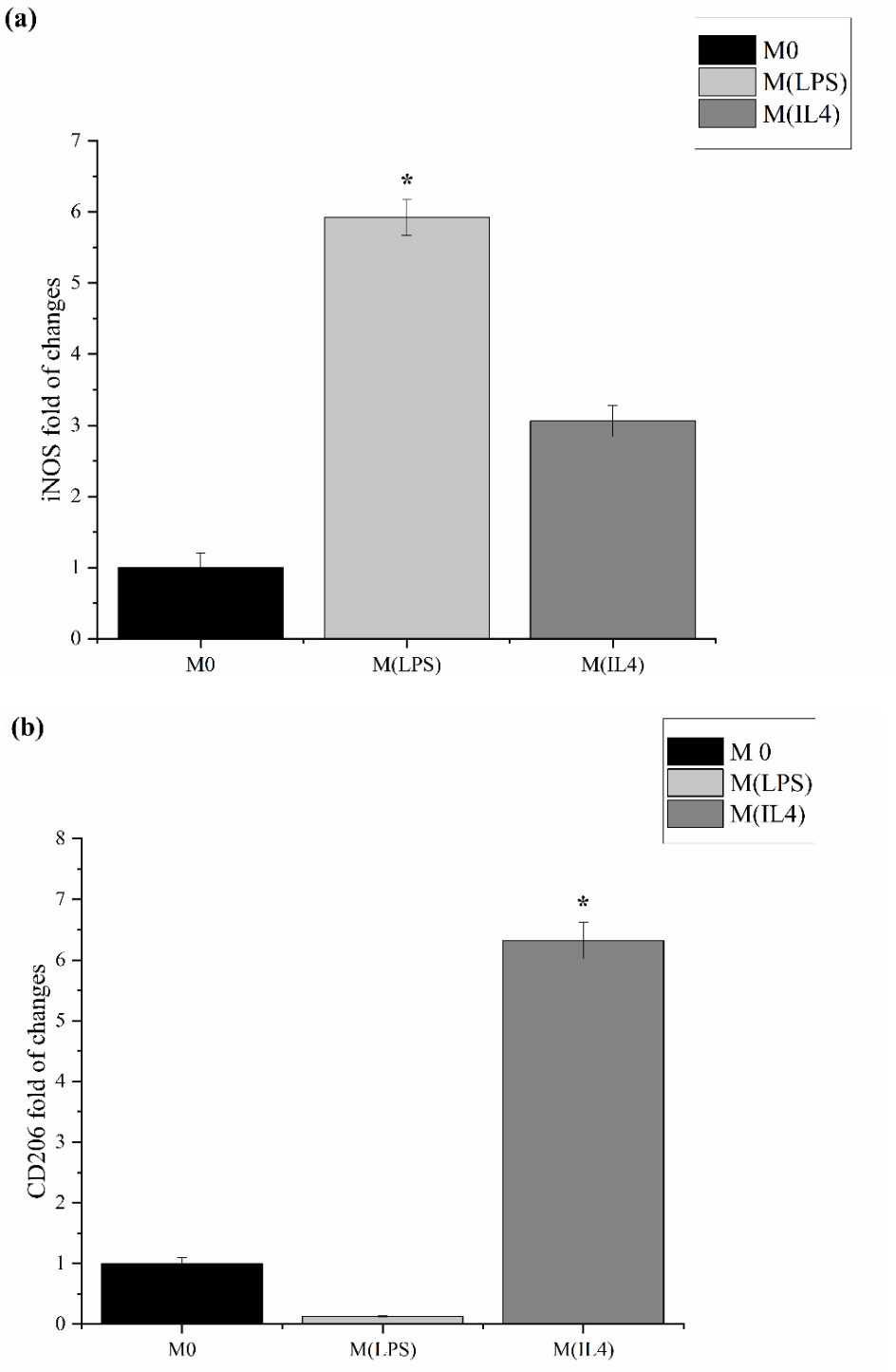

Figure 4.1: *Expression of (a) iNOS2 and (b) CD206 was significantly greater for M(LPS) and M(IL4), respectively. Detection of cell polarization was performed by flow cytometry assay. Statistical analysis through two-way ANOVA and Tukey's HSD post-hoc test. * represent p< .05 for (a) M(LPS) and (b) M(IL4) compared to M(Ø).*

The half-minimal inhibitory concentration (IC_{50}) is a commonly used metric in drug development to determine the potency of an antagonist drug. It represents the concentration of a drug that is required to achieve half-maximal inhibition of a specific biological process. This value can provide important information on the efficacy of a drug and can be used to compare the potency of different drugs. IC_{50} values of DLL and IBLL against M(Ø), M(LPS), and M(IL4) were calculated to determine the concentrations of DLL and IBLL to use for the synergistic studies. A serial dilution of DLL starting at 250 µg/mL and IBLL at 1000 µg/mL was performed on M(Ø), M(LPS), and M(IL4) macrophages. The cells were treated with liposomes for 48 h and then assayed using an MTT assay. The results were plotted on a dose-response curve using Origin(Pro) software. The IC_{50} values of DLL were 4.79 ± 1.26, 3.17 ± 1.16, and 5.37 ± 1.29 µg/mL for M(Ø), M(LPS), and M(IL4), respectively. The IC_{50} values of IBLL were 597 ± 43, 630 ± 37, and 550 ± 23 µg/mL for M(Ø), M(LPS), and M(IL4), respectively. The IC_{50} values of free DOX were 1.70 ± 0.14, 0.78 ± 0.16, and 0.93 ± 0.15 µg/mL and the IC_{50} values of free ibuprofen were 261 ± 21, 223 ± 16, and 214 ± 18 µg/mL for M(Ø), M(LPS), and M(IL4), respectively. Only free DOX IC_{50} showed a statistically significant higher value for M(Ø) compared to M(LPS) and M(IL4). For all other IC_{50} values, no significant differences were seen within the same groups.

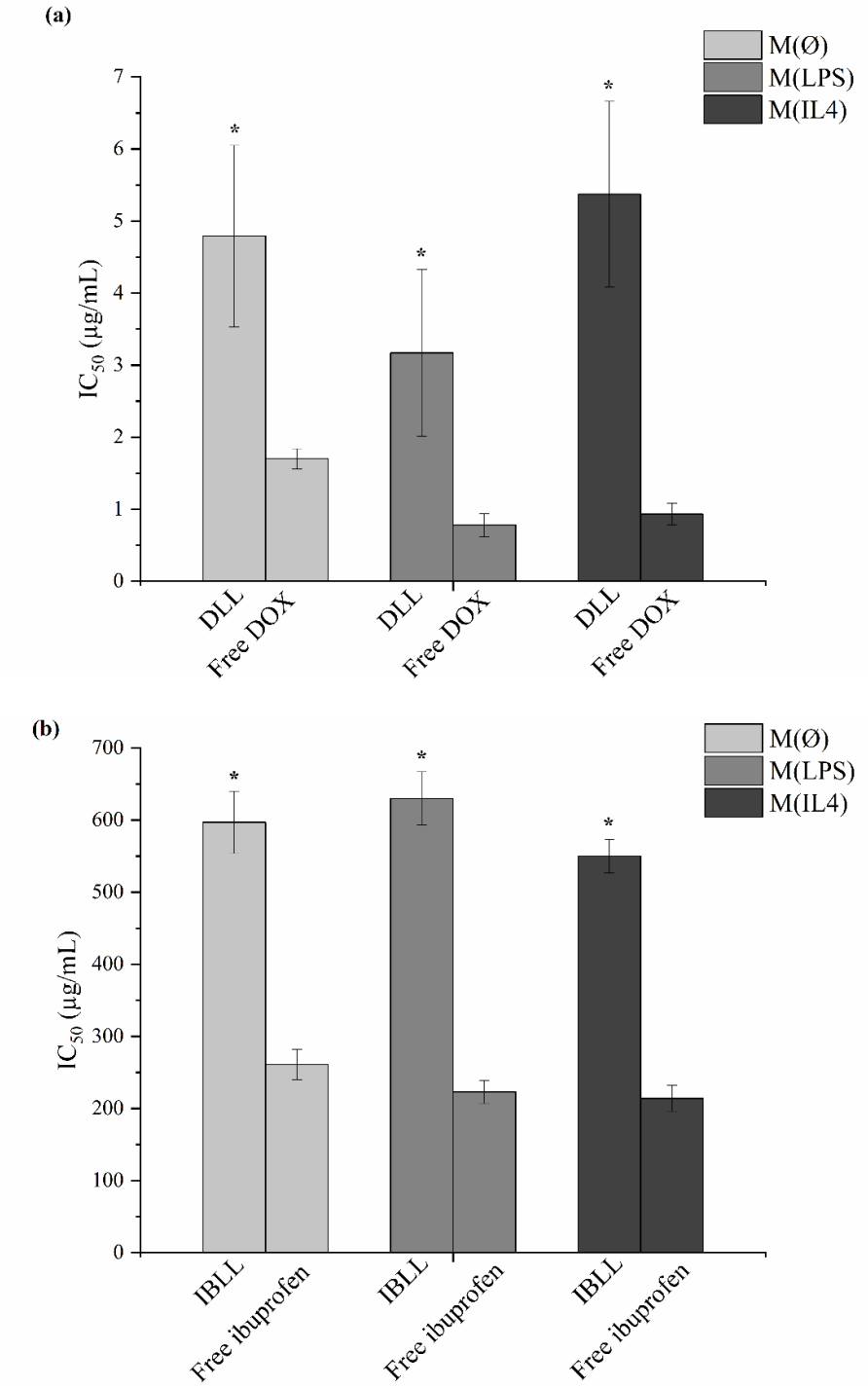

Figure 4.2: *IC50 values of (a) DLL & free DOX, & (b) IBLL & free ibuprofen against M(Ø), M(LPS), and M(IL4). Data represent the mean value of four replicates for each sample ± standard deviation. Statistical analysis through two-way ANOVA and Tukey's HSD post-hoc test. * represent p< .05 for IC50 values of DLL or IBLL compared to the IC50 values of free DOX or free ibuprofen, respectively.*

Figure 4.2 (a) shows the IC_{50} data for DLL and free DOX against M(Ø), M(LPS), and M(IL4), while **Figure 4.2 (b)** presents the IC_{50} data for IBLL and free ibuprofen against M(Ø), M(LPS), and M(IL4). Quadruplicates of each experiment were performed; the mean and standard deviation were calculated. The '*****' on the figure indicates that there was a statistically significant difference ($p<0.05$) between the IC_{50} of DLL or IBLL compared to the IC_{50} value of free DOX or free ibuprofen, respectively.

Furthermore, the IC_{20} and IC_{80} values for IBLL were also calculated against M(Ø). These values were calculated to determine what combinations of IBLL to use with DLL for the synergy studies. The IC20 and IC80 values for IBLL against M(Ø) were 643 ± 18 and 153 ± 17 µg/mL, respectively. The combinations were chosen to cover a range of IBLL concentrations ranging from 5 to 750 µg/mL with a constant concentration of 25 µg/mL for DLL. Nine different combinations were chosen for the synergy studies and are listed in *Table 4.2*. These combinations were used to determine the effect of varying the concentration of IBLL on the synergistic effect of DLL and IBLL.

4.3.4 Synergistic Studies of Various Ibuprofen-loaded Liposomes (IBLL) with Doxorubicin-loaded Liposomes (DLL)

To determine the impact of varying IBLL concentrations when combined with DLL, several MTT assays were conducted on three different sample groups: M(Ø), M(LPS), and M(IL4). These assays involved testing the 9 different IBLL concentrations, a constant concentration of 25 µg/mL DLL, and the combination of each IBLL concentration with the constant DLL concentration. **Figure 4.3** shows the percentage cell viability for these combinations and stand-alone concentrations for **(a)** M(Ø), **(b)** M(LPS), and **(c)** M(IL4).

Table 4.2: list of 9 different concentrations chosen for the synergy studies

Varying concentrations of IBLL (µg/mL)	Fixed concentration of DLL (µg/mL)
750	25
650	25
550	25
450	25
350	25
250	25
150	25
50	25
5	25

Looking at the cell viability values, it was seen that for M(Ø), the percentage cell viability for all IBLL and DLL combinations, except 750 and 650 µg/mL IBLL + 25 µg/mL DLL, resulted in statistically significantly lower values when compared to the percentage cell viability of IBLL only; these statistically significant differences are donated by '*****' with $p<0.05$, seen in **Figure 4.4**. When the same statistical test was performed to compare the percentage cell viability values of the combinations compared to the DLL only, it was seen that all values were statistically significantly lower, except 5 µg/mL IBLL + 25 µg/mL DLL; these statistical differences are shown in **Figure 4.4** using '†'.

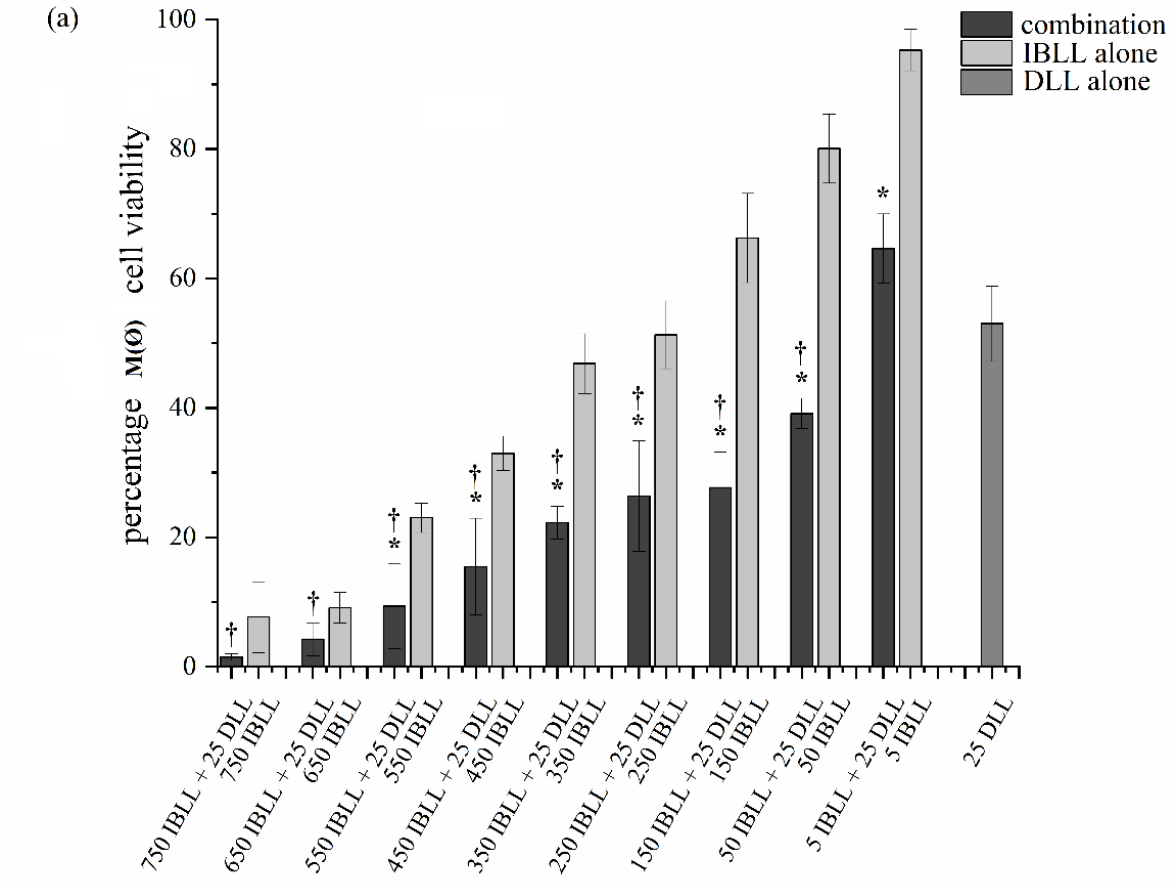

Figure 4.3*: Percentage cell viability of 25 µg/mL DLL, 9 combinations of IBLL, and the combination of 25 µg/mL DLL with 9 different concentrations of IBLL against* ***(a)*** *M(Ø),* ***(b)*** *M(LPS), and* ***(c)*** *M(IL4). Data represent the mean value of four replicates for each sample ± standard deviation using pairwise comparison.* ******* *indicates p< .05 for combinations values compared to cell viability from IBLL only, using pairwise comparison. † donates p< .05 for cell viability values compared to 25 µg/mL DLL alone.*

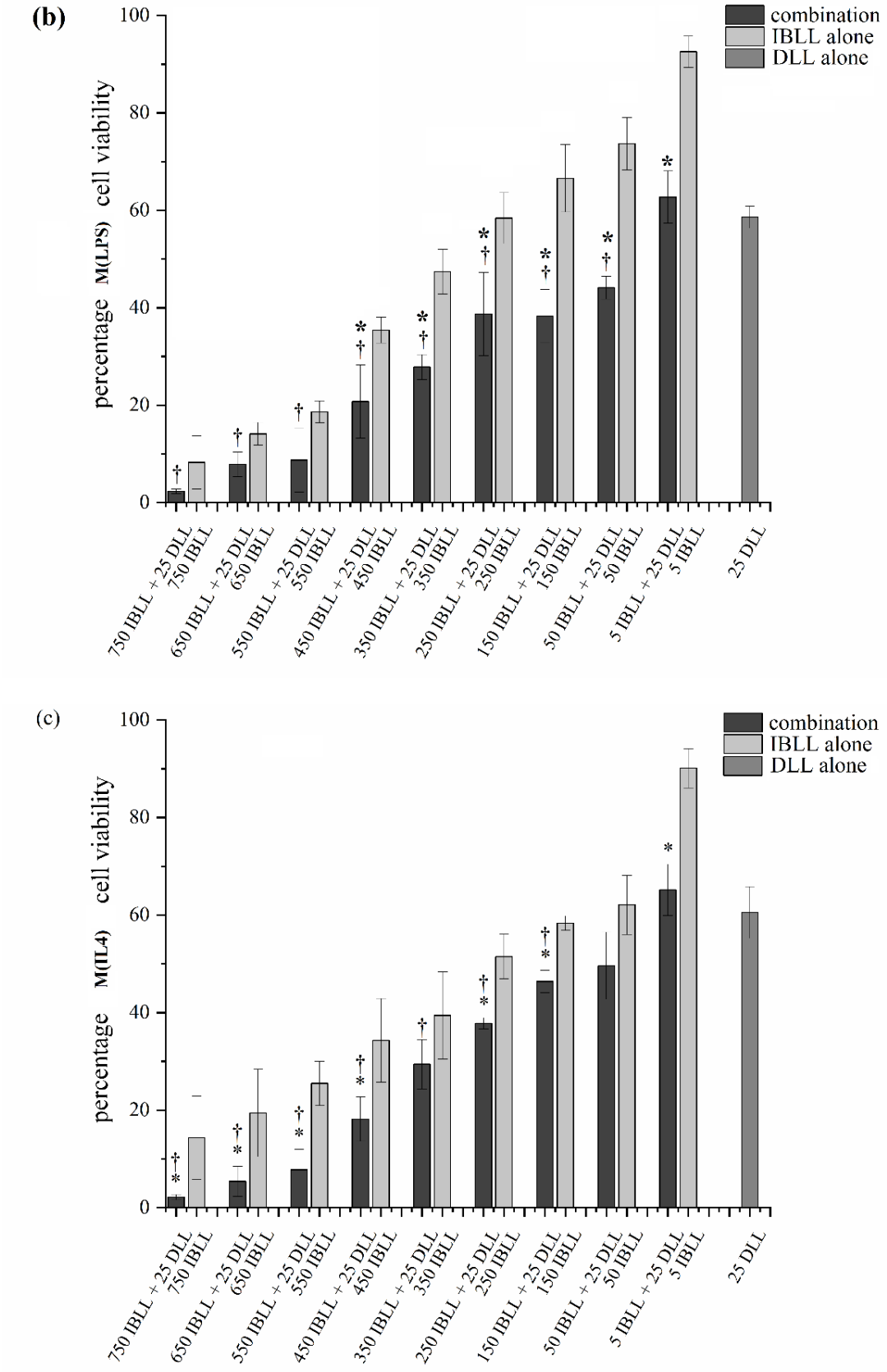

Figure 4.3 continued

Similarly, for M(LPS), all combinations except 750 and 650 µg/mL IBLL + 25 µg/mL DLL showed statistically significantly lower values compared to IBLL only, donated by '*****'. Likewise, all percentage cell viability values were statistically significantly lower, except 5 IBLL + 25 DLL, compared to DLL only, labeled by '†'. The percentage cell viability for M(IL4) showed similar results with a few exceptions. Interestingly, all combinations showed a significantly statistically lower percentage cell viability value for the combination except only 50 µg/mL IBLL + 25 µg/mL DLL, which are denoted by '*****' in **Figure 4.4**. On the other hand, similar results were seen for the statistically significant differences between the combination percentage cell viability values compared to the DLL alone, with a statistically significant difference observed in all values except for combinations of 50 and 5 µg/mL IBLL with 25 µg/mL DLL. These differences are donated by '†' in **Figure 4.4.**

In order to determine the synergistic effects of drugs, it is common to use the combination index (CI) method, which compares the efficacy of the drug combination to the expected efficacy if the drugs were acting independently. A CI value of less than 1 indicates synergism, while a CI value greater than 1 indicates antagonism. By measuring the CI of different drug combinations, researchers can determine which combinations are likely to produce the most effective therapeutic outcomes. Therefore, the CI graphs were used to visualize the results for the synergy studies in this study, as seen in Figure 4.4. The CI (y-axis) was plotted against the fraction affected (Fa, x-axis). The Fa values represent the percentage of cells affected by the treatment or drug combination. It is also known as the "effect level" and is expressed as a fraction of the total cell population. The Fa value ranges from 0 to 1, where 0 indicates no effect (all cells are alive and unharmed), and 1 indicates complete effect (all cells are dead or affected

by the treatment). The Fa values are usually calculated based on a specific endpoint, in this case, cell viability. The Fa values are used to calculate the CI values and determine the degree of synergy or antagonism between the drugs or treatments being tested.

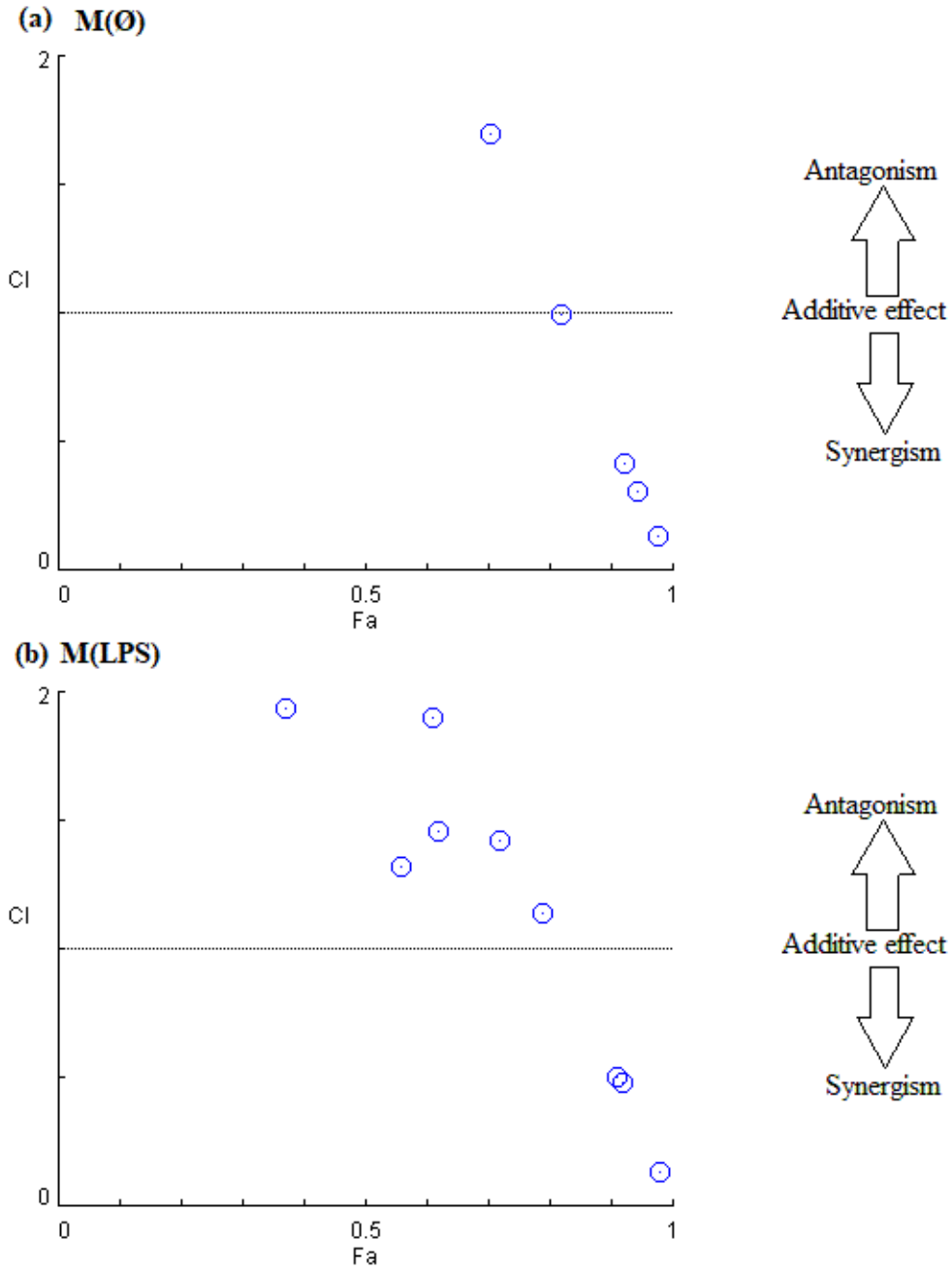

Figure 4.4: Combination index plots of synergy studies using a combination of 9 IBLL concentration with 25 µg/mL DLL for **(a)** M(Ø), **(b)** M(LPS), and **(c)** M(IL4). Y-axis represents the combination index (CI), whereas the x-axis shows the fraction affected (Fa). CI value < 1 indicates synergy, a CI value = 1 indicates additivity, and a CI value > 1 indicates antagonism.

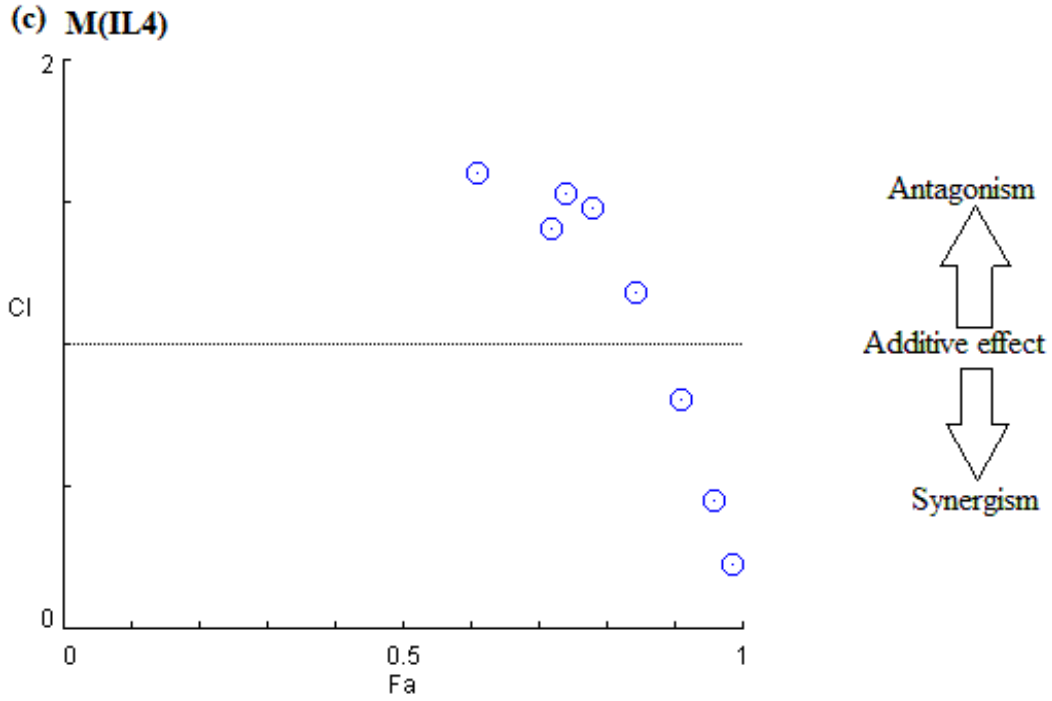

Figure 4.4 continued

It is demonstrated that the combinations of 750, 650, and 550 µg/mL IBLL, with the constant concentration of 25 µg/mL DLL, showed synergistic effects for M(Ø), M(LPS), and M(IL4). In addition, the combination of 450 µg/mL IBLL and 25 µg/mL DLL showed a synergistic effect for M(Ø) with a CI value of 0.99445.

4.4 Discussion

Doxorubicin (DOX) is a well-known chemotherapeutic drug that is used alone or in combination with other drugs for treating a myriad of cancers, including sarcomas, carcinomas, and hematological cancers [207–210]. Whether the tumor is located in the breasts, prostate, ovary, stomach, or liver, DOX has been proven to treat cancers in numerous organs [211–216]. Additionally, in recent years, the role of ibuprofen as an anti-cancer drug has shown promise. A recent study by Pashapour et al. demonstrated that the cell viability of liver cancer cells (HepG2) could be significantly decreased using 1 and 10 mg/mL ibuprofen for 24 h and using 0.001, 0.1, 1, and 10 mg/mL ibuprofen for 72 h [217]. Moreover, Yurtdaş-Kırımlıoğlu et al. reported that ibuprofen-

loaded Eudragit® is a suitable agent for human lung adenocarcinoma cells (A549) [218]. Therefore, in this study, a combination of both DOX and ibuprofen-loaded liposomes was used to examine the synergistic effect of these two drugs.

Loading a drug in the aqueous cavity of liposomes is a relatively easy and efficient process. Typically, there are two loading routes, active and passive loading [219]. DOX was encapsulated in the liposomes using active loading performed through the pH difference between the inside and outside of the liposome cavity. Through the active method, the encapsulation efficiency is higher (>95%) in liposomes [219]. Loading of DLL resulted in an encapsulation efficiency of 97.6 ± 3% in our studies. On the other hand, the passive loading method is a more straightforward method in which the drug is added to the dry lipid layer before hydration; this results in a slightly lower drug loading [220]; our IBLL loading studies, using the passive loading method, resulted in 80.7 ± 4% EE.

Size and zeta potential are two important characteristics of liposomes that affect their cellular uptake [200,221,222]. It is widely known that to capitalize on the enhanced permeability and retention (EPR) effect, the particle size should be smaller than 400 nm [143,144,223]. According to Yoshikawa and Liu, a smaller liposome size (~100 nm) leads to even better cellular uptake [223,224]. Moreover, a negative surface charge of the liposomes is preferred for cellular uptake. When liposomes have a negative charge, they can become coated with proteins, making it easier for them to enter cell membranes through absorptive endocytosis. This makes it more efficient for the cells to take up the liposomes [139]. Furthermore, our previous study has shown a positive correlation between negatively charged liposomes and increased toxicity [200]. Once the liposomes were encapsulated with either DOX or ibuprofen, they were rigorously tested for their size and zeta potential values. To ensure consistency in the size of our liposomes for this study, we used a

100 nm polycarbonate filter to make them fairly monodisperse in size at around 100 nm. Additionally, we made our liposomes negatively charged by using DOPE:DOPC liposomes that have negatively charged ends. Our DLL resulted in a size of 102 ± 7 nm with a zeta potential value of -17.5 ± 1.5 mV, while IBLL and BL produced liposomes with sizes of 102 ± 7 nm and 105 ± 4 nm, respectively, with zeta potential values of -19.1 ± 1.9 and -18.2 ± 0.9 mV, respectively.

Because one of our goals was to observe the synergistic effects of DOX and ibuprofen on tumor-associated macrophages (TAMs), we chose to work with RAW 264.7 cells. These mouse macrophages can easily be transformed from naïve macrophages (MØ) into classically activated (M(LPS)) or alternatively activated (M(IL4)) macrophages using LPS and IL4, respectively [103]. Alternately activated macrophages, also known as M2 phenotype, exhibit similar properties to TAMs and are known to transform into TAMs in tumor microenvironments [206,225,226]. To confirm the transformation of MØ to M(LPS) and M(IL4), known markers for M1 and M2 were chosen and added to the cells. The results were observed under a fluorescent microscope and also through flow cytometry.

NOS2, also known as inducible nitric oxide synthase, is a marker closely associated with the M1 polarization of macrophages [227]. M1 macrophages typically have a pro-inflammatory phenotype and are involved in the clearance of pathogens and cancer cells. NOS2 expression is upregulated in response to pro-inflammatory stimuli such as interferon-gamma (IFN-γ) and lipopolysaccharides (LPS) and is involved in the production of nitric oxide (NO), a molecule that can mediate antimicrobial and antitumor activity [228]. In our results, we observed that M(LPS) showed 5.92 ± 0.2 folds of changes compared to M(Ø), which is consistent with the results seen in the literature [229,230]

On the other hand, CD206, also known as macrophage mannose receptor 1 (MRC1), is a widely used marker for alternatively activated or M2 macrophages [203,231]. M2 macrophages typically have an anti-inflammatory phenotype and are involved in tissue repair and remodeling. CD206 is a scavenger receptor that is involved in the clearance of glycoproteins and plays a role in modulating the immune response to pathogens and cancer cells. In this study, the M(IL4) resulted in 6.32 ± 0.3 fold of changed compared to M(Ø); these results are supported by the literature [230,232].

Overall, the expression of NOS2 and CD206 can serve as useful markers for distinguishing between the M1 and M2 subtypes of macrophages, respectively. As expected, the results from flow cytometry and immunocytometry confirmed that using LPS, the M(Ø)s were converted to the M1 phenotype, and through the use of IL4, M(Ø)s were transformed to the M2 phenotype.

The half-maximal inhibitory concentration (IC_{50}) is a commonly used method for evaluating the cytotoxicity of drugs or particles. This technique provides valuable information about the efficacy and potency of a drug. The IC_{50} is defined as the concentration of a drug that is required to inhibit a biological process by 50%. In pharmacological research, IC_{50} is often used as a measure of a drug's potency as an antagonist. This information is critical for identifying promising drug candidates and optimizing drug dosing in clinical settings. Therefore, IC_{50} is widely considered to be the most informative measure of a drug's efficacy [233–236].

The primary goal of this study was to determine the concentrations at which DLL and IBLL most effectively inhibit the growth of cells and show maximum synergy. To achieve this goal, first, we calculated the IC_{50} values of DLL and IBLL, which resulted in 4.79 ± 1.26, 3.17 ± 1.16, and 5.37 ± 1.29 µg/mL for M(Ø), M(LPS), and M(IL4), respectively, and 597 ± 43, 630 ±

37, and 550 ± 23 µg/mL for M(Ø), M(LPS), and M(IL4), respectively. Based on the resulting values, the DLL concentration was chosen to be 25 µg/mL, as the DOX was loaded in the liposomes at a ratio of 5:1 (liposomes:DOX). Hence, a 25 µg/mL DLL solution contains 5 µg/mL DOX, which is a reflection of its IC_{50} value.

Similarly, we wanted to investigate the effects of IBLL at a range of concentrations that were wider than just the IC_{50} value. To accomplish this, we selected a range of concentrations that covered not only the IC_{50} but also the IC_{20} (643 ± 18 µg/mL) and IC_{80} (153 ± 17 µg/mL) values for IBLL. The IC_{50} value of ibuprofen against macrophages can be influenced by various factors such as the cell line, experimental conditions, and assay method. This study supported the literature-reported IC_{50} values for ibuprofen. Wang et al. and Ouyang et al. recorded IC_{50} values of 668 µg/mL and 520 µg/mL, respectively, for RAW 264.7 macrophages, which were consistent with the IC_{50} value calculated in this study [237,238]. However, Boonnak et al. reported a significantly lower IC_{50} value of 110 µg/mL, which may be attributed to differences in the experimental conditions and methodology [239]. Boonnak used the Griess reagent assay and a smaller cell density (1 x 105 cells/well), which could have contributed to the lower IC_{50} value. Overall, the IC_{50} value of ibuprofen against macrophages should be interpreted cautiously, considering the various factors that can impact the measurement of IC_{50} values.

To ensure that we covered these values as well as some concentrations beyond these, we selected a range of IBLL concentrations starting from 5 µg/mL to a maximum of 750 µg/mL. The interval between each concentration was set to 100 µg/mL to provide a good distribution of values across the range.

When it comes to drug efficacy, it is important to consider not only the potency of a single drug but also the potential interactions between multiple drugs. Synergistic drug combinations are those in which the combined effect of two or more drugs is greater than the sum of their individual effects. This can result in improved therapeutic efficacy, reduced toxicity, and increased therapeutic index of the drugs. Therefore, we used a number of IBLL concentrations in combination with one single concentration of DLL to examine the synergistic effects of the two drugs.

Antagonism and synergism refer to the interaction between two or more drugs or compounds in terms of their combined effect on a particular biological process or system. When the combination of drugs results in a greater effect than what would be expected from the sum of their individual effects, it is called synergy. Synergy is often desirable in drug combinations as it allows for a lower dose of each drug to be used, minimizing potential side effects. In this study, a CI value < 1 and Fa > 0.5 indicate a synergistic effect [240,241].

On the other hand, when the combined effect is less than what would be expected from the sum of their individual effects, it is called antagonism. Antagonism is generally undesirable in drug combinations as it may result in treatment failure or reduced effectiveness[242,243].

In our study, the IC_{50} In the context of this study, the general trend observed was that IBLL concentrations of 550 µg/mL or higher in combination with 25 µg/mL DLL resulted in a synergistic effect. Thus, according to our findings, using DLL and IBLL in combination with these concentrations can inhibit the growth of cancer cells in a better way. Moreover, several studies, including those by Woodman, Greenspan, and Wynne, suggest that ibuprofen may be effective in reducing inflammation associated with cancer in tumors [244–246]. In contrast, DOX is an anthracycline drug that works by blocking the activity of an enzyme called topoisomerase 2,

which is involved in DNA replication and cancer cell growth [247]. By inhibiting this enzyme, DOX can slow or stop the growth of cancer cells. Together, the combination of ibuprofen and DOX, using the concentrations found in this study, can have a synergistic effect, with ibuprofen reducing inflammation and DOX blocking cancer cell growth.

In conclusion, this study highlights the potential synergistic effects of combining ibuprofen-loaded and DOX-loaded liposomes to target TAMs and inhibit cancer cell growth. The results demonstrate that this combination can significantly increase the efficacy of DOX while reducing its toxic effects on healthy cells. These findings could have important implications for the development of new cancer treatments that combine traditional chemotherapy with anti-inflammatory drugs to improve patient outcomes. Furthermore, in future studies, building on these findings, researchers could explore modifying the surface of these liposomes to improve their targeting of TAMs. In particular, they could consider attaching specific targeting agents, such as antibodies or peptides, to the liposomes to increase their binding and uptake by these cells. Such modifications could enhance the effectiveness of this combination therapy and reduce potential side effects by limiting drug exposure to healthy cells.

4.5 Conclusions

In conclusion, the findings of this study suggest that the combination of doxorubicin and ibuprofen-loaded liposomes may be a promising approach for cancer treatment, with potential immunomodulatory effects on macrophages. The liposomes were successfully loaded with high efficiency using both active and passive loading methods for DOX and IBU, respectively, resulting in a size of about 100 nm with a negative zeta potential value. Based on the IC_{50} values of DLL and IBLL, different concentrations of IBLL were chosen to work in combination with a constant concentration of DLL. The synergistic effect 550, 650, and 750 µg/mL IBLL was seen with 25 µg/mL DLL against M(Ø), M1, and M2 phenotypes. Moreover, 450 µg/mL IBLL

showed synergistic results in combination with 25 µg/mL DLL for M(Ø).Using the given concentrations of IBLL may also further reduce the concentration of DLL or DOX needed for chemotherapy.

While further studies are needed to optimize the dosage and treatment duration, the use of IBLL could potentially enhance the efficacy of DOX by reducing the dose required and minimizing its adverse effects. Additionally, the use of ibuprofen as an anti-cancer agent warrants further investigation, as it may provide a novel approach to cancer treatment. Overall, these results highlight the potential of combination therapies and drug delivery systems for improving cancer treatment outcomes. To further improve the potential of using DOX and IBLL combination therapy for cancer treatment, future studies could explore the modification of liposome surfaces to effectively target the M2 phenotype (TAMs in a tumor microenvironment), potentially enhancing the therapeutic efficacy of the treatment.

Acknowledgments

This research has been funded by the Department of Material Science and Engineering, Iowa State University, and the Carol Vohs Johnson Chair Award.

Declaration of competing interest

Surya K. Mallapragada acknowledges financial interest in ImmunoNanoMed Inc.

4.6 References

1. Krämer, S. D. et al. When barriers ignore the “rule-of-five”. Adv. Drug Deliv. Rev. 101, 62–74 (2016).

2. Chagas, C. M., Moss, S. & Alisaraie, L. Drug metabolites and their effects on the development of adverse reactions: Revisiting Lipinski’s Rule of Five. Int. J. Pharm. 549, 133–149 (2018).

3. Amjad, M. T., Chidharla, A. & Kasi, A. Cancer chemotherapy. (2020).

4. Housman, G. et al. Drug resistance in cancer: an overview. Cancers (Basel). 6, 1769–1792 (2014).

5. Rivankar, S. An overview of doxorubicin formulations in cancer therapy. J. Cancer Res. Ther. 10, 853–858 (2014).

6. Slingerland, M., Guchelaar, H.-J. & Gelderblom, H. Liposomal drug formulations in cancer therapy: 15 years along the road. Drug Discov. Today 17, 160–166 (2012).

7. Ajaykumar, C. Overview on the Side Effects of Doxorubicin. Adv. Precis. Med. Oncol. (2020).

8. Demirel, Y. Nonequilibrium thermodynamics : transport and rate processes in physical, chemical and biological systems. (Elsevier, 2007).

9. Brown, T., Sykes, D. & Allen, A. R. Implications of breast cancer chemotherapy-induced inflammation on the gut, liver, and central nervous system. Biomedicines 9, 189 (2021).

10. Vyas, D., Laput, G. & Vyas, A. K. Chemotherapy-enhanced inflammation may lead to the failure of therapy and metastasis. Onco. Targets. Ther. 1015–1023 (2014).

11. Montague, K. & Malcangio, M. The therapeutic potential of monocyte/macrophage manipulation in the treatment of chemotherapy-induced painful neuropathy. Front. Mol. Neurosci. 10, 397 (2017).

12. Upadhyay, A. et al. Ibuprofen-based advanced therapeutics: Breaking the inflammatory link in cancer, neurodegeneration, and diseases. Drug Metab. Rev. 53, 100–121 (2021).

13. Akrami, H., Moradi, B., Borzabadi Farahani, D. & Mehdizadeh, K. Ibuprofen reduces cell proliferation through inhibiting Wnt/β catenin signaling pathway in gastric cancer stem cells. Cell Biol. Int. 42, 949–958 (2018).

14. Akrami, H., Aminzadeh, S. & Fallahi, H. Inhibitory effect of ibuprofen on tumor survival and angiogenesis in gastric cancer cell. Tumor Biol. 36, 3237–3243 (2015).

15. Haycock, J. W. et al. α-Melanocyte-stimulating hormone inhibits NF-κB activation in human melanocytes and melanoma cells. J. Invest. Dermatol. 113, 560–566 (1999).

16. Redpath, M. et al. Ibuprofen and hydrogel-released ibuprofen in the reduction of inflammation-induced migration in melanoma cells. Br. J. Dermatol. 161, 25–33 (2009).

17. van der Koog, L., Gandek, T. B. & Nagelkerke, A. Liposomes and extracellular vesicles as drug delivery systems: A comparison of composition, pharmacokinetics, and functionalization. Adv. Healthc. Mater. 11, 2100639 (2022).

18. Dicheva, B. M. & Koning, G. A. Targeted thermosensitive liposomes: an attractive novel approach for increased drug delivery to solid tumors. Expert Opin. Drug Deliv. 11, 83–100 (2014).

19. Zhao, N., Woodle, M. C. & Mixson, A. J. Advances in delivery systems for doxorubicin. J. Nanomed. Nanotechnol. 9, (2018).

20. Lukyanov, A. N., Elbayoumi, T. A., Chakilam, A. R. & Torchilin, V. P. Tumor-targeted liposomes: doxorubicin-loaded long-circulating liposomes modified with anti-cancer antibody. J. Control. Release 100, 135–144 (2004).

21. Zhang, X. et al. Multicompartmentalized vesosomes containing DOX loaded liposomes and 5FU loaded liposomes for synergistic tumor treatment. New J. Chem. 43, 4895–4899 (2019).

22. Han, H. D. et al. In vivo distribution and antitumor activity of heparin-stabilized doxorubicin-loaded liposomes. Int. J. Pharm. 313, 181–188 (2006).

23. Mohammed, A. R., Weston, N., Coombes, A. G. A., Fitzgerald, M. & Perrie, Y. Liposome formulation of poorly water soluble drugs: optimisation of drug loading and ESEM analysis of stability. Int. J. Pharm. 285, 23–34 (2004).

24. Mattheolabakis, G., Nie, T., Constantinides, P. P. & Rigas, B. Sterically stabilized liposomes incorporating the novel anticancer agent phospho-ibuprofen (MDC-917): preparation, characterization, and in vitro/in vivo evaluation. Pharm. Res. 29, 1435–1443 (2012).

25. He, Y., Luo, L., Liang, S., Long, M. & Xu, H. Influence of probe-sonication process on drug entrapment efficiency of liposomes loaded with a hydrophobic drug. Int. J. Polym. Mater. Polym. Biomater. 68, 193–197 (2019).

26. Galluzzi, L. et al. Molecular mechanisms of cisplatin resistance. Oncogene 31, 1869–1883 (2012).

27. Cardinale, D. et al. Prevention of high-dose chemotherapy–induced cardiotoxicity in high-risk patients by angiotensin-converting enzyme inhibition. Circulation 114, 2474–2481 (2006).

28. Duffy, M. J. & Crown, J. A personalized approach to cancer treatment: how biomarkers can help. Clin. Chem. 54, 1770–1779 (2008).

29. Zhang, L. et al. Amphiphilic depsipeptide-based block copolymers as nanocarriers for controlled release of ibuprofen with doxorubicin. J. Polym. Sci. Part A Polym. Chem. 51, 3213–3226 (2013).

30. Li, Z. et al. A nanomicellar prodrug carrier based on ibuprofen-conjugated polymer for co-delivery of doxorubicin. Front. Pharmacol. 9, 781 (2018).

31. Martinez, F. Martinez, FO & Gordon, S. M1 M2 Paradig. macrophage Act. time Reassess. F1000Prime Rep 6, F1000prime (2014).

32. Biswas, S. K. & Mantovani, A. Macrophage plasticity and interaction with lymphocyte subsets: cancer as a paradigm. Nat. Immunol. 11, 889–896 (2010).

33. Edge, L. Macrophage diversity enhances tumor. Cell 141, G2010 (2010).

34. Mills, C. D. Anatomy of a discovery: m1 and m2 macrophages. Front. Immunol. 6, 212 (2015).

35. Mosser, D. M. & Edwards, J. P. Exploring the full spectrum of macrophage activation. Nat. Rev. Immunol. 8, 958–969 (2008).

36. Noy, R. & Pollard, J. W. Tumor-associated macrophages: from mechanisms to therapy. Immunity 41, 49–61 (2014).

37. Mantovani, A., Sozzani, S., Locati, M., Allavena, P. & Sica, A. Macrophage polarization: tumor-associated macrophages as a paradigm for polarized M2 mononuclear phagocytes. Trends Immunol. 23, 549–555 (2002).

38. Sica, A. & Mantovani, A. Macrophage plasticity and polarization: in vivo veritas. J. Clin. Invest. 122, 787–795 (2012).

39. Kim, J. & Bae, J.-S. Tumor-associated macrophages and neutrophils in tumor microenvironment. Mediators Inflamm. 2016, (2016).

40. Solinas, G., Germano, G., Mantovani, A. & Allavena, P. Tumor-associated macrophages (TAM) as major players of the cancer-related inflammation. J. Leukoc. Biol. 86, 1065–1073 (2009).

41. Qian, B.-Z. & Pollard, J. W. Macrophage diversity enhances tumor progression and metastasis. Cell 141, 39–51 (2010).

42. Mantovani, A., Marchesi, F., Malesci, A., Laghi, L. & Allavena, P. Tumour-associated macrophages as treatment targets in oncology. Nat. Rev. Clin. Oncol. 14, 399–416 (2017).

43. Rehman, T. U. & Bratlie, K. M. Improving selective targeting to cancer-associated fibroblasts by modifying liposomes with arginine based materials. J. Drug Target. 30, 94–107 (2022).

44. Niu, G., Cogburn, B. & Hughes, J. Preparation and characterization of doxorubicin liposomes. Cancer Nanotechnol. methods Protoc. 211–219 (2010).

45. Alyane, M., Barratt, G. & Lahouel, M. Remote loading of doxorubicin into liposomes by transmembrane pH gradient to reduce toxicity toward H9c2 cells. Saudi Pharm. J. 24, 165–175 (2016).

46. Lv, R., Bao, Q. & Li, Y. Regulation of M1-type and M2-type macrophage polarization in RAW264. 7 cells by Galectin-9. Mol. Med. Rep. 16, 9111–9119 (2017).

47. Zhou, W. et al. SENP1-Sirt3 signaling promotes α-ketoglutarate production during M2 macrophage polarization. Cell Rep. 39, 110660 (2022).

48. Song, C. et al. NETs promote ALI/ARDS inflammation by regulating alveolar macrophage polarization. Exp. Cell Res. 382, 111486 (2019).

49. Pan, Y., Yu, Y., Wang, X. & Zhang, T. Tumor-associated macrophages in tumor immunity. Front. Immunol. 11, 583084 (2020).

50. Danesi, R., Fogli, S., Gennari, A., Conte, P. & Del Tacca, M. Pharmacokinetic-pharmacodynamic relationships of the anthracycline anticancer drugs. Clin. Pharmacokinet. 41, 431–444 (2002).

51. Gruber, B. M., Anuszewska, E. L. & Priebe, W. The effect of new anthracycline derivatives on the induction of apoptotic processes in human neoplastic cells. Folia Histochem. Cytobiol. 42, 127–130 (2004).

52. Carvalho, C. et al. Doxorubicin: the good, the bad and the ugly effect. Curr. Med. Chem. 16, 3267–3285 (2009).

53. Sritharan, S. & Sivalingam, N. A comprehensive review on time-tested anticancer drug doxorubicin. Life Sci. 278, 119527 (2021).

54. Muggia, F. M. et al. Phase II study of liposomal doxorubicin in refractory ovarian cancer: antitumor activity and toxicity modification by liposomal encapsulation. J. Clin. Oncol. 15, 987–993 (1997).

55. Sparano, J. A. et al. Phase I trial of pegylated liposomal doxorubicin and docetaxel in advanced breast cancer. J. Clin. Oncol. 19, 3117–3125 (2001).

56. Batist, G. et al. Reduced cardiotoxicity and preserved antitumor efficacy of liposome-encapsulated doxorubicin and cyclophosphamide compared with conventional doxorubicin and cyclophosphamide in a randomized, multicenter trial of metastatic breast cancer. J. Clin. Oncol. 19, 1444–1454 (2001).

57. Burade, V. et al. Lipodox®(generic doxorubicin hydrochloride liposome injection): in vivo efficacy and bioequivalence versus Caelyx®(doxorubicin hydrochloride liposome injection) in human mammary carcinoma (MX-1) xenograft and syngeneic fibrosarcoma (WEHI 164) mouse models. BMC Cancer 17, 1–12 (2017).

58. Sawpari, R. et al. Recent advances and futuristic potentials of nano-tailored doxorubicin for prostate cancer therapy. J. Drug Deliv. Sci. Technol. 104212 (2023).

59. Wang, Y., Chen, X., He, D., Zhou, Y. & Qin, L. Surface-modified nanoerythrocyte loading DOX for targeted liver cancer chemotherapy. Mol. Pharm. 15, 5728–5740 (2018).

60. Pashapour, S., Zabihi, A. & Behrouzi, R. Investigating the cytotoxic effect of ibuprofen concentration in liver cancer cells (HepG2) and normal fibroblast (AGO). Toxicol Adv 4, 15 (2022).

61. Yurtdaş-Kırımlıoğlu, G., Görgülü, Ş. & Berkman, M. S. Novel approaches to cancer therapy with ibuprofen-loaded Eudragit® RS 100 and/or octadecylamine-modified PLGA nanoparticles by assessment of their effects on apoptosis. Drug Dev. Ind. Pharm. 46, 1133–1149 (2020).

62. Ibrahim, M., Abuwatfa, W. H., Awad, N. S., Sabouni, R. & Husseini, G. A. Encapsulation, release, and cytotoxicity of doxorubicin loaded in liposomes, micelles, and metal-organic frameworks: a review. Pharmaceutics 14, 254 (2022).

63. Crommelin, D. J. A. & Van Bloois, L. Preparation and characterization of doxorubicin-containing liposomes. II. Loading capacity, long-term stability and doxorubicin-bilayer interaction mechanism. Int. J. Pharm. 17, 135–144 (1983).

64. Weber, C. et al. Functionalization of liposomes with hydrophilic polymers results in macrophage uptake independent of the protein corona. Biomacromolecules 20, 2989–2999 (2019).

65. Kaźmierczak, Z. et al. Endocytosis in cellular uptake of drug delivery vectors: Molecular aspects in drug development. Bioorg. Med. Chem. 28, 115556 (2020).

66. Yoshikawa, T. et al. Rapid and continuous accumulation of nitric oxide-releasing liposomes in tumors to augment the enhanced permeability and retention (EPR) effect. Int. J. Pharm. 565, 481–487 (2019).

67. Liu, D., Cohen, J. & Turkman, N. PEG2000-DBCO surface coating increases intracellular uptake of liposomes by breast cancer xenografts. Sci. Rep. 12, 10564 (2022).

68. Wu, K. et al. Redefining tumor-associated macrophage subpopulations and functions in the tumor microenvironment. Front. Immunol. 11, 1731 (2020).

69. Vadevoo, S. M. P. et al. The macrophage odorant receptor Olfr78 mediates the lactate-induced M2 phenotype of tumor-associated macrophages. Proc. Natl. Acad. Sci. 118, e2102434118 (2021).

70. Mock, B. A. et al. The inducible form of nitric oxide synthase (NOS2) isolated from murine macrophages maps near the nude mutation on mouse chromosome 11. Int. J. Immunogenet. 21, 231–238 (1994).

71. Barth, K. A., Waterfield, J. D. & Brunette, D. M. The effect of surface roughness on RAW 264.7 macrophage phenotype. J. Biomed. Mater. Res. Part A 101, 2679–2688 (2013).

72. Neog, M. K., Sultana, F. & Rasool, M. Targeting RAW 264.7 macrophages (M1 type) with Withaferin-A decorated mannosylated liposomes induces repolarization via downregulation of NF-κB and controlled elevation of STAT-3. Int. Immunopharmacol. 61, 64–73 (2018).

73. Zhang, B., Yang, Y., Yi, J., Zhao, Z. & Ye, R. Hyperglycemia modulates M1/M2 macrophage polarization via reactive oxygen species overproduction in ligature-induced periodontitis. J. Periodontal Res. 56, 991–1005 (2021).

74. Liu, H.-F. et al. Altered polarization, morphology, and impaired innate immunity germane to resident peritoneal macrophages in mice with long-term type 2 diabetes. J. Biomed. Biotechnol. 2012, (2012).

75. Camell, C. & Smith, C. W. Dietary oleic acid increases m2 macrophages in the mesenteric adipose tissue. PLoS One 8, e75147 (2013).

76. Aykul, S. & Martinez-Hackert, E. Determination of half-maximal inhibitory concentration using biosensor-based protein interaction analysis. Anal. Biochem. 508, 97–103 (2016).

77. Beck, B. et al. Assay operations for SAR support. Assay Guid. Man. [Internet] (2017).

78. Yung-Chi, C. & Prusoff, W. H. Relationship between the inhibition constant (KI) and the concentration of inhibitor which causes 50 per cent inhibition (I50) of an enzymatic reaction. Biochem. Pharmacol. 22, 3099–3108 (1973).

79. CORTÉS, A., CASCANTE, M., CÁRDENAS, M. L. & CORNISH-BOWDEN, A. Relationships between inhibition constants, inhibitor concentrations for 50% inhibition and types of inhibition: new ways of analysing data. Biochem. J. 357, 263–268 (2001).

80. Wang, X. et al. Three-Dimensional RAW264.7 Cell Model on Electrohydrodynamic Printed Poly(ε-Caprolactone) Scaffolds for In Vitro Study of Anti-Inflammatory Compounds. ACS Appl. Bio Mater. 4, 7967–7978 (2021).

81. 238. Ouyang, N., Ji, P. & Williams, J. L. A novel NSAID derivative, phospho-ibuprofen, prevents AOM-induced colon cancer in rats. Int. J. Oncol. 42, 643–650 (2013).

82. Boonnak, N., Chantrapromma, S., Tewtrakul, S. & Sudsai, T. Inhibition of nitric oxide production in lipopolysaccharide-activated RAW264. 7 macrophages by isolated xanthones from the roots of Cratoxylum formosum ssp. pruniflorum. Arch. Pharm. Res. 37, 1329–1335 (2014).

83. Tallarida, R. J. Drug synergism: its detection and applications. J. Pharmacol. Exp. Ther. 298, 865–872 (2001).

84. Greco, W. R. The search for synergy: a critical review from a response surface perspective. Pharmacol Rev 47, 331–385 (1995).

85. Chou, T.-C. Theoretical basis, experimental design, and computerized simulation of synergism and antagonism in drug combination studies. Pharmacol. Rev. 58, 621–681 (2006).

86. Chou, T.-C. Drug combination studies and their synergy quantification using the Chou-Talalay methodsynergy quantification method. Cancer Res. 70, 440–446 (2010).

87. Woodman, T. J. et al. Chiral inversion of 2-arylpropionyl-CoA esters by human α-methylacyl-CoA racemase 1A (P504S)—A potential mechanism for the anti-cancer effects of ibuprofen. Chem. Commun. 47, 7332–7334 (2011).

88. Greenspan, E. J., Madigan, J. P., Boardman, L. A. & Rosenberg, D. W. Ibuprofen inhibits activation of nuclear β-catenin in human colon adenomas and induces the phosphorylation of GSK-3β. Cancer Prev. Res. 4, 161–171 (2011).

89. Wynne, S. & Djakiew, D. NSAID inhibition of prostate cancer cell migration is mediated by Nag-1 induction via the p38 MAPK-p75NTR pathway. Mol. Cancer Res. 8, 1656–1664 (2010).

90. Renu, K., Abilash, V. G., PB, T. P. & Arunachalam, S. Molecular mechanism of doxorubicin-induced cardiomyopathy–An update. Eur. J. Pharmacol. 818, 241–253 (2018).

CHAPTER 5. UTILIZING THIOLYNE CLICK CHEMISTRY TO TARGET M2 MACROPHAGE PHENOTYPE USING FOLATE CONJUGATED LIPOSOMES

Tanzeel Ur Rehman [1,3], Susheel K. Nethi [2,3], Chris J. Cornelius [1,2], Surya K. Mallapragada [1,2,3]

1. Department of Materials Science & Engineering, Iowa State University, Ames, Iowa 50011

2. Department of Chemical & Biological Engineering, Iowa State University, Ames, Iowa, 50011

3. Nanovaccine Institute, Iowa State University, Ames, IA, 50011, USA

Modified from a manuscript to be submitted to the *Journal of Liposome Research*

Abstract

Liposomes are promising drug delivery systems but have limitations, including their stability, drug loading capacity, and ability to target cancer cells specifically. Moreover, Tumor-associated macrophages (TAMs), which are abundant in tumor microenvironments, can contribute to drug resistance and tumor proliferation. Therefore, there is a need to develop new, advanced, and targetable liposomes to address these issues. This study aims to develop a new liposome formulation that can selectively target cancer cells by utilizing thiol-ene click chemistry. To achieve this, we modified DOPE and attached a cysteine on the surface to form cysteine-modified DOPE, and used its thiol group to attach alkyne-bound folic acid (FA). The resulting FA-CYS-DOPE liposomes were stable and showed efficient drug loading, sustained drug release, and low toxicity. In vitro experiments demonstrated that the FA-CYS-DOPE liposomes selectively targeted M2-type macrophages overexpressing folate receptors, which are converted to TAMs in a tumor microenvironment. Moreover, the liposomes were efficiently internalized by the cells, resulting in enhanced cellular uptake and cytotoxicity of the drug. These

findings suggest that the thiol-ene click chemistry approach is a promising strategy for the development of targeted liposomal drug delivery systems that can effectively overcome limitations mediated by TAMs.

5.1 Introduction

Liposomes are promising drug delivery systems due to their biocompatibility, versatility, and ability to encapsulate hydrophilic and hydrophobic drugs [248]. However, one of the major challenges associated with liposomes is achieving efficient and targeted drug delivery to the desired site of action [200,249]. Additionally, tumor-associated macrophages (TAMs) have been shown to promote cancer growth, angiogenesis, and metastasis [250]. Furthermore, TAMs have been shown to promote drug resistance in tumors through various mechanisms, such as promoting tumor cell survival, altering drug metabolism, and inhibiting immune responses [231,251,252]. Therefore, there is a pressing need for advanced liposomes that can target TAMs and enhance drug delivery to tumors. In recent years, several new technologies have been developed to improve liposome functionality, including thiol-ene/yne click chemistry, which allows for easy conjugation of targeting moieties onto liposomes [253,254]. However, there is still much to be done in developing targeted liposomes that can effectively combat TAM-mediated drug resistance and enhance drug delivery to tumors.

Recent advances in liposome technology have led to the development of more sophisticated liposomes that can overcome some of the limitations of traditional liposomes. For example, azide-alkyne click chemistry has been used to attach various targeting moieties, including peptides and antibodies, to liposomes, allowing for more specific delivery to target cells [255–258]. Other advances include the use of pH-sensitive liposomes that can release their contents in response to the acidic environment of tumors, and the development of long-circulating liposomes that can remain in circulation for longer periods of time, allowing for

greater accumulation in tumors [259–261]. Despite recent advances in liposome technology, limited research has focused on optimizing liposomes for thiol-ene/yne click chemistry reactions. Therefore, it is crucial to explore the potential of liposomes in this direction and to develop new approaches for enhancing their effectiveness.

TAMs are a key component of the tumor microenvironment and can promote tumor progression by promoting angiogenesis, suppressing immune responses, and facilitating metastasis [251,262–264]. Additionally, TAMs can contribute to drug resistance by sequestering drugs and preventing their uptake by tumor cells [214,265]. Therefore, targeting TAMs is an important strategy for improving the efficacy of cancer therapy. One promising approach is to use liposomes that are specifically targeted to TAMs, allowing for more efficient drug delivery and potentially reducing drug resistance.

Folic acid is a widely used targeting moiety for liposomes because of its high affinity for the folate receptor β (FRβ), which is overexpressed on TAMs [266–268]. Several studies have demonstrated the effectiveness of folate-targeted liposomes in delivering drugs to TAMs and improving the efficacy of cancer therapy. For example, one study showed that folate-targeted liposomes loaded with doxorubicin were able to inhibit tumor growth and reduce the number of TAMs in a mouse model of breast cancer [269]. Another study demonstrated that folate-targeted liposomes loaded with paclitaxel were able to reduce tumor growth and improve survival in a mouse model of ovarian cancer [270]. These studies highlight the potential of folate-targeted liposomes for improving cancer therapy by specifically targeting TAMs.

In this study, we developed a new liposome formulation that is click chemistry-ready by modifying the amine terminal of DOPE to attach a protected cysteine. We then deprotected the cysteine to make the thiol (-SH) group available for click chemistry reactions. To test the

targeting potential of the liposomes, we used folic acid as the targeting moiety and modified it to have a terminal alkyne group. The liposomes were then synthesized using CYS-DOPE:DOPC and reacted with the alkyne-bound FA through click chemistry to formulate FA-CYS-DOPE:DOPC liposomes. These liposomes were further tested for their toxicity and cellular uptake using DOX and rhodamine, respectively, and against different macrophage phenotypes, including MØ, M1, and M2. Our results showed that folic acid-conjugated liposomes had a higher uptake in M2 macrophages (that are TAMs in a tumor microenvironment), which overexpress FRβ, compared to non-targeted liposomes. Our findings suggest that these thiol-ene/yne click-ready liposomes have the potential to greatly benefit targeted drug delivery in the field of cancer therapeutics by allowing for specific targeting of TAMs and other cancer cells, ultimately leading to increased drug efficacy and reduced toxicity.

5.2 Materials and Methods

5.2.1 Materials

1,2-Dioleoyl-sn-glycero-3-PE (DOPE) and 1,2-Dioleoyl-sn-glycero-3-PC (DOPC) were purchased from Cayman Chemicals (Ann Arbor, MI). Doxorubicin (DOX) was obtained from LC Laboratories (Woburn, MA). Trityl-protected cysteine (Tr-Cys(Tr)-OH) was purchased from Bachem (Torrance, CA), and Trityl-protected succinimidyl-activated cysteine (Tr-Cys(Tr)-OSu) was prepared according to a literature procedure [271]. (1,4-diazabicyclo[2.2.2]octane) (DABCO) was purchased from Sigma Aldrich. (2,2-dimethoxy-2-phenylacetophenone) (DMPA) was acquired from Fisher Scientific. Folic acid anhydride and dichloromethane (DCM) were purchased from TCI (Portland, OR). Interleukin 4 (IL4) was purchased from Biotechne (Minneapolis, MN), and Lipopolysaccharides (LPS) were purchased from eBiosciences, ThermoFisher Scientific (Waltham, MA). (3-(4,5-Dimethylthiazol-2-yl)-2,5-Diphenyltetrazolium bromide) (MTT) was purchased from ThermoFisher Scientific (Waltham, MA). Citric acid

anhydrous, sodium hydroxide, hydrochloric acid, chloroform, and phosphate buffer saline (PBS) were purchased from Fisher Scientific (Hampton, NH). Dimethyl sulfoxide (DMSO) was purchased from VWR Scientific (Radnor, PA). All other solvents and chemicals were purchased from Sigma-Aldrich (St. Louis, MO) and were used as received unless otherwise stated. Fresh deionized (DI) water (Milli-Q, Thermo Scientific Nanopure, Waltham, MA) was used throughout this study.

5.2.2 Methods

5.2.2.1 Conjugation of Cysteine-Functionalized 1,2-Dioleoyl-sn-glycero-3-PE (DOPE)

DOPE was chosen as the lipid to attach cysteine to because of its favorable physicochemical properties, such as its ability to form stable bilayers and its high propensity for fusogenicity, which can aid in drug delivery to the target cells [272]. Moreover, DOPE has been previously used in our lab for surface modification and has shown the potential to improve drug delivery to various cells [97,103,200]. Cysteine was conjugated with the terminal amine of DOPE, according to the method described by Sanne et al. [273]. Briefly, 200 mg (268.8 µmol) DOPE was dissolved in 2 mL DCM under an argon atmosphere. Next, 80 µL (568 µmol) triethylamine was added to the solution, followed by 224 mg (322 µmol) Tr-Cys(Tr)-OSu. The reaction was stirred at room temperature overnight. The solvent was removed using rotary evaporation, and the crude product was dissolved in 2 mL chloroform. This product was then purified using column chromatography (silica, $CHCl_3$/MeOH, 19:1 v/v to 9:1 v/v). Following the purification, trityl-protected Cys-DOPE was obtained in 30 % yield. This intermediate product was analyzed using ^{1}H-NMR to confirm the conjugation of trt-Cys-DOPE.

Subsequently, the trityl protection was removed from the product. Trityl-protected Cys-DOPE was dissolved in 25 µL (158 mmol) triethyl silane, followed by a solution of DCM and trifluoroacetic acid (1:1 v/v). The resulting solution was stirred for 2 h at room temperature and concentrated under reduced pressure. Finally, the crude product was precipitated in diethyl ether, filtered, and dried under vacuum. The final product was obtained at a yield of 90% (~55 mg). The final product was analyzed using ^{1}H-NMR.

5.2.2.2 Synthesis of Alkyne-Bound Folic Acid

Folate receptor β (FRβ) is a glycosylphosphatidyl (GPI)-anchored plasma membrane protein that is expressed on alternatively activated macrophages, i.e., M(2) type macrophages [274]. Therefore, folic acid (FA) was chosen as a targeting moiety for this study to click with the Cys-DOPE. In order to utilize the thiol-yne click chemistry, FA was modified to have a terminal alkyne group. The terminal alkyne was added to the FA through the Schotten-Baumann method [275,276], and the method of Hayashi et al. was followed with a few alterations [277]. Briefly, 200 mg (0.45 mmol, 1 equivalent) FA was dissolved in 30 mL DMSO. The solution was stirred at 16 ^{o}C for 2 h, followed by 1 hr stirring at 70 ^{o}C. Finally, a solution of 15% aq. KOH (1.2 equivalent) was added to eliminate HBr. The solvent was removed under reduced pressure.

The resulting dark yellow solid was recrystallized using a 10% ethanol solution, forming an orange powder. This final product was dried under vacuum overnight. Subsequently, the product was treated with dilute HCl and washed with water to obtain alkyne-bound FA. To confirm the presence of the alkyne group, ^{1}H-NMR was performed. ^{1}H NMR [278,279].

5.2.2.3 Synthesis of Cysteine-Functionalized 1,2-Dioleoyl-sn-glycero-3-PE (CYS-DOPE) and 1,2-Dioleoyl-sn-glycero-3-PC (DOPC) Liposomes

Liposomes were synthesized based on the approach published earlier [103,200]. 50 mg (57.8 µmol) of the obtained Cys-DOPE was dissolved in 5 mL chloroform, followed by 23 mg (29.2 µmol) DOPC. After stirring for 15 min, the organic solvent was evaporated using a rotary evaporator at 40 ^{o}C for 5 min; a thin lipid film was seen at the bottom of the flask. Subsequently, the lipid film was rehydrated using DI water through vigorous scraping with a spatula and placing the flask in a sonication bath for 15 min. A milky white solution was seen; the liposomes were lyophilized and kept at -20 ^{o}C for further use. As a control, liposomes without FA were also synthesized, using only DOPE:DOPC (2:1) using the same procedure.

5.2.2.4 Thiol-yne Click Reaction

After obtaining cysteine-functionalized DOPE (Cys-DOPE) and DOPC liposomes, and alkyne-bound FA, both of these were reacted through thiol-yne click chemistry. Briefly, 50 mg of CYS-DOPE:DOPC liposomes were dissolved in DMSO, followed by the addition of alkyne-bound FA and dropwise addition of DMPA. The reaction was magnetically stirred at 70 ^{o}C for one hour, followed by the addition of DABCO. The reaction was then stirred at 37 ^{o}C for 24 h. Next, the organic solvent was removed under vacuum. The final product was placed in a dialysis bag (MWCO: 3,500) to remove any excess organic solvents or reagents. Finally, the liposome solution was lyophilized and kept at -20 ^{o}C for further use. To confirm the click reaction, ^{1}H NMR was conducted, and the results were analyzed.

5.2.2.5 Doxorubicin Loading and Release Studies

To investigate drug delivery using liposomes, doxorubicin (DOX) was encapsulated and used as a model drug. Initially, a 10 mg/mL DOX solution in DI water was prepared to load into the liposomes. Next, 5 mg of lyophilized liposomes were dissolved in 1 mL of 150 mM citric

acid (pH 4.0), and the solution was extruded 21 times through a 100 nm polycarbonate filter membrane using an Avanti Mini-Extruder (Avanti Polar Lipids, Inc. Alabaster, AL). Subsequently, the pH of the liposome solution was then adjusted to 7.4 using HCl and NaOH. The DOX solution and liposome solution (both at pH 7.4) were heated to 65°C for 10 minutes to reach thermal equilibrium. Subsequently, 100 µL of the DOX solution was added to the liposome solution and kept at 65°C for another 45 minutes. Afterward, the DOX-loaded liposomes solution was centrifuged at 3000 rpm for 10 minutes, and the supernatant was carefully removed and tested for DOX loading efficiency. The liposomes were stored at -20°C for future use in cell culture.

To assess the efficiency of DOX loading in liposomes, a standard calibration curve was generated by serially diluting a 1 mg/mL DOX solution in a 96-well plate. Then, 100 µL of supernatant was added to the same plate. The experiments were conducted in triplicate, and a SpectraMax M3 plate reader (Molecular Devices, San Jose, CA) was used to measure absorbance at 470 nm with a reference at 630 nm. The DOX encapsulation efficiency was calculated using the following formula:

$$Encapsulation\ efficiency\ (\%) = \frac{(C_{start} - C_{supernatant})}{C_{start}} X\ 100\% \qquad (1)$$

Here, C_{start} is the concentration of DOX solution added to the liposomes, and $C_{supernatant}$ is the concentration of DOX in the supernatant. Since the liposomes were synthesized using two different lipids, for the rest of this article, the DOX-loaded liposomes with FA are referred to as FADLL, while DOX-loaded non-FA liposomes are referred to as DLL.

DOX release studies were carried out using FADLL, according to procedures outlined in [103]. FADLLs were enclosed in a dialysis membrane with a molecular weight cutoff of 3500 and placed in a 100 ml beaker containing PBS. The beaker was sealed and kept at a temperature of

37°C. At specified intervals (3, 6, 12, 24, 48, and 72 h), 1 ml samples were taken and added to a 96-well plate. To maintain a consistent volume, 1 ml of PBS was added to the beaker after each sample was taken. Finally, the plate was read at an absorbance of 470 nm with a reference at 630 nm using the SpectraMax M3 plate reader.

5.2.2.6 Rhodamine-loaded liposomes

A flow cytometry analysis was performed at the end of the study to measure the cellular uptake of liposomes by each phenotype. To measure the number of liposomes internalized by cells, FA-DOPE:DOPC and plain DOPE:DOPC liposomes were loaded with rhodamine using the method by Kang et al. [280]. Briefly, either FA-DOPE:DOPC (2:1) or DOPE:DOPC (2:1) were dissolved in chloroform and added to a round bottom flask along with the addition of rhodamine (dissolved in methanol at 2mg/mL). The rotary evaporator was used to remove the organic solvents under reduced pressure, leaving a dried thin film on the inner surface of the flask. The thin film was then hydrated in 100 mM phosphate-buffered saline (PBS, pH 7.4) and incubated for 30 minutes at room temperature to form a suspension of multilamellar liposomes. The liposome suspension was sonicated in a bath-type sonicator at 37°C for 1 hour. To remove any unloaded rhodamine, the liposomes were loaded onto a Sephadex G-50 column, passed through a 100 nm polycarbonate filter, and extruded 21 times. Finally, rhodamine-loaded liposomes were stored at 4°C until use. The concentration of rhodamine loaded in the liposomes was determined by lysing the liposomes with 1% Triton X-100 and assaying the concentration of rhodamine using a plate reader, with a known concentration of free rhodamine used as a standard.

5.2.2.7 Size and zeta potential

The size and zeta potential of DLL and FADLL were measured using a Zetasizer Nano Z instrument (Malvern Instruments Ltd. Malvern, UK). For each liposome type, a 1% w/v solution (100 µL) was prepared and added to three test tubes containing 5 mL of deionized (DI) water.

The liposome solution was then extruded through a 100 nm polycarbonate membrane filter using the Avanti Mini-Extruder. To avoid any interference from ions in the water, the pH of the freshly extruded liposome solutions was adjusted to 7.4 using HCl and NaOH before the size and zeta potential measurements were taken.

5.2.2.8 Cell line and culture

The RAW 264.7 macrophages from ATCC (Manassas, VA) were cultured in complete medium at 37 ^{o}C with 5% CO_2. The CM comprised Dulbecco's modified Eagle's medium (DMEM) supplemented with 10% fetal bovine serum (FBS), 1% penicillin, and 1% streptomycin. The cells were passaged every three to four days using a cell scraper, with subculturing performed between approximately 6.4 x 10^3 and 2.7 x 10^4 cells per cm^2. To differentiate the macrophages from their naïve state (MØ) to either classically activated or proinflammatory macrophages (M1), 5 ng/mL LPS was used. For differentiation to alternatively activated or anti-inflammatory (proangiogenic) (M2) phenotype, 25 ng/mL IL-4 was used.

5.2.2.9 Detection of Cell Polarization by Immunocytochemistry

To confirm the polarization of naïve macrophages to M1 and M2, the cells were treated with their respective antibodies and were imaged under a fluorescent microscope. For M1, nitric oxide synthase 2 (NOS2) is a known marker, while CD206 is known to be overexpressed in M2 [203,281]. Therefore, the cells were grown for 24 h with the addition of either LPS or IL-4, followed by washing of cells using PBS. After incubation for 24 hours, the cells were washed twice with PBS. Next, the nuclei of the cells were stained using DAPI. The cells were then observed under a fluorescent microscope, and images were taken to confirm the polarization of M0 to M1 and M2.

5.2.2.10 Cell viability assay

To confirm the safety and biocompatibility of the liposomes on cells, RAW 264.7 macrophages (MØ, M1, and M2) were seeded at 5 x 10^4 cells/cm^2 in a 96-well plate and allowed to grow for 24 hours. Next, the media was carefully aspirated, and 100 µL of 250 µg/mL unloaded DOPE:DOPC liposomes and unloaded FA-DOPE:DOPC liposomes in CM were added to the cells, with positive and negative controls also included. The plate was then incubated at 37 ^oC for 48 h. To determine cell viability, a methyl thiazol tetrazolium (MTT) assay was used, with 100 µL of 0.5 mg/mL MTT solution added to each well and incubated for an additional 2 hours at 37 ^oC. The resulting insoluble purple formazan crystals were dissolved in DMSO, and the plate was read at 570 nm with a reference of 630 nm using a plate reader. This experiment was performed in triplicate.

5.2.2.11 Half-minimal Inhibitory Concentration (IC_{50})

Macrophages and their phenotypes (MØ, M1, and M2) were cultured in a 96-well plate with a density of 5 x 10^4 cells/cm^2 in complete media at 37 ^oC for 24 h. To determine the cell viability, a positive control was added with cells without liposomes and a negative control with liposomes without cells. The cells were then treated with 250 µg/mL FADLL and with 50 µg/mL free DOX. Two different sets of experiments were conducted; one was concluded after 24 hr of treatment, while the second one was concluded after 48 h of the treatment. After either 24 h or 48 h of incubation at 37 ^oC, an MTT assay was conducted, and the data were normalized to the positive controls. Using a sigmoidal dose-response curve, the IC_{50} values were calculated for FADLL and free DOX at 24 and 48 h. Each experiment was performed in four replicates.

5.2.2.12 Cellular uptake

To determine the cellular uptake of liposomes in MØ, M1, and M2, a flow cytometry analysis was performed using rhodamine-loaded liposomes. Firstly, macrophages and their phenotypes were passaged and allowed to grow for 24 h. Next, the old media was carefully aspirated, and fresh media with 250 µg/mL rhodamine-loaded FA-DOPE:DOPC liposomes and rhodamine-loaded DOPE:DOPC liposomes were added to the cells. The cells were treated with the liposomes for 2 h, then washed twice with PBS and tested for cellular uptake using flow cytometry.

5.2.2.13 Statistical analyses

The data from all experiments were presented as mean ± standard deviation (SD), and four replicates were performed for each experiment. Tukey's honest significant test was utilized to assess pairwise comparisons, with statistical significance considered at $p < .05$. Pairwise comparisons were conducted to analyze the IC_{50} values of FADLL and free DOX at 24 and 48 h against MØ, M1, and M2 as well as for the cellular uptake of liposomes by all three phenotypes.

5.3 Results

5.3.1 Cysteine-Functionalized DOPE:DOPC Liposomes React with Alkyne-Bound Folic Acid through Click Chemistry

In this study, we successfully synthesized a liposome capable of reacting with a targeting agent consisting of a double or triple bond by modifying the terminal amine of DOPE to have a cysteine attached using the method by Sanne et al. (**Figure 5.1 (a)**). The was confirmed through ^{1}H NMR analysis, as shown in **Figure 5.2**. The appearance of multiple peaks between 7.0-7.5 ppm in **Figure 5.2 (b)** confirms the attachment of DOPE-CYS (protected) to the DOPE, while the removal of these peaks (7.0-7.5 ppm) in **Figure 5.2 (c)** confirms the deprotection of DOPE-CYS. A soft peak at 1.31 ppm was observed, corresponding to the thiol group (-SH).

To enable thiolyne-click chemistry, we introduced an alkyne group to folic acid (FA) (**Figure 1 (b)**), which was confirmed through ^{1}H NMR spectra, as shown in **Figure 5.2**. The emergence of a peak at 2.8 ppm **in Figure 5.2 (e)** confirms the presence of the terminal alkyne group that was absent in **Figure 5.2 (d)**, representing the ^{1}H NMR of pure FA.

After obtaining DOPE-CYS and alkyne-bound FA, a click reaction was conducted between the two using DMPA as the thermal initiator and DABCO as the catalyst. The final product was analyzed using ^{1}H NMR to confirm the completion of the thiolyne click chemistry, as shown in **Figure 5.2 (f)**. The loss of the peak at 1.31 ppm (belonging to the thiol group) and the addition of the peak at 8.4 ppm corresponding to the amide group in FA confirms the successful conjugation of DOPE-CYS-FA. These FA-bound liposomes were then loaded with doxorubicin (DOX) as a model drug and were tested for their toxicity and cellular uptake against macrophages and their phenotypes (MØ, M1, and M2).

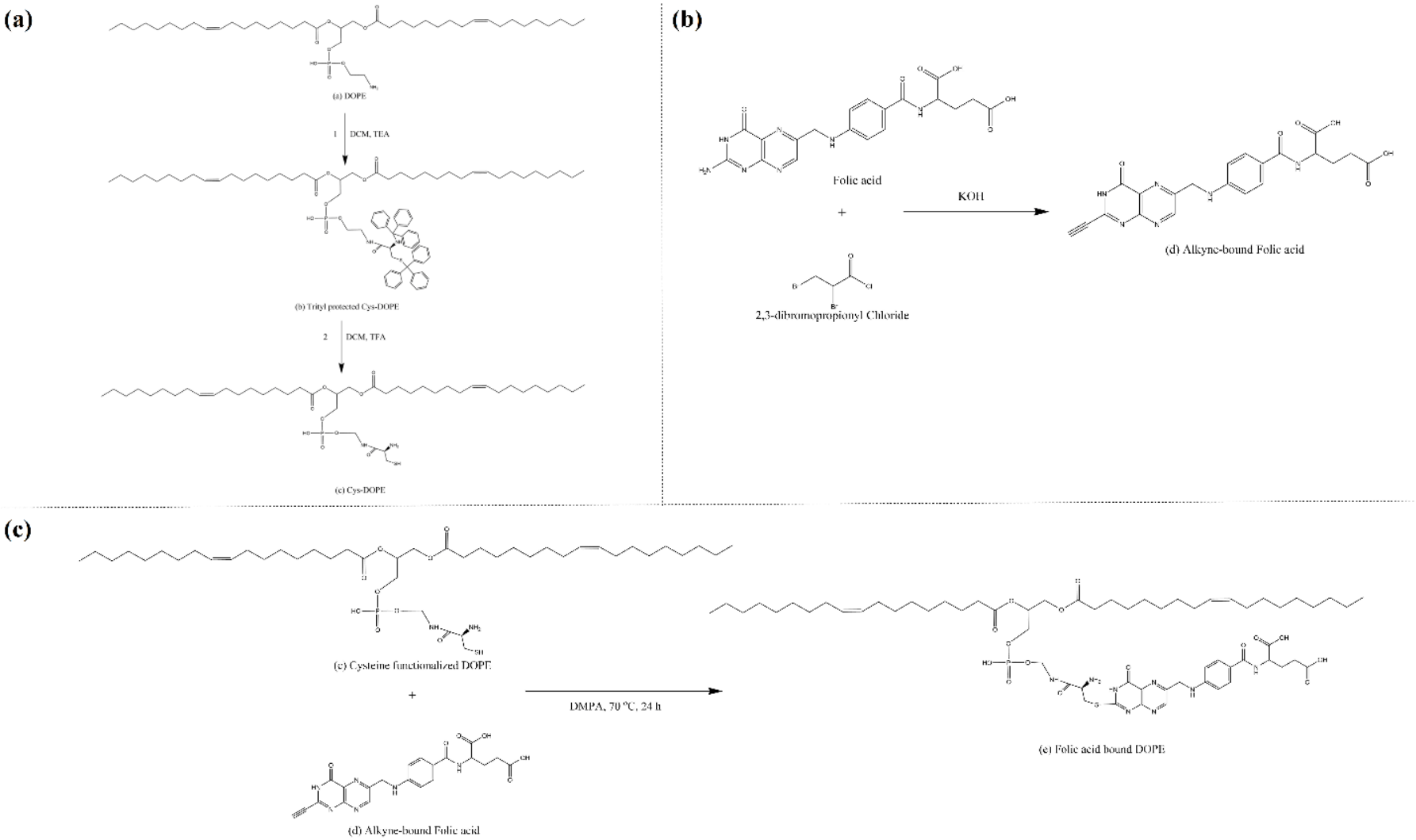

Figure 5.1*: Schematic of* ***(a)*** *modification of DOPE to attach (Tr-Cys(Tr)-OH) and unprotect the thiol (-SH) group,* ***(b)*** *reaction to obtain a terminal alkyl group to FA, and* ***(c)*** *thiolyne click chemistry between DOPE-CYS and alkyne-bound FA.*

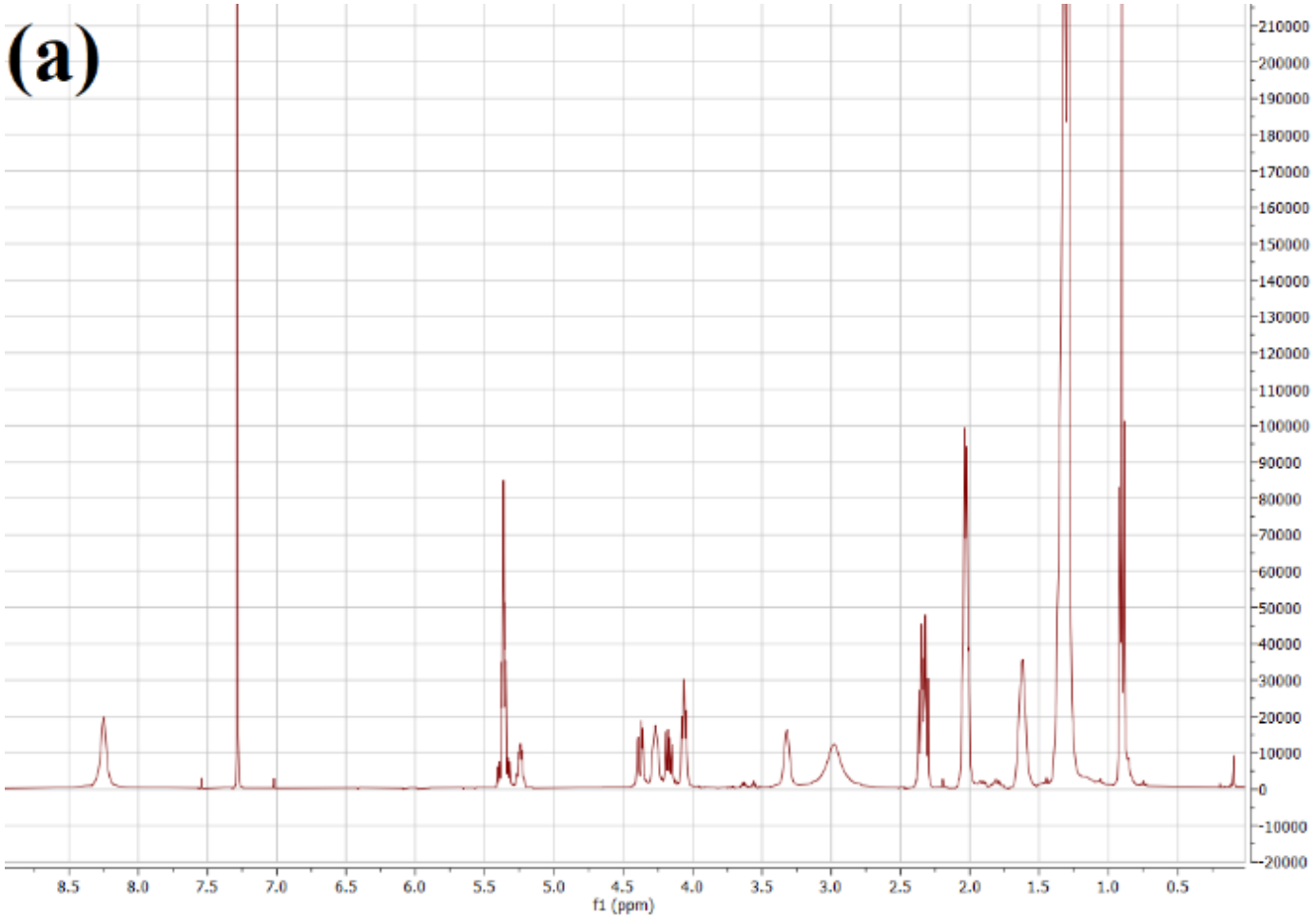

***Figure 5.2**: The ^{1}H NMR spectra of the reactions. **(a)** pure DOPE; **(b)** DOPE-CYS (protected); **(c)** DOPE-CYS (unprotected); **(d)** pure folic acid (FA); **(e)** alkyne-bound FA; and **(f)** DOPE-CYS-FA click chemistry*

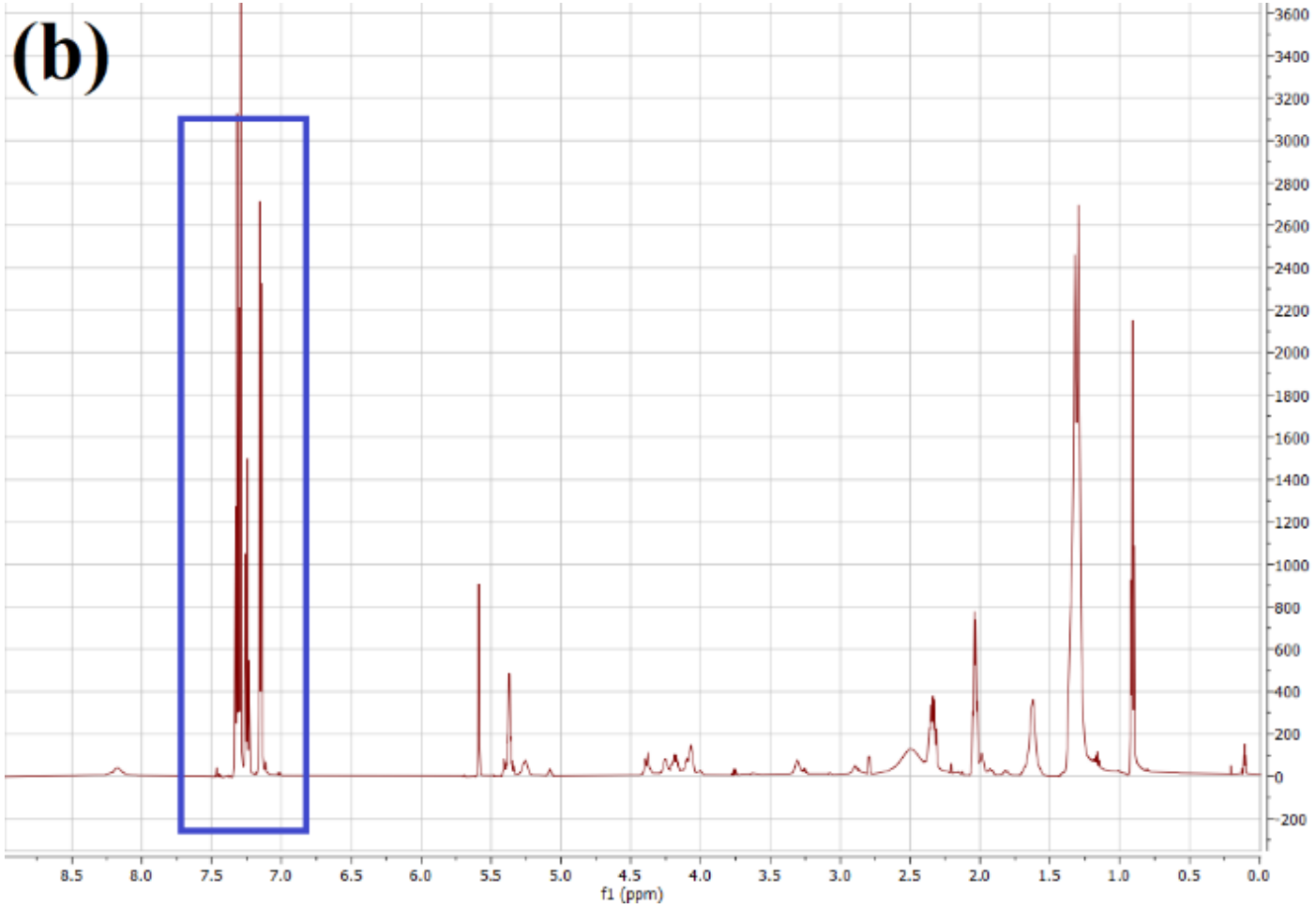

Figrue 5.2 continued

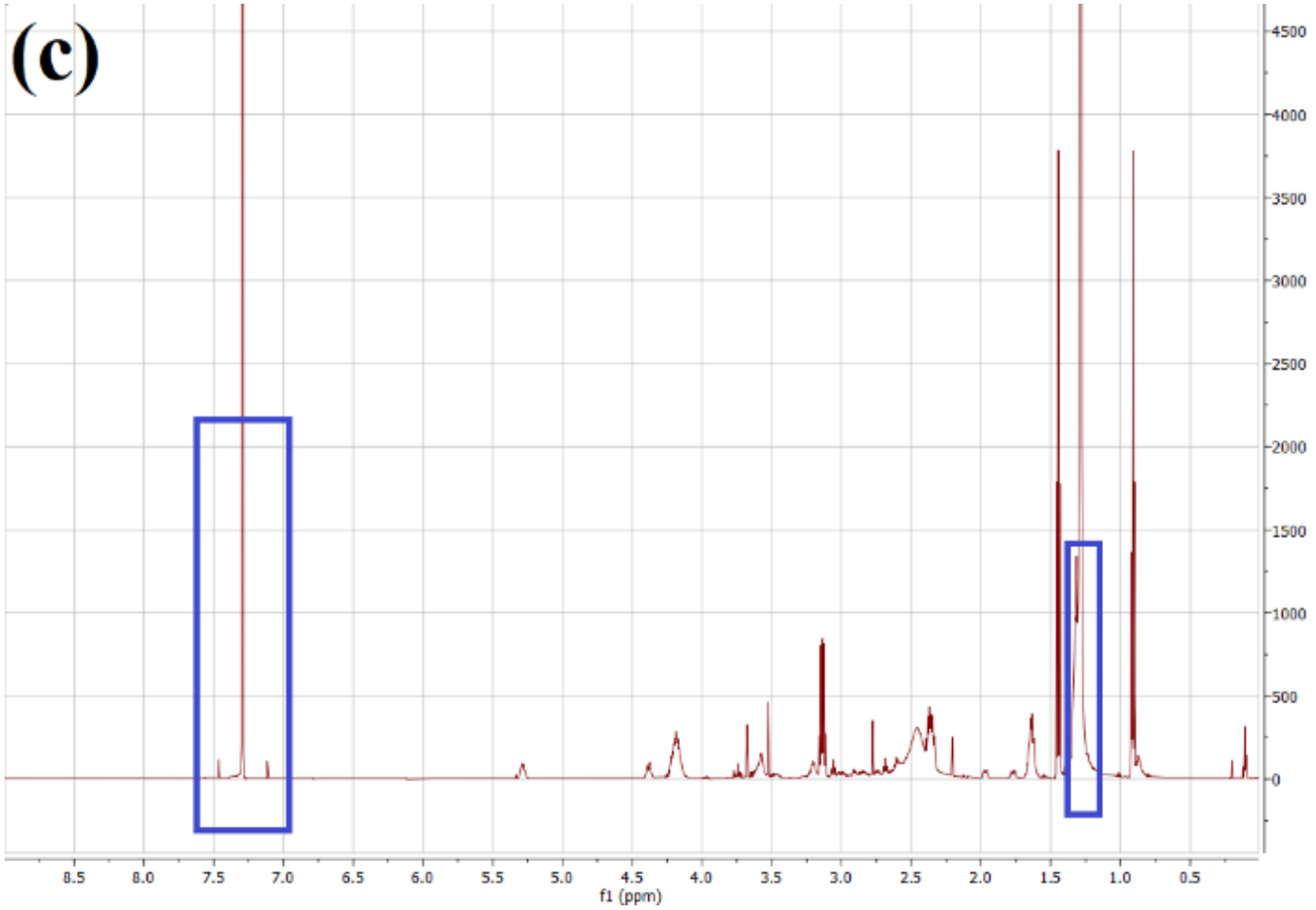

Figrue 5.2 continued

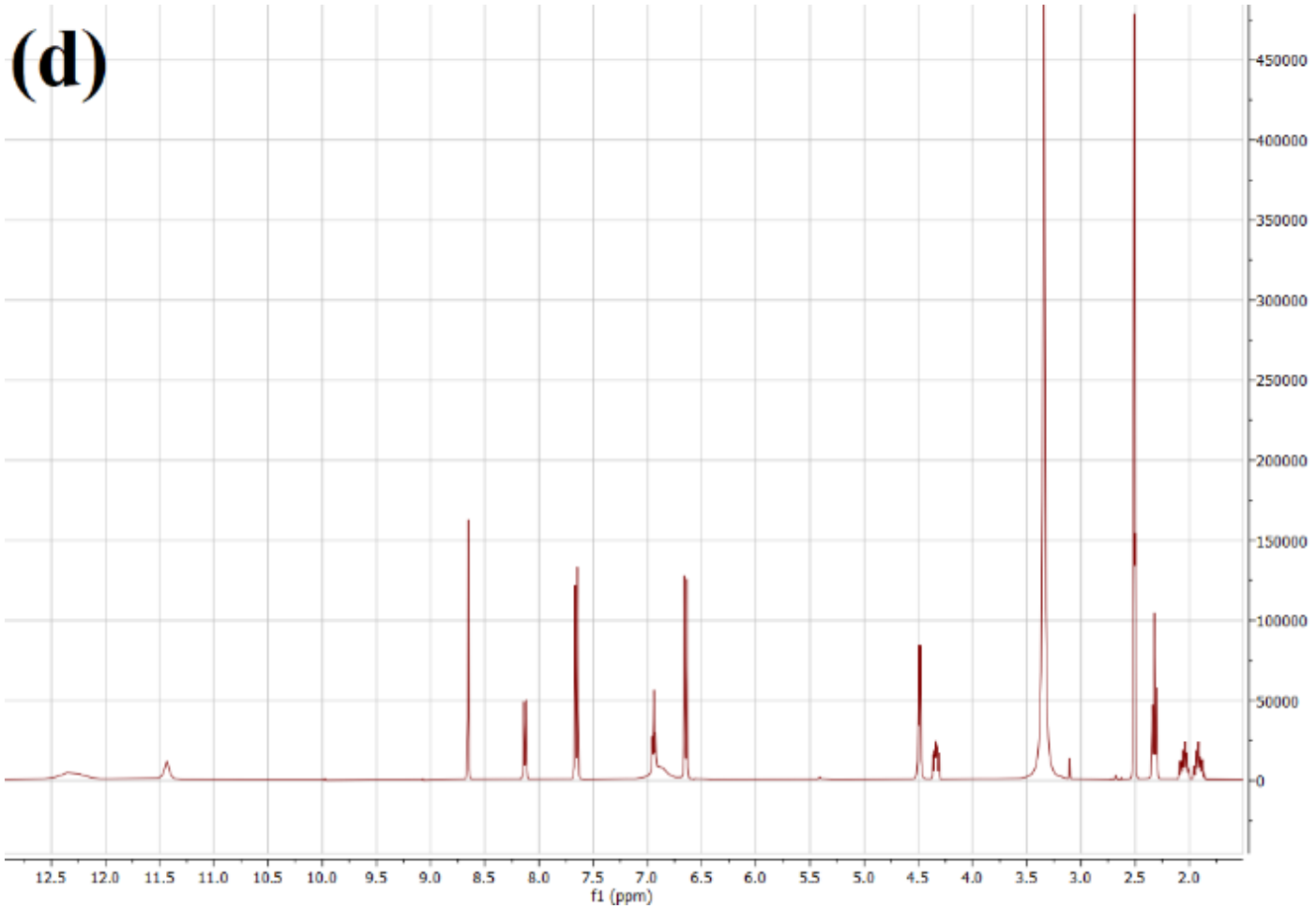

Figrue 5.2 continued

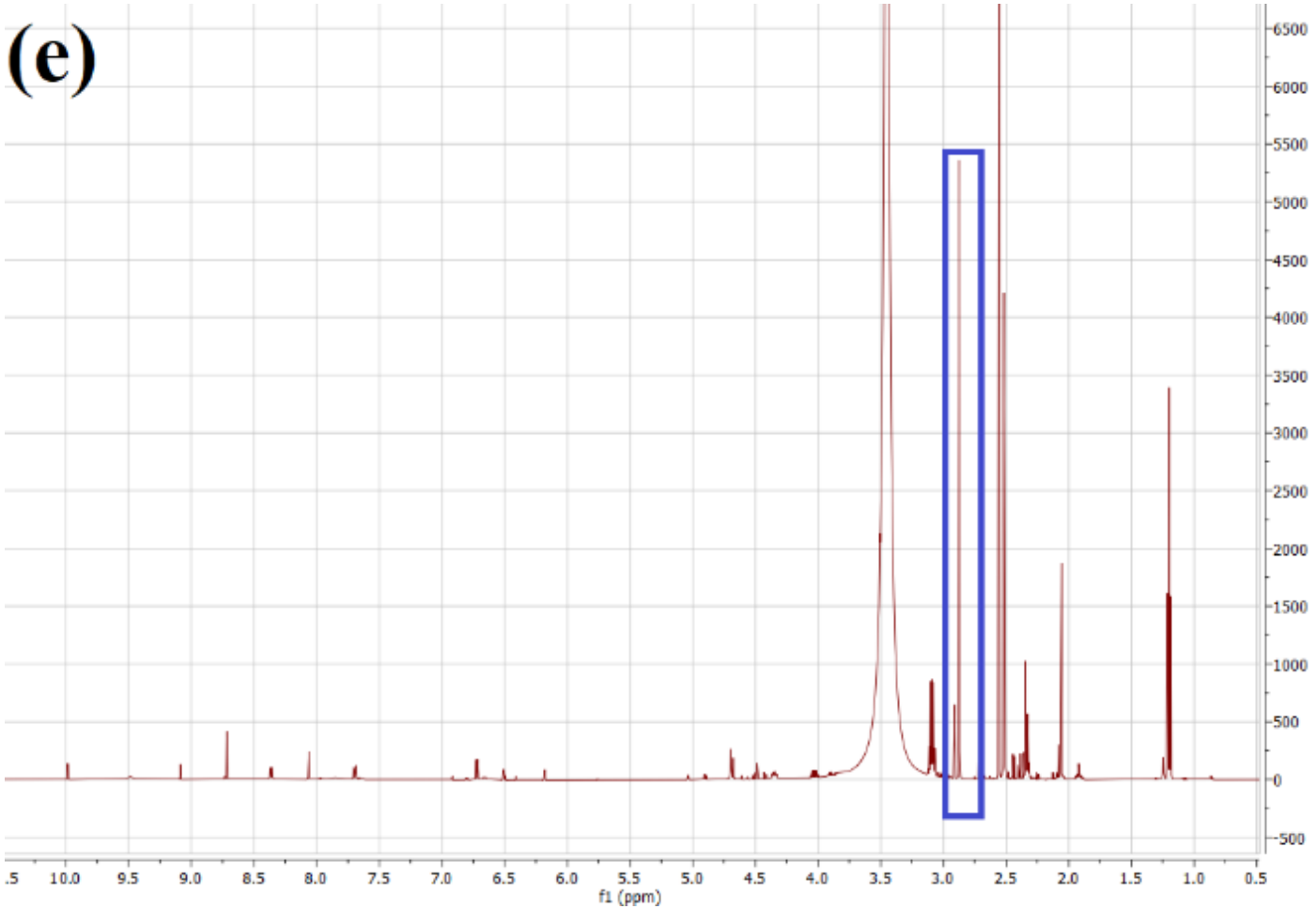

Figrue 5.2 continued

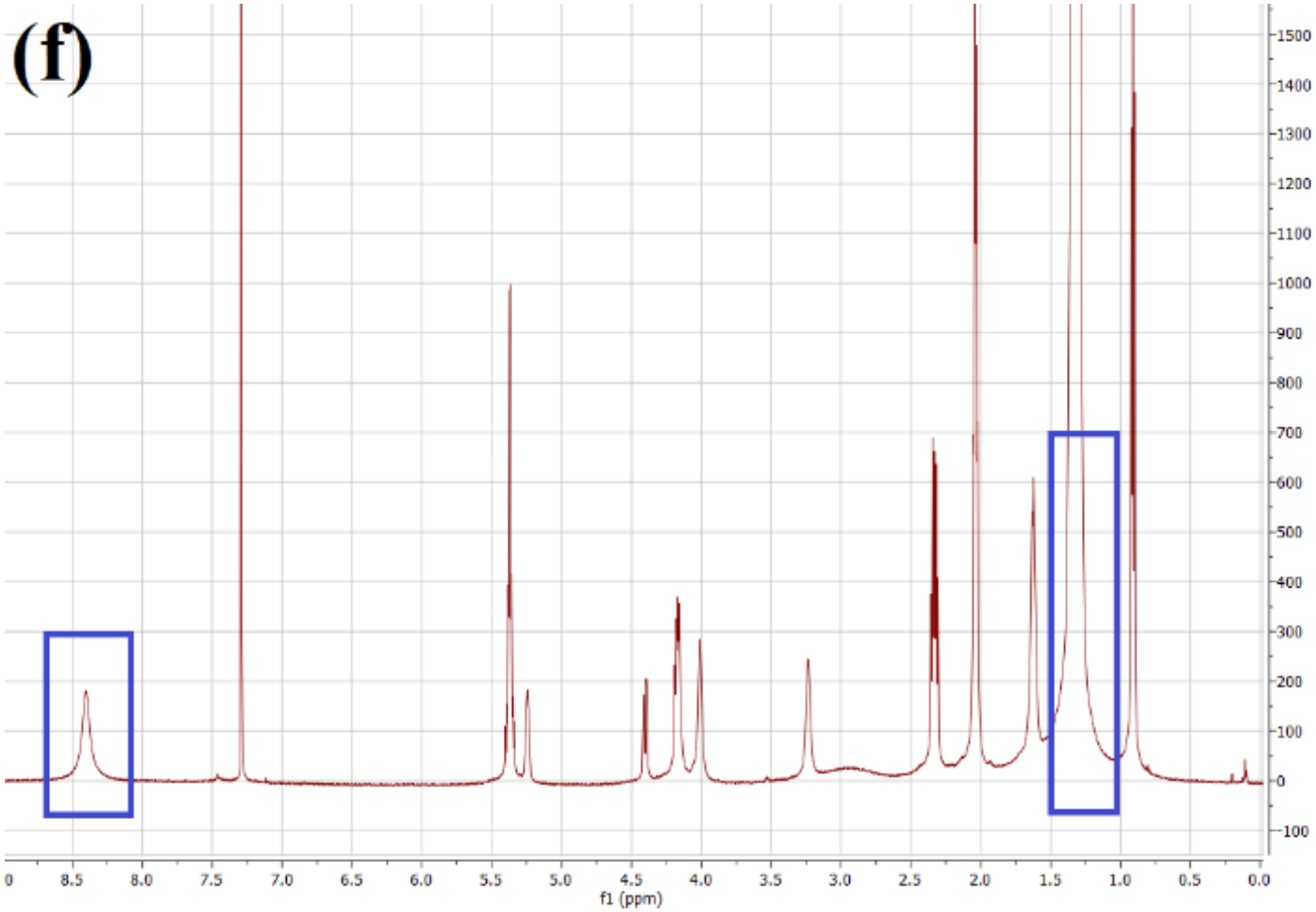

Figrue 5.2 continued

5.3.2.2 Liposome Characterization

The DOPE-CYS-FA:DOPC liposomes were carefully characterized for their physical properties, including size and zeta potential. The size and zeta potential of liposomes are critical factors in determining their cellular uptake [282]. The use of a 100 nm polycarbonate filter during liposome extrusion resulted in liposomes with a diameter of 109 ± 7 nm, which is consistent with the expected value. The zeta potential value of these liposomes was found to be -7.17 ± 1.02 mV. Similarly, DLL (unmodified) liposomes showed a size and zeta potential of 102 ± 5 nm and -5.1 ± 1.9 mV, respectively. *Table 5.1* lists the size and zeta potential values for FADLL and DLL.

Table 5.1: Characterization of folic acid doxorubicin-loaded liposomes and doxorubicin-loaded liposomes.

	Size (nm)	Zeta potential (mV)	Doxorubicin encapsulation efficiency (%)	Rhodamine encapsulation efficiency (%)
FADLL	109 ± 7	-7.2 ± 1.02	95.7 ± 0.5	99.1 ± 0.4
DLL	102 ± 5	-5.1 ± 1.9	93.8 ± 1.2	98.7 ± 0.5

5.3.2.3 Rhodamine and Doxorubicin Loading and Doxorubicin Release Studies

To evaluate the drug encapsulation efficiency of liposomes, we loaded the liposomes with both DOX and rhodamine, and calculated their encapsulation efficiency using a standard calibration curve. DOX is typically actively loaded into liposomes based on the pH gradient between the liposomal cavity and the surrounding solution, resulting in a high encapsulation efficiency [154,200]. In our study, the FADLL demonstrated an encapsulation efficiency of 95.7 ± 0.5 % for DOX, while rhodamine showed a 99.1 ± 0.4 % encapsulation efficiency. Similarly, DLL showed a DOX encapsulation efficiency of 93.8 ± 1.2 % and rhodamine encapsulation efficiency of 98.7 ± 0.5 %. *Table 1* enlists the encapsulation efficiencies of DOX and rhodamine for FADLL and DLL.

To investigate the release of DOX from the liposomal cavity, we conducted drug release studies. The results demonstrated an initial burst release of 31% of the DOX within the first 24 hours, followed by a slower release rate for the next 48 hours. The total amount of DOX released at the end of 72 hours was 65%, as shown in **Figure 5.3**.

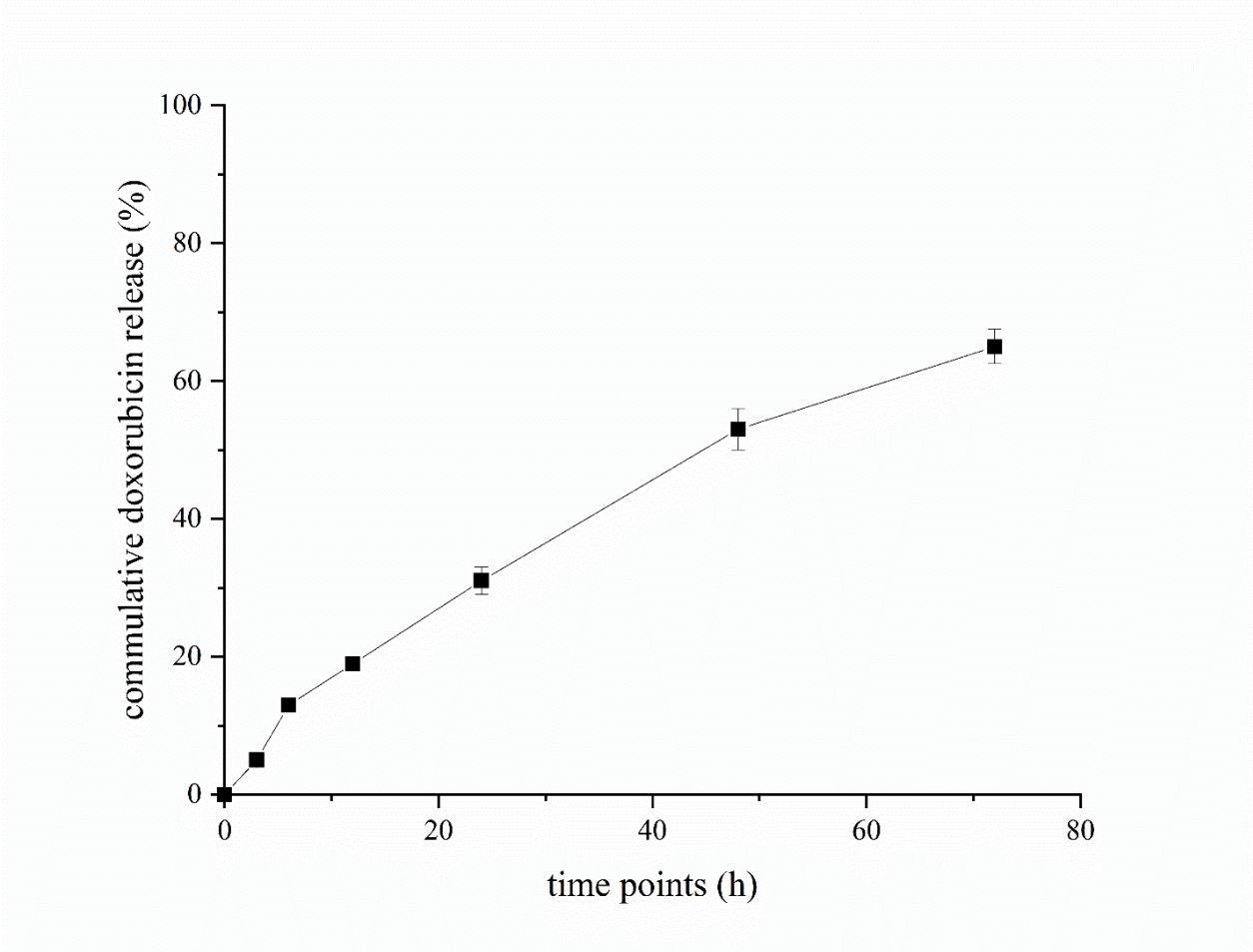

Figure5. 3*: cumulative drug release of DOX from the FADLL over a time of 72 h.*

5.3.2.4 Polarization of M0 to M1 and M2

To assess the polarization of naïve macrophages (MØ) to M1 and M2, we performed an immunocytochemistry analysis using specific markers. The M1 and M2 macrophages were identified by the expression of iNOS and CD206, respectively. The cells were treated with LPS

or IL-4 to promote polarization to M1 or M2 macrophages, respectively. After incubation, the cells were stained with PE-labeled iNOS and FITC-labeled CD206 and then observed under a fluorescence microscope. The nuclei of the cells were counterstained with DAPI.

Our results demonstrated that the M1 macrophages exhibited a strong red fluorescence signal from iNOS staining, indicating the expression of this marker. In contrast, the M2 macrophages exhibited a strong green fluorescence signal from CD206 staining, indicating the expression of this marker. The images from these results are shown in **Figure 5.4**. These findings confirmed the successful polarization of MØ to M1 and M2 macrophages using LPS and IL-4 treatment, respectively.

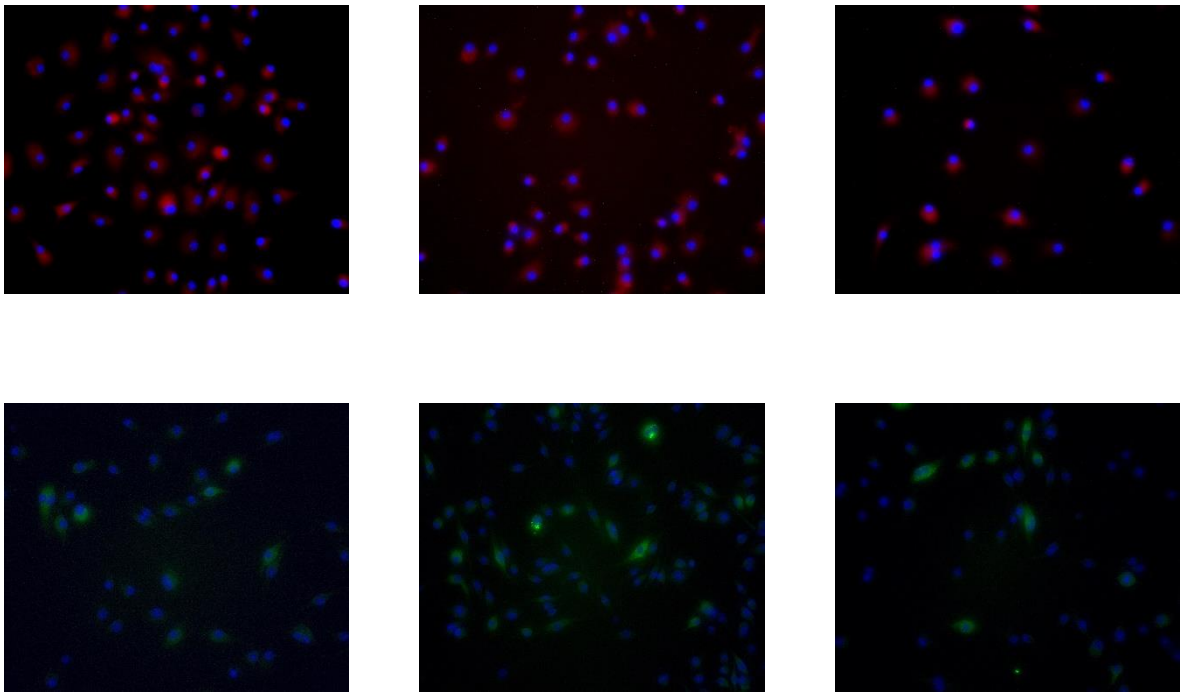

Figure 5.4: *shows the expression of (top) PE-labeled iNOS attached to M1 macrophages, while (bottom) shows the expression of FITC-labeled CD206 attached to M2 macrophages, confirming the polarizations.*

5.3.2.5 Cytotoxicity of FADLL

Since the goal of this study was to develop a thiol-ene/yne click chemistry-ready liposome; to show the proof of concept, we used folic acid (FA) as the targeting agent in this study. It is well-known that the folate receptor β (FRβ) is highly expressed in TAMs and has been identified as a promising target for antimacrophage and antiinflammatory therapies [283,284]. Folic acid was conjugated with the liposomes using the thiolyne click chemistry and used to target the M2. However, before targeting the cells, the FADLL were tested for their cell viability to ensure that the FA did now cause any significant cell death. Moreover, the IC_{50} of FADLL and free DOX was calculated at 24 and 48 h to understand how fast the cells uptake and react with the DOX.

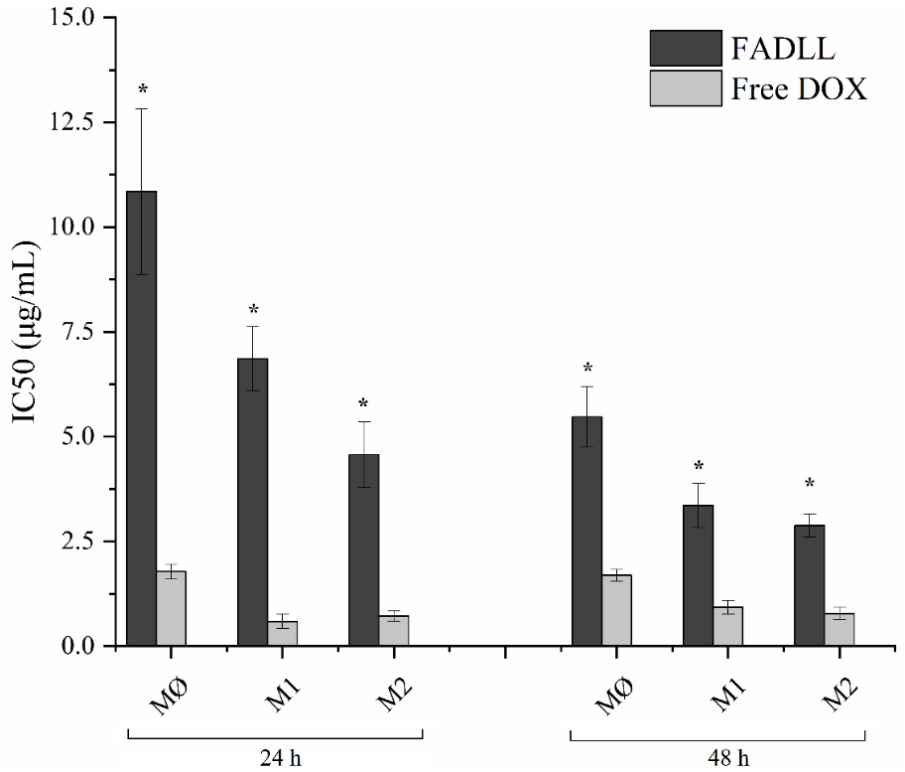

Figure 5.5**: Half-minimal inhibitory concentration (IC_{50}) of FADLL and free DOX against MØ, M1, and M2 at 24 and 48 h time points. '**' represent a significant difference between the same cell type for FADLL and free DOX with $p < 0.05$.*

It was seen that after 24 h, the IC_{50} values for FADLL against MØ, M1, and M4 were calculated to be 10.85 ± 1.98, 6.86 ± 0.76, and 4.57 ± 0.78 µg/mL, respectively; while the IC_{50} values of free DOX against MØ, M1, and M2 were 1.78 ± 0.18, 0.59 ± 0.17, and 0.72 ± 0.12 µg/mL, respectively. When the IC_{50} was calculated at 48 h, the results for FADLL against MØ, M1, and M2 came out to be 5.47 ± 0.72, 3.36 ± 0.52, and 2.88 ± 0.28 µg/mL, respectively. For free DOX, the IC_{50} values were calculated to be 1.69 ± 0.14, 0.93 ± 0.16, and 0.78 ± 0.15 µg/mL for MØ, M1, and M2, respectively. When performed the statistical analyses, it was seen that the IC_{50} values for FADLL at both 24 and 48 h time points have significantly higher values ($P < 0.05$) compared to the free DOX IC_{50} values for all three cell types; this significant difference has been denoted by '*****' in **Figure 5.5**.

5.3.2.6 Cellular uptake of FADLL

The cellular uptake of FADLL against MØ, M1, and M2 was evaluated using flow cytometry analysis. Rhodamine-loaded liposomes with and without FA were synthesized using DOPE:DOPC and DOPE-CYS-FA:DOPC lipids, incubated at 37°C for 2 hours, and tested for cellular uptake. **Figure 6** clearly indicates that the liposomes with FA were significantly taken up by M(IL4) cells compared to MØ and M(LPS), whereas the non-FA-loaded liposomes did not show such an increase in cellular uptake. The significant difference is shown in **Figure 6** using '*****' with $p < 0.05$.

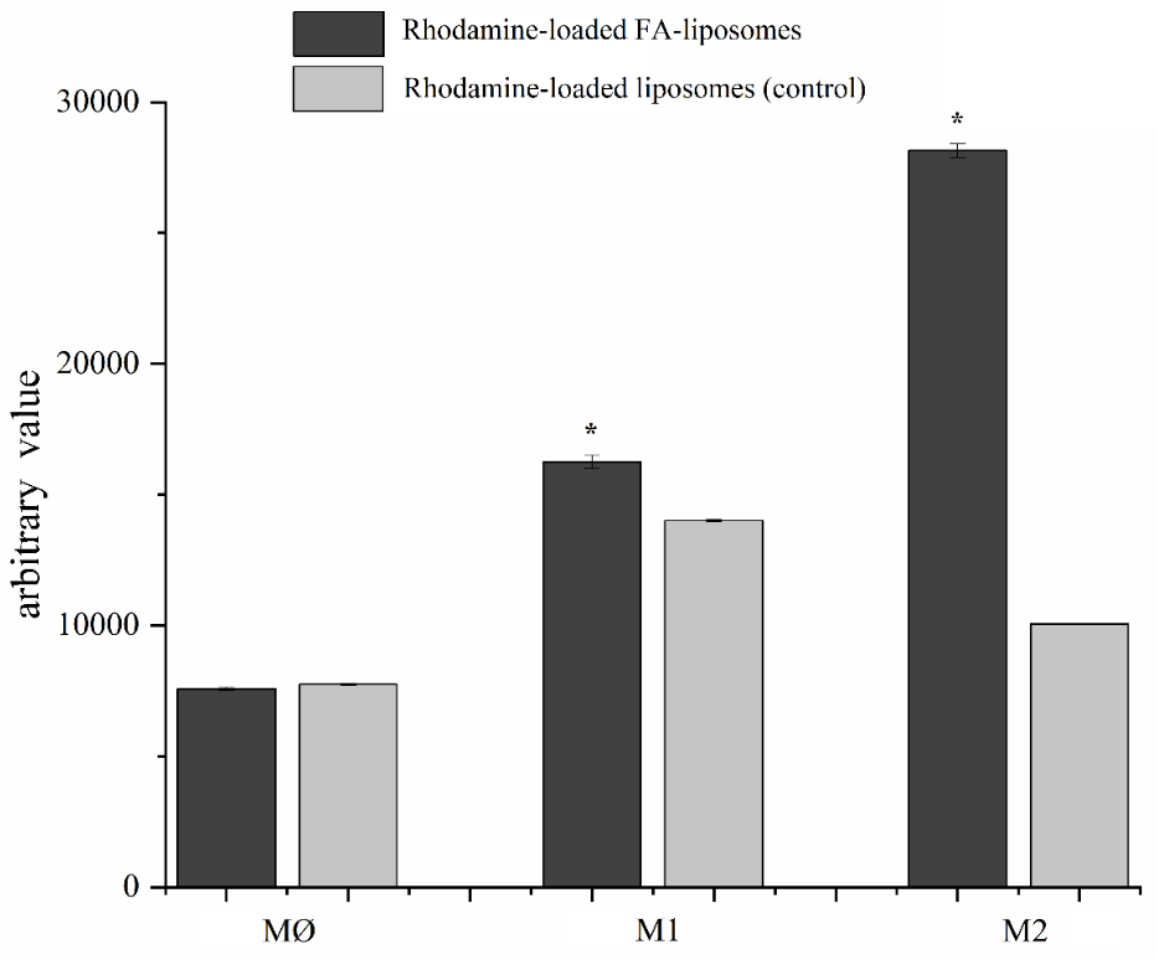

Figure 5.6**: Cellular uptake of rhodamine-loaded DOPE-CYS-FA:DOPC liposomes and rhodamine-loaded DOPE:DOPC liposomes. A significant increase in liposomes containing FA can be seen for M2. "**' representing a significant difference is present for liposomes containing FA compared to non-FA liposomes with $p < 0.05$.*

5.4 Discussion

5.4.1 The addition of cysteine on DOPE and folic acid on the liposomes does not affect liposome properties and toxicity

The size and zeta potential of liposomes play a critical role in cellular uptake. Nanoparticles smaller than 200 nm can be internalized by cells more efficiently compared to larger particles [285,286]. This is because smaller liposomes can diffuse more easily through the cell membrane, which is usually around 7-10 nm thick. Furthermore, the surface charge of

liposomes, as determined by their zeta potential, also affects their cellular uptake. Positively charged liposomes can cause liposomes to aggregate, leading to decreased cellular uptake [287]. Conversely, negatively charged liposomes are less prone to aggregation. A study by Lee et al. showed that other than the surface charge, cellular uptake also depends on the cell type, and for macrophage-like cell lines, negatively charged liposomes are better suited for uptake [288]. In this study, we modified the primary amine of DOPE to attache a cysteine, and futher used the -SH bond of cysteine to attach folic acid to the surface of the liposomes.

Our results show that the addition of cysteine on DOPE and folic acid on the liposomes did not affect the size and polydispersity index of the liposomes. Additionally, there was no significant change observed in the zeta potential of the liposomes. This suggests that the addition of cysteine and folic acid did not alter the surface charge and stability of the liposomes.

Toxicity is a crucial factor to consider in the development of liposomes for drug delivery. In our study, we tested the toxicity of both the unmodified and modified liposomes on MØ, M1, and M2. We found that the addition of cysteine and folic acid did not affect the cell viability compared to the unmodified liposomes. This is an important finding, as one of the deciding factors in choosing both cysteine and FA was their biocompatibility. Numerous studies have used cysteine, both in vitro and in vivo, and it has been proven not to affect the toxicity of the delivery system. Marty et al. used cysteine to introduce thiol groups onto ligands such as antibodies and peptides for site-specific functionalization [289,290].

Similarly, FA has been widely used as a targeting ligand for cancer cells due to its biocompatibility and specificity. Moghimipour et al. studied how FA liposomes can be used to deliver 5-fluorouracil to CT26 cells [291]. Another study by Wang et al. studied the potential of FA-modified liposomes for the delivery of curcumin for targeted delivery to HeLa cells [292]. Our

results of toxicity align with the previous studies, and the lack of significant toxicity observed in our study suggests that the addition of cysteine and folic acid to the liposomes did not compromise their biocompatibility.

Furthermore, the toxicity results obtained in our study indicate that the IC_{50} values of FADLL were higher at 24 h compared to the free DOX, which can be attributed to the difference in drug release for FADLL. Our drug release study showed that after 24 h, FADLL released 31% DOX while free DOX was just present in each well to be internalized without a controlled release. This release behavior corresponds to the higher $IC5_0$ values of FADLL at 24 h. Similarly, at 48 h, FADLL released 53% DOX; this release behavior corresponds to the half-fold values of IC_{50} for FADLL at 48 h compared with 24 h. A study conducted by Handali et al. demonstrated comparable outcomes in drug release when they encapsulated 5-Fluorouracil (5FU) in folate-PEG-DSPE liposomes. Corresponding to our results, the cells internalized the free 5FU within a few hours, whereas nearly 55% of the 5FU encapsulated in the liposomes was released within the first 24 h, and approximately 80% was released at the end of 48 h [293].

The slow and controlled drug release observed in our study through the use of folate-conjugated liposomes can have significant benefits in drug delivery. It allows for a prolonged therapeutic effect, as the drug is released in a controlled manner over a longer period of time. Additionally, liposomes have been shown to delay the release of the drug while increasing its accumulation at the tumor site. This is particularly important as it can reduce the amount of drug required for effective treatment, potentially minimizing toxic side effects in non-cancerous tissues.

5.4.2 Cysteine conjugated DOPE:DOPC liposomes are ideal for thiolyne click chemistry

Thiolene or thiolyne click chemistry is a promising strategy for conjugating molecules to liposomes due to its high efficiency, mild reaction conditions, and specificity. Thiolyne click chemistry involves the reaction between a thiol and an alkyne functional group, forming a carbon-sulfur bond. This reaction has been used for various applications, including drug delivery and imaging.

In a recent study by Dey et al., the researchers used sunlight-mediated thiolyne click reaction to synthesize and deliver DNA transfection using liposomes. The optimized reaction conditions successfully synthesized a series of small molecules and lipids in a single step, including cationic lipids that effectively bind with genetic materials for potential use in gene delivery [294]. A study by Liu et al. showed how thiol-ene chemistry was used to modify the surface of inorganic nanocrystals, which are commonly stabilized by hydrophobic ligands [254].

Similarly, our study utilized cysteine-conjugated liposomes as a platform for thiolyne click chemistry. The presence of the thiol group on the cysteine-modified liposomes allows for efficient and specific conjugation with alkyne-containing molecules. This approach offers a versatile and efficient method for targeted drug delivery, as a variety of targeting molecules can be easily conjugated to the liposomes using thiolyne click chemistry. Overall, cysteine conjugated DOPE:DOPC liposomes are ideal for thiolyne click chemistry and represent a promising platform for targeted drug delivery applications.

5.4.3 Folid acid-conjugated Doxorubicin-loaded liposomes show a higher uptake in M2 macrophages

Folic acid (FA) is commonly used as a targeting agent for cancer therapy due to its high affinity to the folate receptor, which is overexpressed in many cancer cells, and this has led to the development of folic acid-conjugated drug delivery systems for cancer therapy. n our study, we

used folic acid as a proof of concept for selective targeting of M2 macrophages. M2 macrophages are a subtype of macrophages that play a role in tissue repair and have been implicated in many pathological conditions, including cancer. M2 macrophages have been shown to overexpress the folate receptor β (FRβ), and this has led to the development of folic acid-conjugated drug delivery systems for M2 macrophage-targeted therapy. In our study, we used folic acid-conjugated liposomes loaded with DOX to target M2 macrophages.

Our results showed that FADLL had a higher uptake in M2 macrophages compared to unmodified liposomes. This demonstrated the potential of FA as a targeting ligand for M2 macrophages. Other studies have shown similar results, with folic acid-conjugated nanoparticles showing selective targeting to cancer cells that overexpress the FRβ. In a recent study, folic acid liposomes were used to deliver 5-Fluorouracil to HT-29, Caco-2, CT26, HeLa, and MCF-7 cell lines [293]. Furthermore, similar to our study, Hattori et al. used FA-linked liposomes to target TAMs and deliver zoledronic acid to the cells to evaluate its antitumor properties [283].

In conclusion, the FADLLs with conjugated folic acid showed higher uptake in M2 macrophages due to the overexpression of FRβ on their surface. This study demonstrated the potential of FADLLs as a targeted drug delivery system. Future studies could focus on testing these FADLLs in vivo for biodistribution, toxicity, and therapeutic efficacy. Additionally, other targeting ligands could be explored to further improve the specificity and effectiveness and make use of cysteine-conjugated liposomes in delivering drugs to specific cells or tissues. Overall, the use of thiol-ene/yne click chemistry-ready liposomes provides a promising platform for targeted drug delivery, with potential applications in a variety of disease conditions.

5.5 Conclusions

In this study, we have successfully developed a novel liposome platform with cysteine attached on the surface, allowing for efficient conjugation of targeting moieties through thiol-ene/yne click chemistry. The incorporation of folic acid as a proof of concept demonstrated selective targeting of M2 macrophages with higher expression of the folate receptor β. Our study also showed improved drug delivery efficacy of DOX in FADLL compared to free drug. The stability and biocompatibility of the FADLL platform were also demonstrated, making it a promising candidate for targeted drug delivery applications. Future studies could explore the in vivo biodistribution and therapeutic efficacy of FADLL in relevant disease models. Overall, our study presents a simple yet new and effective approach for targeted drug delivery using thiol-ene/yne click chemistry. This platform can be further expanded by conjugating different targeting agents, such as peptides, antibodies, or aptamers, for specific applications. The development of this liposome platform has the potential to revolutionize the field of drug delivery and personalized medicine.

Acknowledgments

This research has been funded by the Department of Material Science and Engineering, Iowa State University and the Carol Vohs Johnson Chair Award.

Declaration of competing interest

Surya K. Mallapragada acknowledges financial interest in ImmunoNanoMed Inc.

5.6 References

[1] W. Al-Jamal and K. Kostarelos, “Liposomes: from a clinically established drug delivery system to a nanoparticle platform for theranostic nanomedicine,” Acc. Chem. Res., vol. 44, no. 10, pp. 1094–1104, 2011.

[2] M. Bilal, M. Qindeel, A. Raza, S. Mehmood, and A. Rahdar, “Stimuli-responsive nanoliposomes as prospective nanocarriers for targeted drug delivery,” J. Drug Deliv. Sci. Technol., vol. 66, p. 102916, 2021.

[3] T. U. Rehman and K. M. Bratlie, “Improving selective targeting to cancer-associated fibroblasts by modifying liposomes with arginine based materials,” J. Drug Target., vol. 30, no. 1, pp. 94–107, 2022.

[4] L.-Q. Fu, W.-L. Du, M.-H. Cai, J.-Y. Yao, Y.-Y. Zhao, and X.-Z. Mou, “The roles of tumor-associated macrophages in tumor angiogenesis and metastasis,” Cell. Immunol., vol. 353, p. 104119, 2020.

[5] H.-F. Liu et al., “Altered polarization, morphology, and impaired innate immunity germane to resident peritoneal macrophages in mice with long-term type 2 diabetes,” J. Biomed. Biotechnol., vol. 2012, 2012.

[6] E. Yang, X. Wang, Z. Gong, M. Yu, H. Wu, and D. Zhang, “Exosome-mediated metabolic reprogramming: the emerging role in tumor microenvironment remodeling and its influence on cancer progression,” Signal Transduct. Target. Ther., vol. 5, no. 1, p. 242, 2020.

[7] C. Anfray, A. Ummarino, F. Torres Andon, and P. Allavena, “Current strategies to target tumor-associated-macrophages to improve anti-tumor immune responses,” Cells, vol. 9, no. 1, p. 46, 2019.

[8] Y. Zheng et al., “Remote drug loading into liposomes via click reaction,” Mater. Horizons, vol. 9, no. 7, pp. 1969–1977, 2022.

[9] B. Liu, X. Deng, Z. Xie, Z. Cheng, P. Yang, and J. Lin, “Thiol–ene click reaction as a facile and general approach for surface functionalization of colloidal nanocrystals,” Adv. Mater., vol. 29, no. 36, p. 1604878, 2017.

[10] E. O. Blenke, G. Klaasse, H. Merten, A. Plückthun, E. Mastrobattista, and N. I. Martin, “Liposome functionalization with copper-free ‘click chemistry,’” J. Control. Release, vol. 202, pp. 14–20, 2015.

[11] C. D. Hein, X.-M. Liu, and D. Wang, “Click chemistry, a powerful tool for pharmaceutical sciences,” Pharm. Res., vol. 25, pp. 2216–2230, 2008.

[12] B. Frisch, F. S. Hassane, and F. Schuber, “Conjugation of ligands to the surface of preformed liposomes by click chemistry,” Liposomes Methods Protoc. Vol. 1 Pharm. Nanocarriers, pp. 267–277, 2010.

[13] F. Said Hassane, B. Frisch, and F. Schuber, “Targeted liposomes: convenient coupling of ligands to preformed vesicles using ‘click chemistry,’” Bioconjug. Chem., vol. 17, no. 3, pp. 849–854, 2006.

[14] H. Karanth and R. S. R. Murthy, “pH-Sensitive liposomes-principle and application in cancer therapy,” J. Pharm. Pharmacol., vol. 59, no. 4, pp. 469–483, 2007.

[15] S. Simões, J. N. Moreira, C. Fonseca, N. Düzgüneş, and M. C. P. De Lima, “On the formulation of pH-sensitive liposomes with long circulation times,” Adv. Drug Deliv. Rev., vol. 56, no. 7, pp. 947–965, 2004.

[16] S. R. Paliwal, R. Paliwal, and S. P. Vyas, “A review of mechanistic insight and application of pH-sensitive liposomes in drug delivery,” Drug Deliv., vol. 22, no. 3, pp. 231–242, 2015.

[17] K. J. O’Byrne, A. G. Dalgleish, M. J. Browning, W. P. Steward, and A. L. Harris, “The relationship between angiogenesis and the immune response in carcinogenesis and the progression of malignant disease,” Eur. J. Cancer, vol. 36, no. 2, pp. 151–169, 2000.

[18] W. Liang and N. Ferrara, “The complex role of neutrophils in tumor angiogenesis and metastasis,” Cancer Immunol. Res., vol. 4, no. 2, pp. 83–91, 2016.

[19] E. Safarzadeh, M. Orangi, H. Mohammadi, F. Babaie, and B. Baradaran, “Myeloid-derived suppressor cells: important contributors to tumor progression and metastasis,” J. Cell. Physiol., vol. 233, no. 4, pp. 3024–3036, 2018.

[20] V. Burade, S. Bhowmick, K. Maiti, R. Zalawadia, H. Ruan, and R. Thennati, “Lipodox®(generic doxorubicin hydrochloride liposome injection): in vivo efficacy and bioequivalence versus Caelyx®(doxorubicin hydrochloride liposome injection) in human mammary carcinoma (MX-1) xenograft and syngeneic fibrosarcoma (WEHI 164) mouse models,” BMC Cancer, vol. 17, pp. 1–12, 2017.

[21] C. Ngambenjawong, H. H. Gustafson, and S. H. Pun, “Progress in tumor-associated macrophage (TAM)-targeted therapeutics,” Adv. Drug Deliv. Rev., vol. 114, pp. 206–221, 2017.

[22] A. Rodriguez-Garcia et al., “CAR-T cell-mediated depletion of immunosuppressive tumor-associated macrophages promotes endogenous antitumor immunity and augments adoptive immunotherapy,” Nat. Commun., vol. 12, no. 1, p. 877, 2021.

[23] T. Nagai et al., “Targeting tumor-associated macrophages in an experimental glioma model with a recombinant immunotoxin to folate receptor β,” Cancer Immunol. Immunother., vol. 58, pp. 1577–1586, 2009.

[24] A. Puig-Kröger et al., “Folate Receptor β Is Expressed by Tumor-Associated Macrophages and Constitutes a Marker for M2 Anti-inflammatory/Regulatory MacrophagesFolate Receptor β Is an M2 Macrophage Marker,” Cancer Res., vol. 69, no. 24, pp. 9395–9403, 2009.

[25] N. M. La-Beck, X. Liu, H. Shmeeda, C. Shudde, and A. A. Gabizon, “Repurposing amino-bisphosphonates by liposome formulation for a new role in cancer treatment,” in Seminars in Cancer Biology, 2021, vol. 68, pp. 175–185.

[26] M. K. Prajapati, R. Pai, and P. Vavia, “Tuning ligand number to enhance selectivity of paclitaxel liposomes towards ovarian cancer,” J. Drug Deliv. Sci. Technol., vol. 66, p. 102809, 2021.

[27] I. van Baal et al., “Multivalent peptide and protein dendrimers using native chemical ligation,” Angew. Chemie, vol. 117, no. 32, pp. 5180–5185, 2005.

[28] I. Ermilova and J. Swenson, “DOPC versus DOPE as a helper lipid for gene-therapies: molecular dynamics simulations with DLin-MC3-DMA,” Phys. Chem. Chem. Phys., vol. 22, no. 48, pp. 28256–28268, 2020.

[29] K. Neuberger, A. Boddupalli, and K. M. Bratlie, “Effects of arginine-based surface modifications of liposomes for drug delivery in Caco-2 colon carcinoma cells,” Biochem. Eng. J., vol. 139, pp. 8–14, 2018.

[30] L. Ma, H. C. Bygd, and K. M. Bratlie, “Improving selective targeting to macrophage subpopulations through modifying liposomes with arginine based materials,” Integr. Biol., vol. 9, no. 1, pp. 58–67, 2017.

[31] S. W. A. Reulen, W. W. T. Brusselaars, S. Langereis, W. J. M. Mulder, M. Breurken, and M. Merkx, “Protein− liposome conjugates using cysteine-lipids and native chemical ligation,” Bioconjug. Chem., vol. 18, no. 2, pp. 590–596, 2007.

[32] D. M. S. H. Chandrupatla, C. F. M. Molthoff, A. A. Lammertsma, C. J. van der Laken, and G. Jansen, “The folate receptor β as a macrophage-mediated imaging and therapeutic target in rheumatoid arthritis,” Drug Deliv. Transl. Res., vol. 9, pp. 366–378, 2019.

[33] J. C. Sheehan and A. K. Bose, “The Synthesis and Reactions of Some Substituted β-Lactams,” J. Am. Chem. Soc., vol. 73, no. 4, pp. 1761–1765, 1951.

[34] A. K. Bose, B. N. Ghosh-Mazumdar, and B. G. Chatterjee, “Ease of Cyclization to the β-Lactam Ring1,” J. Am. Chem. Soc., vol. 82, no. 9, pp. 2382–2386, 1960.

[35] K. Hayashi, M. Moriya, W. Sakamoto, and T. Yogo, “Chemoselective synthesis of folic acid− functionalized magnetite nanoparticles via click chemistry for magnetic hyperthermia,” Chem. Mater., vol. 21, no. 7, pp. 1318–1325, 2009.

[36] C. Bonechi et al., “Solution structure of folic acid: Molecular mechanics and NMR investigation,” Spectrochim. Acta Part A Mol. Biomol. Spectrosc., vol. 60, no. 7, pp. 1411–1419, 2004.

[37] R. M. Silverstein, F. X. Webster, and D. J. Kiemle, “Spectrometric identification of organic compounds. New York: Jonh Wiley and Sons,” Inc.[Google Sch., 1981.

[38] D. Il Kang, H.-K. Kang, H.-S. Gwak, H.-K. Han, and S.-J. Lim, “Liposome composition is important for retention of liposomal rhodamine in P-glycoprotein-overexpressing cancer cells,” Drug Deliv., vol. 16, no. 5, pp. 261–267, 2009.

[39] R. Lv, Q. Bao, and Y. Li, “Regulation of M1-type and M2-type macrophage polarization in RAW264. 7 cells by Galectin-9,” Mol. Med. Rep., vol. 16, no. 6, pp. 9111–9119, 2017.

[40] P. Puddu et al., “IL-12 induces IFN-gamma expression and secretion in mouse peritoneal macrophages.,” J. Immunol. (Baltimore, Md. 1950), vol. 159, no. 7, pp. 3490–3497, 1997.

[41] C. He, Y. Hu, L. Yin, C. Tang, and C. Yin, “Effects of particle size and surface charge on cellular uptake and biodistribution of polymeric nanoparticles,” Biomaterials, vol. 31, no. 13, pp. 3657–3666, 2010.

[42] S. A. Abraham, D. N. Waterhouse, L. D. Mayer, P. R. Cullis, T. D. Madden, and M. B. Bally, “The liposomal formulation of doxorubicin,” in Methods in enzymology, vol. 391, Elsevier, 2005, pp. 71–97.

[43] Y. Hattori, J. Yamashita, C. Sakaida, K. Kawano, and E. Yonemochi, “Evaluation of antitumor effect of zoledronic acid entrapped in folate-linked liposome for targeting to tumor-associated macrophages,” J. Liposome Res., vol. 25, no. 2, pp. 131–140, 2015.

[44] Y. Lu et al., “Antiinflammatory activity of a novel folic acid targeted conjugate of the mTOR inhibitor everolimus,” Mol. Med., vol. 21, pp. 584–596, 2015.

[45] D. Liu, A. Mori, and L. Huang, “Role of liposome size and RES blockade in controlling biodistribution and tumor uptake of GM1-containing liposomes,” Biochim. Biophys. Acta (BBA)-Biomembranes, vol. 1104, no. 1, pp. 95–101, 1992.

[46] S. Spagnou, A. D. Miller, and M. Keller, “Lipidic carriers of siRNA: differences in the formulation, cellular uptake, and delivery with plasmid DNA,” Biochemistry, vol. 43, no. 42, pp. 13348–13356, 2004.

[47] M. Ferreira et al., “Liposomes as antibiotic delivery systems: A promising nanotechnological strategy against antimicrobial resistance,” Molecules, vol. 26, no. 7, p. 2047, 2021.

[48] K.-D. Lee, K. Hong, and D. Papahadjopoulos, “Recognition of liposomes by cells: in vitro binding and endocytosis mediated by specific lipid headgroups and surface charge density,” Biochim. Biophys. Acta (BBA)-Biomembranes, vol. 1103, no. 2, pp. 185–197, 1992.

[49] C. Marty and R. A. Schwendener, “Cytotoxic tumor targeting with scFv antibody-modified liposomes,” Adopt. Immunother. methods Protoc., pp. 389–401, 2005.

[50] C. Marty et al., “Cytotoxic targeting of F9 teratocarcinoma tumours with anti-ED-B fibronectin scFv antibody modified liposomes,” Br. J. Cancer, vol. 87, no. 1, pp. 106–112, 2002.

[51] E. Moghimipour et al., “Folic acid-modified liposomal drug delivery strategy for tumor targeting of 5-fluorouracil,” Eur. J. Pharm. Sci., vol. 114, pp. 166–174, 2018.

[52] W.-Y. Wang, Y.-X. Cao, X. Zhou, and B. Wei, “Delivery of folic acid-modified liposomal curcumin for targeted cervical carcinoma therapy,” Drug Des. Devel. Ther., pp. 2205–2213, 2019.

[53] S. Handali et al., “A novel 5-Fluorouracil targeted delivery to colon cancer using folic acid conjugated liposomes,” Biomed. Pharmacother., vol. 108, pp. 1259–1273, 2018.

[54] S. Dey, A. Gupta, A. Saha, S. Pal, S. Kumar, and D. Manna, “Sunlight-Mediated Thiol–Ene/Yne Click Reaction: Synthesis and DNA Transfection Efficiency of New Cationic Lipids,” ACS omega, vol. 5, no. 1, pp. 735–750, 2019.

CHAPTER 6. GENERAL CONCLUSION

In conclusion, the research presented in this thesis aimed to develop novel liposomal drug delivery systems that could effectively target cancer-associated fibroblasts (CAFs) and tumor-associated macrophages (TAMs), which play critical roles in tumor progression and metastasis. These cells promote tumor growth and survival by secreting cytokines and growth factors that facilitate angiogenesis, immune suppression, and tissue remodeling; there is an urgent need for a vehicle to target these cells, specifically. Targeting these cells presents a promising avenue for cancer therapy, as they are relatively stable components of the tumor microenvironment and have been shown to be resistant to traditional cytotoxic treatments. By specifically targeting CAFs and TAMs with liposomal drug delivery systems, it may be possible to not only overcome the limitations of current cancer therapies but also mitigate some of the devastating effects of cancer on patients' lives.

Chapter 2 investigated the effects of different sizes of liposomes on drug delivery, efficacy, and cellular uptake, which provided valuable insights into optimizing the liposomal design for targeted drug delivery. Chapter 3 explored the use of various surface modifications on liposomes to specifically target CAFs (myofibroblasts), demonstrating the potential of liposomes to deliver drugs directly to the tumor microenvironment and limit off-target effects.

Chapter 4 presented a novel combination therapy approach, utilizing liposomes loaded with doxorubicin and ibuprofen to test the drug delivery and uptake to macrophage and its phenotypes. This study demonstrated the potential of liposomes to deliver multiple drugs simultaneously, which may improve treatment efficacy and overcome drug resistance. Chapter 5, on the other hand, focused on synthesizing a thiol-ene/yne click reaction-ready liposome formulation that could be conjugated with any targeting moiety possessing an alkene or alkyne

bond. The study demonstrated the use of alkyne-bound folic acid to specifically target TAMs, providing a potential strategy to improve drug delivery to these cells and reduce the negative impact of TAMs on cancer treatment outcomes.

Future studies may include in vivo testing of these liposomal formulations to better understand their mechanisms of action, biodistribution, and efficacy in targeting CAFs and TAMs. These studies can be extended to investigate the pharmacokinetics of these formulations, as well as their toxicity and immunogenicity profiles. Additionally, further exploration of alternative targeting moieties, such as antibodies or peptides, can be investigated to improve the specificity and selectivity of these liposomes toward cancer-associated cells.